Master Thesis Project

Impedance analysis of harmonic resonance in HVDC connected Wind Power Plants

Author: **Igor Sowa**

Advisors: Dr. José Luis Domínguez
Dr. Oriol Gomis

Call: July 2016

Escola Tècnica Superior
d'Enginyeria Industrial de Barcelona

Abstract

During the last years the development of HVDC connected offshore wind power plants increased. As the first wind farms of this type were commissioned, an unexpected phenomenon occurred. Electrical harmonic resonance in offshore AC grid led to outages of the HVDC transmission system. The thesis introduces the phenomenon and compare different methods of its analysis.

The study focuses on harmonic frequencies identification excited through the resonance phenomena between the elements within WPP's inner AC network. The analysis includes observations from three tested topology cases by different methods: frequency sweep and harmonic resonance modal analysis. The comparison is performed for diverse converter models: voltage source based, current source based and nonlinear impedance model obtained by harmonic linearization method. The results of the analysis are verified by the outcome attained in DIgSILENT Power Factory software. The study also includes the stability analysis based on Nyquist criterion and interpreted in Bode diagrams.

Furthermore, the result of investigation exposes the clues for possible subsequent implementation of harmonic filters as well as for beneficial control of converters. Feasible measures for resonance mitigation from literature are described and proposed.

Acknowledgement

I would first like to thank my thesis advisors Dr. José Luis Domínguez and Dr. Oriol Gomis who provided me an opportunity to join their team as intern. I am very grateful for their very valuable comments on this thesis.

I thank my fellow master programme colleagues for the stimulating discussions, for the time we were working together before deadlines, and for all the fun we have had in the last two years.

Finally, I must express my very gratitude to my parents and to whole my family for providing me with unfailing support and encouragement throughout my years of study abroad including the process of researching and writing this thesis. This accomplishment would not have been possible without them. Thank you.

Contents

I Introduction **1**

I.1 Background of the study . . . 1

I.2 Motivation . . . 3

I.3 Theoretical introduction . . . 4

I.3.1 Basic information about harmonics . . . 4

I.3.2 Harmonic indices . . . 5

I.3.3 Sources of harmonics . . . 5

I.3.3.1 Harmonics from power electronics elements . . . 6

I.3.4 Harmonic Resonance . . . 6

I.3.4.1 Series AC resonance . . . 7

I.3.4.2 Parallel AC resonance . . . 8

I.3.4.3 Tank circuit parallel AC resonance . . . 10

I.3.4.4 Factors affecting resonance frequency in power system . . . 11

I.3.5 Effects of harmonics . . . 11

I.3.6 Park Transformation . . . 12

I.4 Methods of analysis . . . 13

I.4.1 Frequency Sweep . . . 13

I.4.2 Harmonic Resonance Modal Analysis . . . 13

I.4.3 Critical Modes and Resonance Condition comparison between FS and HRMA . . . 15

II Harmonics and Stabilty in WPP **16**

II.1 Harmonics in WPP . . . 16

II.1.1 Converter topology in WPP . . . 16

II.1.2 Mitigation of harmonics and harmonic resonance . . . 17

II.1.3 Short circuit current at PCC . . . 17

II.1.4 Internal WPP harmonic impedance resonance . . . 17

II.2 Stability of WPP . . . 18

II.2.1 Harmonic Stability . . . 18

ETSEIB

II.2.2 Impedance-based stability evaluation model . . . 18
II.2.3 Stability assessment . . . 20

III Modelling of elements 22
III.1 Transformers . . . 22
III.2 Cables . . . 22
III.3 Filter reactors . . . 23
III.4 Power converters . . . 23
III.4.1 Voltage Source (VS) and Current Source (CS) models . . . 23
III.4.2 Frequency dependent impedance model Z(s) . . . 24
III.4.2.1 Wind turbine converter (inverter) . . . 24
III.4.2.2 HVDC link converter (rectifier) . . . 25

IV Harmonics and power quality regulations 27

V Simulations 28
V.1 System description . . . 28
V.1.1 Network impedance model . . . 30
V.1.2 Topology cases . . . 32
V.1.3 Power converters models . . . 33
V.2 Comparison of resonance frequencies between different topology cases and converter models . . . 35
V.2.1 Case 1 . . . 36
V.2.2 Case 2 . . . 45
V.2.3 Case 3 . . . 55
V.2.4 Comparison between models . . . 65
V.2.4.1 VS model . . . 65
V.2.4.2 CS-WT model . . . 69
V.2.4.3 Z(s) model . . . 72
V.3 Stability study with respect to topology cases . . . 74
V.3.1 Case 1 stability . . . 75
V.3.2 Case 2 stability . . . 77
V.3.3 Case 3 stability . . . 79
V.3.4 Comparison to FS and HRMA . . . 81

VI Approaches to resonance mitigation 83
VI.1 Passive elements . . . 83
VI.2 Active filters, active damping . . . 84
VI.3 Tuning of converter control . . . 85

VII Conclusions **86**

VIII Related environmental impact and costs of the thesis development **89**

VIII.1 Environmental impact of offshore WPP 89

VIII.2 Temporary planning and costs of thesis development 90

Reference **92**

Chapter I

Introduction

I.1 Background of the study

At the end of 2015 total wind power was estimated as 3.7% of Global Electricity Production. It gives the wind power sector the second position within RES production, behind hydro power. What is more important, in 2015 total renewable power generating capacity saw its largest annual increase ever, with en estimated 147 GW of renewable capacity added [1]. That gave an estimated 1849 GW of RES at 2015 year's end. 63.7 GW out of all installed RES capacity in 2015 comes from wind power. This number is wind installations record during one year ever. This power gives a global growth rate of 17.2% comparing to installed capacity at the end of 2014 [2]. Figure I.1 from [1] clearly shows increasing global capacity as well as increasing yearly amount of installed capacity from 2005.

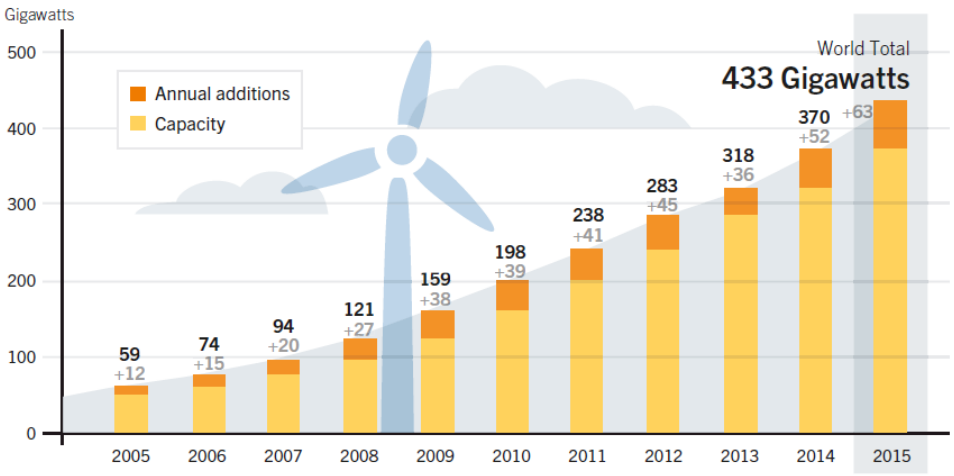

Figure I.1: Wind Power Global Capacity and Annual Additions, 20052015. Figure 23. from [1].

Moreover, as stated in GWEC Global Wind Report [3], the last year's deployment was accompanied by record low prices for forthcoming renewable electricity in countries that combined RES with appropriate policies and market frameworks.

2015 was also a very good year for offshore wind installations. At the end of last year the total globally capacity reached over 12 GW, while only during 2015 new capacity totalled nearly 3.4 GW. More than 11 GW of total installed offshore wind capacity in 2015 is located in Europe and the rest in Asia [3]. Europe, as the biggest offshore wind energy market, installed only in 2015 the capacity of 3019 MW what is 108% more than capacity added in 2014 [4]. At the beginning of 2016, there are 84 offshore wind farms in 11 European countries and still six offshore projects

under construction which will bring additional capacity of 1.9 GW.

Once the total installed capacity of offshore wind power increases over last years, there are also some trends observed regarding the technology itself of offshore wind farms. These trends involves the average power of single turbines, the average water depth and the average distance from the shore. The average size of the turbines increased due to increased deployment of 4-6 MW wind turbines [4]. Depth of the water which is also constantly increasing leads to development of so-called floating offshore wind turbines in the future. The distance from the shore is increasing is determined mainly by higher energy production further from the shore, where the average wind speed values reach higher values. The Figure I.2 shows the average water depth and distance to shore of online farms, the ones under construction and only consented wind farms.

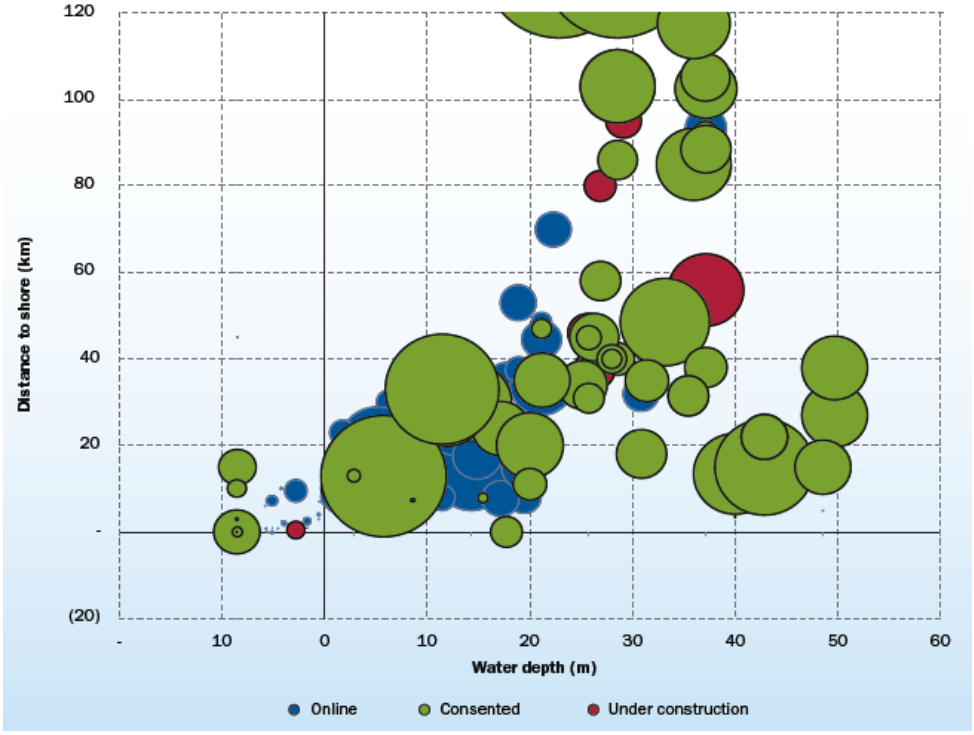

Figure I.2: Average water depth and distance to shore of online, under construction and consented wind farms. Figure 25. from [4].

It clearly shows the increasing trend of size and distance to the shore of already planned wind farms comparing to the existing ones. The average distance to shore of wind farms installed in Europe in only 2015 was 43.3 km. This brings very important concerns regarding transmission of produced power onshore.

The power from offshore wind farm substation has to be transmitted by submarine cables. High voltage AC cables are characterized by a large capacitance. Therefore, a so-called capacitive charging current I_c will flow through the cable (Equation I.1).

$$I_c = UC\omega l \tag{I.1}$$

where l is the length of cable, ω is angular frequency, U is the phase voltage and C is unitary capacitance of cable, which is very high for submarine cables. The charging current limits amount of active power that can be transmitted over the cable to the onshore substation.

As we can clearly see from Equation I.1, the charging current depends also on the length of a submarine cable (l). For long AC cables, the transmission can be highly inhibited due to very high charging current. This current can be limited by additional devices compensating capacitive

reactive power, however it usually requires additional offshore substations and compensating devices, what brings economical concerns.

This limitation of AC cables can be overcome by high voltage direct current (HVDC) transmission. In HVDC cables the charging current does not appear due to transmission at zero-frequency by direct current (DC) instead of alternating current (AC). Besides the length limitations of HVAC cables, there are other issues that should be considered in order to choose between HVAC or HVDC transmission.

Due to DC transmission the losses over the transmission cables are limited, comparing to AC transmission. On the other hand, the losses in HVDC converters exceed the losses in transformers in HVAC systems and have higher risk of failure. For higher distances from the shore the HVDC transmission becomes more competitive mainly due to very high costs of offshore substations, which could be inevitable for long-distance AC transmission due to the necessity of reactive power compensation described above. In the [5] the authors estimate the energy transmission costs for case of 400 MW offshore wind farm for HVAC transmission and HVDC transmission. In the Figure I.3 we observe the transmission distances for which the energy transmission cost by HVAC becomes more expensive than for HVDC. With respect to that study [5], depending on the technology of HVDC conversion, the break-even distance is between 55 and 85 km.

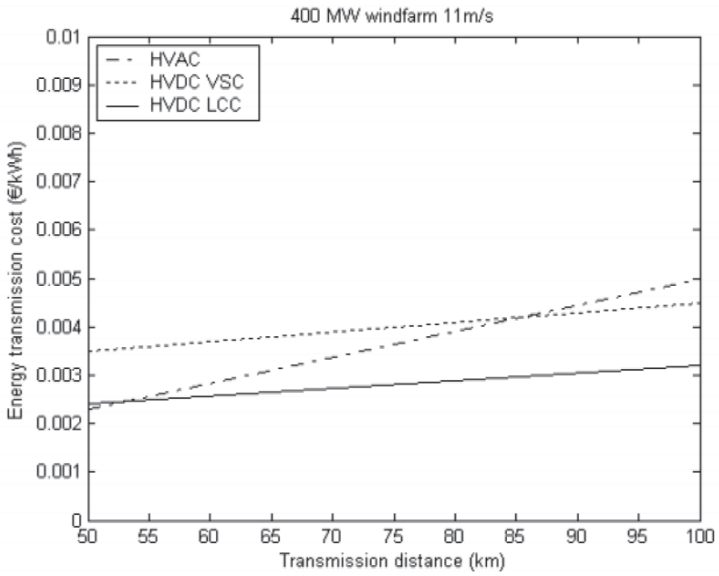

Figure I.3: Energy transmission cost from for 50-100 km. Figure 6. from [5].

To sum up, HVAC or HVDC transmission is usually decided on a project per project basis and is highly dependent on a number of factors.

I.2 Motivation

The study presented in this thesis is motivated by recent experiences in operation of first high-power HVDC connected offshore wind power plant. In that plant the harmonic resonance has occured under normal operation [6]. The authors state that the following conditions bring the problems forth.

Due to the HVDC connection of that grid the offshore AC network is decoupled from main network. This grid is dominated by cables and power electronic converters. The presence of cables brings down the resonant frequency to lower level where the other harmonics occur and could be amplified. Moreover, due to many power electronic devices the damping of resonance

in such a grid is much lower than in the onshore main grid. As the result, in such a *weak grid* power converters can go into resonance between each other causing oscillations and instabilities in AC network [6].

The problems described above were not considered during planning period of that WPP. Due to very strong development of HVDC connected offshore wind farms now and in the future, to avoid such problems, new methods of investigation and analysis for resonance should be developed or current ones should be extended.

The purpose of the thesis is to analyse, understand and compare the resonance in off-shore wind farm AC grids. Deployment of some available methods in order to detect possible occurrence of resonance is considered. Furthermore, the study is coupled with stability analysis based on Nyquist stability criterion and interpreted on the Bode diagram. The accuracy of this study is significantly determined by the quality of utilized model and its elements therefore, for comparison, we use different approaches to power converters modelling.

I.3 Theoretical introduction

I.3.1 Basic information about harmonics

Generation of electricity in power system is usually at the frequency operational level of either 50Hz or 60Hz. Waveforms produced by rotating generator is practically sinusoidal and in this shape they should be delivered to every customer. However, when sinusoidal waveform is applied. Such a current leads to not perfectly sinusoidal voltage drop due to system impedance. Hence, the voltage distortion at load terminals is produced. The presence of these distortions is not new in the power system. However the devices responsible for producing distorted waveforms and devices suffering from presence of the distortions have changed down the years.

A distorted, non-sinusoidal waveform can be expressed in a very simple way as a sum of so-called harmonic components. Harmonic component in power system is a perfectly sinusoidal waveform that has frequency equal to integer multiple of the fundamental frequency:

$$f_h = h \cdot f_1 \tag{I.2}$$

where h is an integer (harmonic order) and f_1 is fundamental frequency (usually 50 Hz or 60 Hz). If h is not an integer, such a waveform is called *interharmonic* component. As aforementioned, any sinusoidal waveform can be expressed as sum of its harmonic components. Exemplary distorted current waveform for fundamental frequency and 3^{rd}, 5^{rd} and 7^{rd} harmonics could be expressed as follows:

$$I = I_1 sin(\omega t) + I_3 sin(3\omega t + \delta_3) + I_5 sin(5\omega t + \delta_5) + I_7 sin(7\omega t + \delta_7) \tag{I.3}$$

where I_1, I_3, I_5, I_7 are peak RMS values of fundamental component and harmonic components and $\delta_3, \delta_5, \delta_7$ are possible phase shifts of each harmonic.

Concerns for harmonics rises from power quality requirements. Power quality requirements are introduced to prevent from negative effects on electrical equipment which are sensitive to poor power quality. The most popular regulations describing power quality with respect to harmonic content are summarized in Chapter IV. Poor power quality leads to damages of equipment, in other words, causes great money losses for industry. Moreover, certain types of equipment, if exposed to distorted waveforms, lead to further generation of harmonics [7].

Even though, the word *harmonics* frequency refers only to the integer multiple of the fundamental frequency, we often use this notion for frequencies which are non-integer multiple of fundamental frequency (which should be called *interharmonics*) if the distinction between these two concepts is not crucial.

I.3.2 Harmonic indices

There are two most common indices to describe content of the harmonics in a time domain signal as one number: *Total Harmonic Distortion* (THD) and *Total Demand Distortion* (TDD).

THD, which usually relates to voltage waveforms, is defined as RMS values (V_{nRMS}) of the harmonics expressed relatively to fundamental components (V_{1RMS}):

$$THD = \frac{\sqrt{\sum_{n=2}^{N} V_{nRMS}^2}}{V_{1RMS}} \tag{I.4}$$

where n is the harmonic order and N is maximum harmonic order to be considered. For most application, it is sufficient to consider harmonic order range up to 25^{th} harmonic, but most standards recommend up to 50^{th} [7].

Since THD of current waveform can be misleading when load is low and could result in very high value, RMS values of harmonic currents (I_{nRMS}) can be related to rated (I_{rRMS}) or maximum current magnitude rather than to fundamental current (like in THD):

$$TDD = \frac{\sqrt{\sum_{n=2}^{N} I_{nRMS}^2}}{I_{rRMS}} \tag{I.5}$$

This reflects distortion in more intuitive way since the electrical power supply systems are design to withstand rated (or maximum) values, while relation to fundamental components when load is far lower from rated value can give impression of much more significant distortion.

I.3.3 Sources of harmonics

As mentioned before the sources of harmonic distortions have changed down the years. In early power systems harmonic distortions were mainly caused by saturation of transformers, industrial arc furnaces and other arc devices like electric welders. On the other hand, the main concern was the effect of those distortions on electric machines, telephones and on increased risk of failure from overvoltage [8].

Nowadays, generally speaking, harmonics, interharmonics and subharmonics in power systems are produced due to many phenomena, for example, ferroresonance, magnetic saturation, subsynchronous resonance, and nonlinear and electrically switched loads. These days, harmonic emission from nonlinear loads dominates [9].

In transformers, harmonics appear as result of saturation, switching, high-flux densities, winding connections and grounding. Also, energizing a power transformer generates a high order of harmonics and a DC component [7].

In rotating machines, the construction elements and their limitations of both generators and motors like [7]: armature windings, phase windings, teeth, phase spread etc. affects EMF in the phase windings, therefore rotating machines are also not pure linear elements. Even synchronous machine generates deviated voltage at its terminal, however the voltage is almost sinusoidal.

In presence of system capacitance, some inductive elements like transformers or reactors can lead to so-called ferroresonance phenomena, due to nonlinearity and saturation of reactance. This causes short current surges that generate overvoltages. Moreover, presence of capacitance in sinusoidal circuits can magnify existing harmonics by creating harmonic resonance condition. More about harmonic resonance in Section I.3.4.

I.3.3.1 Harmonics from power electronics elements

Besides the classical power system elements described above, power electronics equipments are the main source of harmonics in the power system. We can include in this group devices like: power converters (rectifiers and inverters) and power electronic basic elements like diodes, diacs, triacs, GTOs etc. [7].

Among the power electronics devices, many of them are controlled with pulse width modulation (PWM). We can distinguish several techniques of PWM: single PWM, multiple PWM, sinusoidal PWM, modified sinusoidal PWM. Inverters which use PWM can be divided into three groups: VSI (voltage source inverters), CSI (current source inverters) and ZSI (impedance source inverters). These elements (controlled by PWM) usually emit so-called characteristic harmonics which are those produced by power electronic converters during normal operation. They are still integer multiply of fundamental frequency [7]. Such a device can be viewed as a matrix of static switches that provides an interconnection between input and output nodes of an electrical power system. In rectifying process, current is allowed to pass through semiconductor devices during only a fraction of the fundamental frequency cycle, for which power converters are often regarded as energy-saving devices [8]. Power electronic devices also produce some non-characteristic harmonics when some non-ideal condition of control occurs (for example unbalanced PWM signal). Then, harmonics emitted will be unbalanced and also interharmonics can appear. Since mitigation of harmonics is usually designed for characteristic harmonics, the non-characteristic harmonics can cause significant problems [7].

In large power converters, generally, there is much higher inductane on the DC than on the AC side. Thus, the DC current is practically constant and the converter acts as a harmonic voltage source on the DC side and as a harmonic current source on the AC side [8].

In the study cases of the thesis, VSI (Voltage Source Inverters) are used in the considered wind power plant. VSIs use switching devices like GTO, IGBT, MTO which have both turn off and turn on control. Because of this, much more accurate control comparing to CSI is possible, also including power flow control. Further details about utilized models of converters and other elements are provided in Chapter III.

The harmonics from Wind Power Plants are becoming very important in the power system these days due to increasing number of these sources. As stated in the Introduction, the main subject of this thesis is to analyse harmonics created and possibly emitted to the power system to the grid due to the phenomenon of harmonic resonance in Wind Power Plants inner grid. Further details about Wind Power Plants as a source of harmonics in Section II.1.

I.3.4 Harmonic Resonance

Harmonic resonance is an important factor affecting the system harmonic levels. Resonant conditions involve the reactance of capacitive elements that at some point in frequency equals the inductive reactance of the inductive elements. These two elements combine to produce series or parallel resonance [8]. Harmonic waveform generated in other part of the grid can be magnified many times due to this phenomenon [7]. For such a harmonic resonance problems, there must be a sufficient level of harmonic source voltages or currents at or near the resonant

frequency to excite the resonance [10].

Most of the networks are considered inductive, therefore presence of capacitive elements can result in local system resonances, which lead in turn to possibly subsequent damage [9]. Depending on the type of the grid these are usually capacitor banks, cables, overhead lines, compensators etc. Since harmonic resonance either amplify existing harmonics or creates new, the negative effects of this phenomenon are very similar to the effects caused by harmonics described in Section I.3.5. Moreover, it can overload the capacitor and may result in nuisance fuse operation causing severe amplification of the harmonic currents resulting in waveform distortions, which has consequent deleterious effects on the power system components [7].

As circuit theory says, resonance harmonics can occur in series RLC or parallel RLC circuits (the connection type between L and C elements). The resonance frequency depends on values of the inductance and capacitance. The smaller the size of the capacitor, the higher is the resonant frequency [7]. This conclusion we observe in the results presented in Chapter V.

The resonance problem in power system is a serious potential problem. It leads to many negative (shut-downs, failures). It may appear unexpected at certain operating condition of the power system. Moreover, it can also appear partially or disappear with no negative effect. Due to these problems, prevention may require long-term online measurements to establish the disturbing source in the system [7].

Major concerns about elusive harmonic resonances are [7]:

- the resonant frequency is present in a grid (for example separated industrial grid or inner collection grid of WPP) and depends very strongly on topology of considered network,
- expansion or disconnection of some parts of the network may bring out a resonant condition not existing before (for example switching on the capacitor for power factor improvements),
- even when some elements are designed to prevent from harmonic resonance (e.g. harmonic filters), after any modification of the topology, immunity from resonant conditions cannot be guaranteed since the considered network in the new state could have the resonance frequencies at different levels than in the state before modification.

In the thesis we describe some methods for monitoring the resonance in the grid and identification of an element responsible for certain emission (Section I.4). As aforementioned, there are two basic cases of resonance: series and parallel resonance. Following sections describes these two circumstances.

I.3.4.1 Series AC resonance

The simple series connection of resonant element is presented in the Figure I.4.

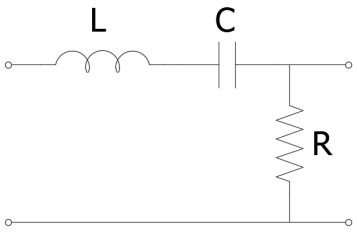

Figure I.4: Exemplary circuit for series LC resonance.

The impedance of such a circuit is as follows:

$$Z = R + j\omega L + \frac{1}{j\omega C} \tag{I.6}$$

In the case of series resonance, the total impedance at the resonance frequency is reduced exclusively to the resistive circuit component. Assuming $R = 0$, the series resonance occurs at certain resonant frequency f_r, when the impedance is minimum i.e.:

$$j\omega L + \frac{1}{j\omega C} = 0 \tag{I.7}$$

What leads to:

$$\omega_r = \frac{1}{\sqrt{LC}} \tag{I.8}$$

Impedance magnitude of the system from Figure I.4 and its angle is presented in the in the Figure I.5.

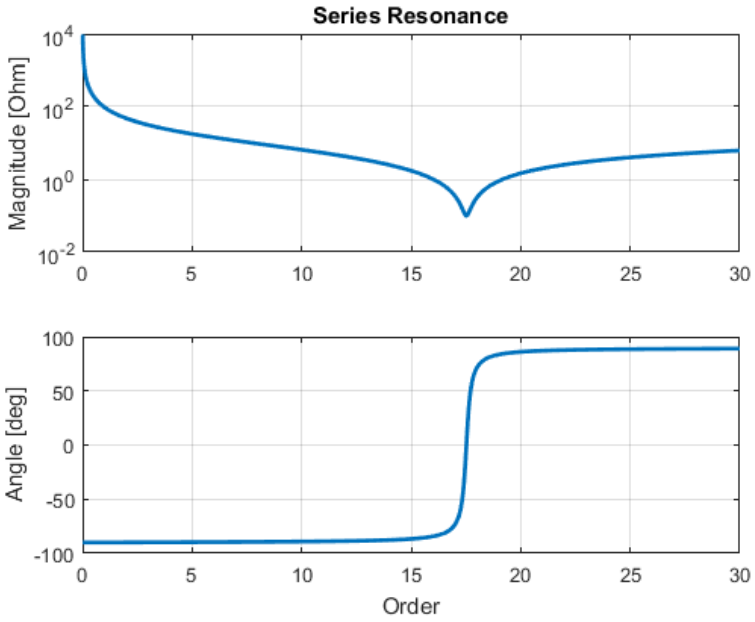

Figure I.5: Series resonance in LC circuit at frequency 876 Hz (17^{th} frequency order).

Since the impedance reduced for resonance frequency, the current can reach very high values:

$$I_r = \frac{V_1}{R} = \frac{V_2}{R} \tag{I.9}$$

Thus, we can see that the current is limited only by resistance. In the pure LC case the currents tends to infinity and if R is very small, current can be high.

I.3.4.2 Parallel AC resonance

The parallel resonance occurs in parallel RLC circuit (see the example circuit in the Figure I.6) when the total impedance at the resonant frequency is very large (theoretically tends to infinite).

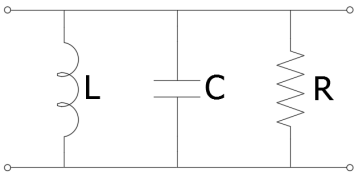

Figure I.6: Exemplary circuit for parallel LC resonance.

$$\frac{1}{Z} = \frac{1}{R} + \frac{1}{j\omega L + j\omega C} \tag{I.10}$$

In this circuit, the resonant condition is (ignoring R - open-circuit):

$$\omega C - \frac{1}{\omega L} = 0 \tag{I.11}$$

Thus, the resonant frequency is as follows:

$$\omega_r = \frac{1}{\sqrt{LC}} \tag{I.12}$$

Exemplary impedance magnitude and angle plots of the system from Figure I.6 are plotted at Figure I.7.

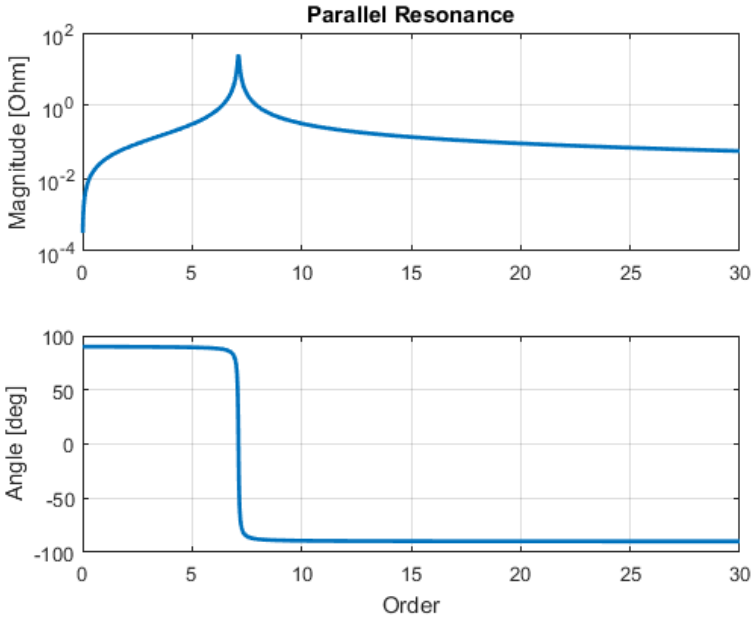

Figure I.7: Parallel resonance in LC circuit at frequency 356 Hz ($7^{th} frequency order$).

This condition may produce a large overvoltage between the parallel-connected elements, even under small harmonic currents. Therefore, resonant conditions may represent a hazard for solid insulation in cables and transformer windings and for the capacitor bank and their protective devices as well [8].

I.3.4.3 Tank circuit parallel AC resonance

More practical LC circuit i.e. with inductor modelled with non-zero value of resistance and capacitor modelled without resistance is called Tank circuit [7]. Figure I.8 presents such a circuit.

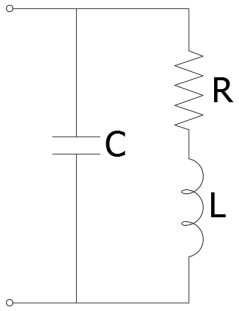

Figure I.8: Tank circuit for parallel LC resonance.

In this circuit the aggregate admittance seen from the terminals is as follows:

$$Y = j\omega C + \frac{1}{R + j\omega L} \tag{I.13}$$

In other form:

$$Y = \frac{R}{R^2 + \omega^2 L^2} + j\left(\omega C - \frac{\omega L}{R^2 + \omega^2 L^2}\right) \tag{I.14}$$

The plot of exemplary impedance for such a system is presented in the Figure I.9.

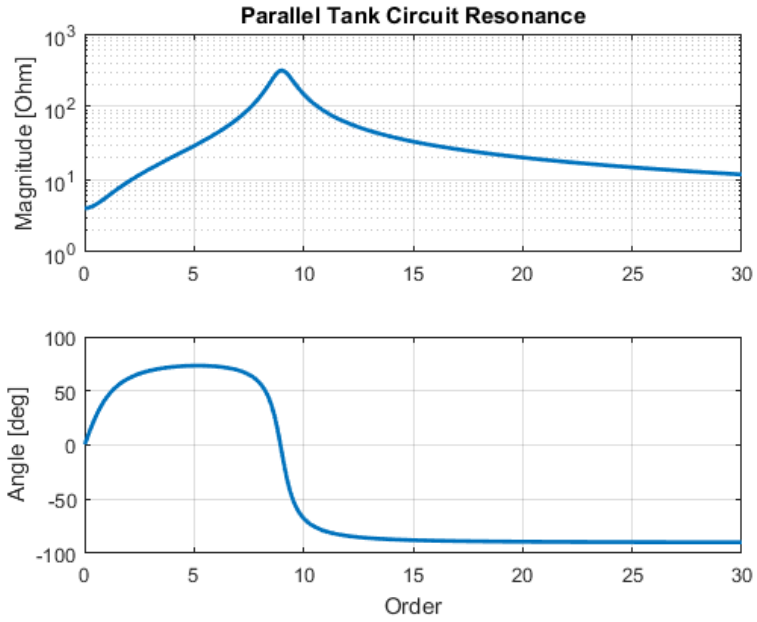

Figure I.9: Parallel resonance in tank circuit between LC elements at frequency 447 Hz ($9^{th} frequency order$).

In the circuit with zero-resistance (lossless circuit), resonance occurs if impedance of inductor equals impedance of capacitor i.e. when the circuit works as short-circuited. In this case,

resonance occurs in similar situation, even though the resistance stays unchanged in the circuit. In other words resonance occurs when power factor of admittance above equals zero [7].

$$\omega C - \frac{\omega L}{R^2 + \omega^2 L^2} = 0 \tag{I.15}$$

That gives resonance frequency:

$$\omega_r = \sqrt{\frac{1}{LC} - \frac{R^2}{L^2}} \tag{I.16}$$

Moreover, as distinct from the series resonance, where resonance can occur from any value of resistance, in this case resonance occurs only if following equation is true:

$$\frac{R^2}{L^2} \leq \frac{1}{LC} \tag{I.17}$$

In other words, resonance does not occur if:

$$R > \sqrt{\frac{L}{C}} \tag{I.18}$$

I.3.4.4 Factors affecting resonance frequency in power system

Generally speaking, in the power system, the following factors, by modification of network impedance, can impact resonance frequency values (based on [7]):

- Synchronous and asynchronous sources and loads in the power system. They can absorb some harmonics but also change the resonance points. Correct modelling of these elements is crucial.
- Impedance of the utility source. In models connected to such a source they are given by the three-phase short-circuit current, which corresponds to certain impedance.
- Shunt power capacitors. They are not recommended in presence of other devices producing harmonics. They shift resonance frequencies and can cause secondary resonance if applied at multi-voltage levels.
- Single phase loads. From impedance point of view, single phase loads are unsymmetrical loads, therefore lead to unsymmetrical phenomena.
- Already applied harmonic mitigating devices (e.g. passive filters). They does not remove the resonant conditions, but by introduction of new impedance, these devices only shift resonance frequency to the other level.
- Topology of the network. Any switching action will change the resonant frequency, since tha aggregated impedance of the network changes.

I.3.5 Effects of harmonics

The harmonic resonance in a power system cannot be tolerated and must be avoided. The magnified harmonics will have serious effects on equipment heating, harmonic torque generation,

nuisance operation of protective devices, derating of electrical equipment, damage to the shunt capacitors due to overloading, can precipitate shutdowns etc.

Some of the harmonic deleterious effects on electrical equipment are gathered in [11]:

- Capacitor bank failure because of reactive power overload, resonance, and harmonic amplification. Nuisance fuse operation.
- Excessive losses, heating, harmonic torques, and oscillations in induction and synchronous machines, which may give rise to torsional stresses.
- Increase in negative sequence current loading of synchronous generators, endangering the rotor circuit and windings.
- Generation of harmonic fluxes and increase in flux density in transformers, eddy current heating, and consequent derating.
- Overvoltages and excessive currents in the power system, resulting from resonance.
- Derating of cables due to additional eddy current heating and skin effect losses.
- Inductive interference with telecommunication circuits.
- Signal interference in solid-state and microprocessor-controlled systems.
- Relay malfunction.
- Interference with ripple control and power line carrier systems, causing misoperation of the systems, which accomplish remote switching, load control, and metering.
- Unstable operation of firing circuits based on zero-voltage crossing detection and latching.
- Interference with large motor controllers and power plant excitation systems.
- Possibility of subsynchronous resonance.
- Flickers.

I.3.6 Park Transformation

Park transformation is necessary to obtain the positive and negative impedances for converters equations presented in Section III.4.2.

Park transformation, also called dq0-transformation is a space vector transformation of three-phase time-domain signals from a stationary phase coordinate system (abc) to a rotating coordinate system ($dq0$) as follows [12]:

$$\begin{bmatrix} u_d \\ u_q \\ u_0 \end{bmatrix} = \frac{2}{3} \begin{bmatrix} cos(\Theta) & cos(\Theta - \frac{2\pi}{3}) & cos(\Theta + \frac{2\pi}{3}) \\ -sin(\Theta) & -sin(\Theta - \frac{2\pi}{3}) & -sin(\Theta + \frac{2\pi}{3}) \\ \frac{1}{2} & \frac{1}{2} & \frac{1}{2} \end{bmatrix} = \begin{bmatrix} u_a \\ u_b \\ u_c \end{bmatrix} \tag{I.19}$$

where $\Theta = \omega t + \delta_A$ is the angle between the rotating and fixed coordinate system at each time t and δ_A is an initial phase shift of the voltage.

The inverse transformation from the $dq0$ frame to the abc frame:

$$\begin{bmatrix} u_a \\ u_b \\ u_c \end{bmatrix} = \begin{bmatrix} cos(\Theta) & -sin(\Theta) & 1 \\ cos(\Theta - \frac{2\pi}{3}) & -sin(\Theta - \frac{2\pi}{3}) & 1 \\ \cos(\Theta + \frac{2\pi}{3}) & -sin(\Theta + \frac{2\pi}{3}) & 1 \end{bmatrix} = \begin{bmatrix} u_d \\ u_q \\ u_0 \end{bmatrix} \tag{I.20}$$

I.4 Methods of analysis

In this study we focus on the methods of analysis in frequency-domain like the ones described below. Therefore methods of harmonic analysis in time-domain like Fourier Series, Discrete Fourier Transform (DFT) or Fast Fourier Transform (FFT) etc. are not included in this description.

The phenomenon of harmonic resonance seems well understood in the literature, however tools available to analyse it are very limited [13]. Method of frequency scan (frequency sweep) is the most general and common method to identify the resonance frequencies in networks [14]. However, this method is limited. The resonance is between two elements (capacitive and inductive) in the system and networks usually consists of many elements. The result of frequency sweep does not indicate which elements exchange energy between each other, causing resonance.

The method of Harmonic Resonance Modal Analysis (HRMA) was developed to face this problem [13]. This method involves only analysis of parallel resonance which is more dangerous in the power system. From HRMA the buses which excite a particular resonances can be identified. Thus, we can observe which components are more involved in a resonance than other. From these results we can conclude where a resonance can be observed more easily or how far the resonance can propagate in the system [13].

I.4.1 Frequency Sweep

Frequency Sweep (or Frequency Scan) analysis is a characterization of the system equivalent impedance at a bus in the system as a function of frequency [10]. As the result, curve of impedance in frequency domain is obtained. The peaks in the curve suggest frequencies when parallel resonance occurs (very high impedance at certain frequency) while dips indicate the frequencies when series resonance occurs (very low impedance at certain frequency).

In Wind Power Plants frequency scans are often done at various grid locations or at the collector bus [10]. The magnitude of computed impedances depends also on the level of equivalent voltage used in the calculations. However, the single value of identified peak impedance does not determine if a dangerous harmonic resonance occurs. For harmonic problems, there must also be a sufficient level of harmonic source voltages or currents at or near the resonant frequency to excite harmonic resonance [10]. Also, the impedance value itself has to be analysed in particular case to identify the value that could cause harm. To do this, the best way is to obtain specific data by measurements, but also data provided by manufacturers of devices in the network.

I.4.2 Harmonic Resonance Modal Analysis

The method is based on analysis of well-known admittance matrix - $\boldsymbol{Y}$. It focuses on the large elements of inverted $\boldsymbol{Y}$. In the extreme case (very large elements) the admittance matrix tends to singularity and element of inverted $\boldsymbol{Y}$ tends to infinity, thus very high voltages can be produced, which is in principle parallel resonance.

The elements are identified on the basis of eigenvalues of $\boldsymbol{Y}$ matrices. Since matrix becomes singular when even one of the eigenvalue becomes zero, the principle can be clearly used. Eigenvalues correspond to certain mode of harmonic resonance, therefore the study consists of identification of critical resonance modes. The equations describing the method including the identification of certain buses and elements are presented below.

The admittance matrix on the network is constructed for certain frequency $\boldsymbol{Y_f}$. Admittance matrix fulfils equation:

$$\boldsymbol{V_f} = \boldsymbol{Y_f^{-1}} \boldsymbol{I_f} \tag{I.21}$$

where: $\boldsymbol{Y_f}$ is the network admittance matrix $\boldsymbol{V_f}$ is the nodal voltage and $\boldsymbol{I_f}$ is the nodal current injection. All matrix values are at frequency f.

To investigate if $\boldsymbol{Y_f}$ approaches singularity, the theory of eigen-analysis is applied. According to [15], matrix $\boldsymbol{Y_f}$ can be decomposed into (index f is neglected in the next equations for simplicity):

$$\boldsymbol{Y} = \boldsymbol{L} \cdot \boldsymbol{\Lambda} \cdot \boldsymbol{T} \tag{I.22}$$

where $\boldsymbol{\Lambda}$ is the diagonal eigenvalue matrix and $\boldsymbol{L}$ and $\boldsymbol{T}$ are the left and right eigenvector matrices.

Defining $\boldsymbol{U} = \boldsymbol{TV}$ as the modal voltage vector and $\boldsymbol{J} = \boldsymbol{TI}$ as the modal current vector, the equation can be derived:

$$\boldsymbol{U} = \boldsymbol{\lambda^{-1}J} \tag{I.23}$$

or

$$\begin{bmatrix} U_1 \\ U_2 \\ ... \\ U_n \end{bmatrix} = \begin{bmatrix} \lambda_1^{-1} & 0 & 0 & 0 \\ 0 & \lambda_2^{-1} & 0 & 0 \\ 0 & 0 & ... & 0 \\ 0 & 0 & 0 & \lambda_n^{-1} \end{bmatrix} = \begin{bmatrix} J_1 \\ J_2 \\ ... \\ J_n \end{bmatrix} \tag{I.24}$$

where each λ^{-1} has the unit of impedance and is named modal impedance Z_m. From matrix Equation I.22, one can easily identify the location of resonance in the modal domain due to corresponding modal currents and voltage. If $\lambda_1 = 0$ or is very small, a small injection of modal 1 current J_1 will lead to a large modal 1 voltage U_1 [13]. Thus, we can identify that a resonance takes place for specific mode (or modes) and it is not related to a particular bus injection since the values are in modal domain. The smallest eigenvalue is called the critical mode of harmonic resonance and its left and right eigenvectors are the critical eigenvectors.

The modal currents J are a linear projections of the physical currents in the direction of the first eigenvectors by: $\boldsymbol{J} = \boldsymbol{TI}$. Also the physical nodal voltages are related to the modal voltages by: $\boldsymbol{V} = \boldsymbol{LU}$. More details in [13]. In summary, the critical eigenvectors characterize the excitability of the critical mode (right critical eigenvector) and observability of the critical mode (left critical eigenvector). The excitability and observability of modes are characterized with respect to the location.

It is also possible to combine the excitability and observability into a single index according to the theory of selective modal analysis [16]:

$$\boldsymbol{V} = \boldsymbol{L\Lambda^{-1}TI} \tag{I.25}$$

However, this approximation is made possible because $1/\lambda_1$, the critical modal impedance, is much larger than the other modal impedances. If there are more impedances at the similar level as critical impedance, we will observe some inaccuracies in the results.

Assuming one critical modal impedance, much larger than the others, the diagonal elements of the above matrix $\boldsymbol{LT}$ characterize the combined excitability and observability of the critical mode at the same bus. They are called participation factors (PF's) of the bus and are defined as follows [13]:

$$PF_{bm} = L_{bm} \cdot T_{mb} \tag{I.26}$$

where b is the bus number and m is the mode number.

Generally speaking, from the calculation on the basis of admittance matrix (decomposition into eigenvectors and eigenvalues) and the approximation above (Equations I.22 - I.26) we obtain: the set of participating factors for each bus for each critical mode (the modes when the modal impedance peaks), which occurs for certain frequency at certain number of mode. Moreover, the participation factors of all buses sum up to 1, therefore the comparison of participation factors between buses is simple and we express them in percentage values.

I.4.3 Critical Modes and Resonance Condition comparison between FS and HRMA

As mentioned, resonant conditions identified in this method depends on the value of eigenvalue, which is very small if resonance occurs. This is equal in other words to very high modal impedance. As seen from comparison with frequency scan impedance curves, the sharp peaks occur for the same frequencies. One has to remember that in frequency scan method, the impedance curves are seen from the certain point in the grid, while in HRMA the impedance curves are divided into modes, which does not correspond exactly to the physical buses, even though the number of modes and the number of buses is the same.

Moreover the values of maximum impedances at peak point from both methods are different. The reason is again due to comparison between *real* impedance and *modal* impedance. Modal impedance should be investigated referring to every specific case in order to identify the threshold value or the range, above which the harmful resonance occurs. In this study, values of interests identified by both methods are the frequencies when resonances occurs, therefore the harmful impedance, neither real nor modal are not identified.

Chapter II

Harmonics and Stabilty in WPP

II.1 Harmonics in WPP

Wind Power Plants, due to intermittency of the wind, are usually supported by great number of power electronic converters which enable effective operation of WPP. These non-linear devices are sources of significant amounts of harmonics in Wind Farms.

Harmonics produced by converters first of all are introduced into inner grid of WPP. Before any waveform produced by wind turbines and converted by wind turbines converters is introduced into the power system (through PCC between WPP and external grid), it is exposed to dangerous phenomenon of harmonic resonance in inner grid of WPP.

Internal harmonic resonance depends essentially on the elements that the inner grid consists of (including possible HVDC link converter) and the way of their connection (topology). As described in Section I.3.4 harmonic resonance contributes to amplification of existing harmonics and is able to create new harmonic components.

As a result, overall external emission of harmonics (to the power system) from Wind Power Plants, not decoupled by HVDC link, depends on [7] (i) converter topology, (ii) applied harmonic filters and (iii) short-circuit current at PCC. These three features has to be completed by the above problem of (iv) internal harmonic impedance resonance of the WPP inner grid. If the wind farm is connected by HVDC link, then the emission of harmonics to the external grid depends on the DC/AC conversion at the PCC behind HVDC connection. Even though, the emission to the main grid of such HVDC connected WPP is less serious problem, harmonic phenomena still creates a many issues in the inner WPP AC grid, which is considered as a *weak grid* due to domination of power electronic converters and luck of resistive damping.

Main focus of the thesis is understanding and description harmonic resonance appearing in inner grids of Wind Power Plants. Moreover, stability issues due to the harmonic resonance are put forward. As mentioned in the Section I.2, the analysis of these problems has recently become very important due to serious problems observed in first HVDC connected offshore wind farm during its first years of operation. For future implementation of HVDC connected offshore WPP the problem is currently investigated.

II.1.1 Converter topology in WPP

Topology of WT-converters in WPP's is partially determined by the electrical machine that is used in wind turbine to generate electricity. According to the level of power that flows through a converter, full scale converter can be distinguished. It provides control over total power produced

in generator. On the other hand, there are also Wind Turbine application where only part of the power produced can flows through converter. The ratings of the converter, so also its costs, are reduced, however control of the power produced in wind turbine is limited.

Within the full-scale converters, the most popular utilized in these days in wind turbines are: 2-level converters, 3-level NPC converters, multi-level converters, also matrix converters and tandem converters [17].

Regarding the harmonics propagation problem from each WT-converter, when it comes to the scale of the wind farm, as stated in [7], the greater the number of turbines the lower is the magnitude of the harmonics and subharmonics, especially of the lower order.

In this study, only models of full rate wind turbine converters are considered. On the other hand, HVDC link converter is modelled with respect to principles described in the Section III.4.

II.1.2 Mitigation of harmonics and harmonic resonance

The two main methods for controlling harmonics in WPP are avoiding producing of harmonics and implementing filters to mitigate them [10]. To avoid the production of harmonics, network of WPP has to be designed properly, however implementation of harmonic filters anyway can be necessary due to topology changes or even very insignificant modifications which change resonance levels. The designing of filters should be based on measurements and simulations in order to control resonance properly.

Second method - implementation of filters - is the most common approach to the harmonic resonance [10]. The design and implementation of filters is not considered in detail in this study, however the Section VI introduces basic methods to control and mitigate these phenomena.

II.1.3 Short circuit current at PCC

From the main grid side, the short circuit level at the point of application is also not fixed. It varies with operational condition in the grid. The weaker the external grid, the more it varies usually, therefore the resonant frequency can float around. These fluctuations are not considered in the thesis.

II.1.4 Internal WPP harmonic impedance resonance

The phenomenon of electrical resonance due to harmonic impedance is described in Section I.3.4. As mentioned, if the resonance is not properly controlled, it leads to failures, instabilities, shut-downs or even damage of components. If the internal grid of WPP is separated from external grid for example by HVDC connection, electrical behaviour of the WPP grid can be different from the main grid.

In such a WPP inner grid there is no rotating mass that establishes physical binding of power and frequency [6]. Thus, the frequency of internal WPP and the infeed from the WTs can and should be completely controlled by converters. Moreover, every converter has its own control schemes that can have a bandwidth of several hundred hertz. Thus, converters are able to amplify oscillations which are in the system [6].

The resonance in Wind Power Plant is the main reason of the instability in first HVDC connected offshore WPP, described in motivation part of the thesis (Section I.2).

II.2 Stability of WPP

In modern wind power plants the presence of power converters is inevitable due to the power control questions. We can distinguish two main types of power converters: Voltage Source Converters (VSC) and Current Source Converters (CSC). In VSC converters the bandwidth of control signals are several times of the fundamental frequency. Such high-frequency control introduces dynamics above fundamental frequency, creating potential for high frequency instabilities and resonances that are not present in CSC [18]. Since the VSC does not need reactive power support, has higher controllability and the ability of black start the system, this type of converter is getting more popular in new Wind Farms. In the offshore WPP Bard Offshore 1 introduced in Section I.2 VSC converters are utilized [6]. However the problem of grid resonances caused by these converters was not considered during planning phase of the WPP. Thus, also stability problems due to converters interactions were not considered.

As stated in [19] and [18] converters could go into resonance with the grid causing instabilities if the grid impedance exceed the input impedance of the converter. On the basis of this statement, the analysis of stability is performed. The essence of the method is presented in [20]. Stability problems happen due to more advanced nonlinear power electronic elements included in the converters. The problem of modelling converter impedance nonlinear behaviour is described in Section III.4.2. This sort of problems does not occur between, for example, synchronous generators since power electronic elements influence in these elements is limited.

II.2.1 Harmonic Stability

The stability criterion based on Nyquist stability criterion is described in [19] and is still under development [6]. The main advantage of this method is that it does not require all details about converter which are always considered as intellectual property of manufacturers. Due to this advantage it could be right choice at the planning phase of an investment. Only frequency dependent impedances of converter are needed [6]. The method also avoids the need to remodel each inverter and repeat its loop stability analysis when the grid impedance changes [19].

In contrast to EMT simulations and eigenvalue analysis only relatively simple stability criterion is developed. Thus, this method is very fast and can evaluate new topology if any switching action occurs [6]. The simplicity is achieved by aggregation of all wind farms with their controllers into one element. Then, the aggregated system is evaluated by Nyquist stability criterion interpreted in Bode diagram that provides information about frequency and phase margin. As mentioned, the manufacturers have to provide only frequency dependent impedance of their generation unit (converter), including passive elements impedance and impedance changes due to active controls. In other words, the main advantage of this approach is that the frequency dependent impedance can be calculated with analytic model (providing appropriate data from manufacturer) or calculated with an EMT-tool but also measured at a real generation unit [6].

II.2.2 Impedance-based stability evaluation model

With the proper data and assumptions described above, we use the simple model to evaluate the stability consisting of voltage source with internal impedance and the impedance of the grid (Figure II.1) [6, 19].

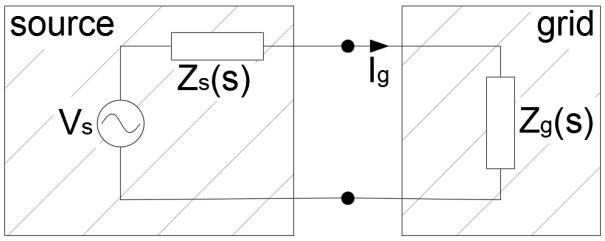

Figure II.1: Model for stability analysis consisting of voltage source with internal impedance (*source*) and grid impedance (*grid*).

In such a network the current I_g depends on both Z_s and Z_g impedances:

$$I_g = \frac{V_s(s)}{Z_s(s) + Z_g(s)} = \frac{V_s(s)}{Z_g(s)} \frac{1}{1 + \frac{Z_s(s)}{Z_g(s)}} \tag{II.1}$$

The equation of the network I_g current (Eq. II.1) can be expressed in as loop gain for the system in the Figure II.2.

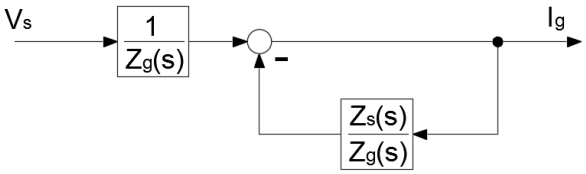

Figure II.2: Loop gain corresponding to the stability model in the Figure II.1.

On the basis on the Equation (II.1) we conclude that the system is stable if the source has a zero and the load an infinite output impedance. For stability, the value of ratio $|Z_s(s)/Z_g(s)|$ has to be at least below 1 to for all frequencies [19] in other words the system is stable if $Z_s(s)/Z_g(s)$ satisfies the Nyquist stability criterion [20].

The first problem with the model above is the division point between the *source* (Z_s) and the *grid* (Z_g). This point indicates what part an investigated network belongs to either the *source* or the *grid*. The best point of division is still under investigation [6]. A change of this division brings changes to both aggregate impedances, therefore could significantly influence the results. In this study the network is divided behind the HV transformer from the HVDC link point of view (Bus 2) (see Figure V.2).

There is also other conceptual problem with the presented approach. As either the inverter of WT of HVDC inverter could be treated as the *source*, the results about stability could be very different [19]. In this study we perform only one approach where the aggregated WT converter is treated as *source* and HVDC link converter as *grid* and the point of division is always as described above.

Finally, the stability criterion requires frequency impedances of converters which could be modelled as either voltage or current sources. The problems and details about these two models are explained in [19]. The *source* part and the *grid* part of the network can be modelled by its Thevenin equivalent circuit (voltage source) or Norton equivalent circuit (current source).

The Thevenin model for stability criterion was presented above. However, it is also possible to represent converters by current source [19] (Figure II.3).

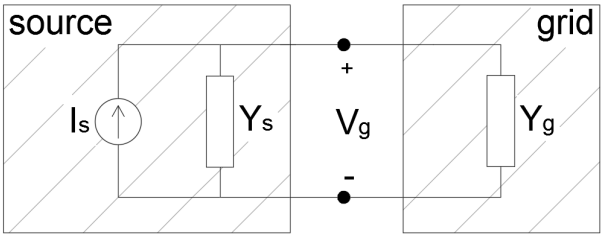

Figure II.3: Model for stability analysis consisting of current source with internal admittance (*source*) and grid admittance (*grid*).

The stability criterion is, analogously to Equation (II.1), based on the system equation:

$$V(s) = I_s(s)Z_g(s)\frac{1}{1 + Z_s(s)/Z_g(s)} \tag{II.2}$$

where, for stability, the ratio of the load input impedance to the source output impedance should meet the Nyquist stability criterion.

Comparing Equation (II.1) to Equation (II.2) one can see that stability requirement for CS system is opposite to that for VS system. The distinction between these models is described in [19] and it boils down to the comparison between the Norton and Thevenin equivalent circuits and in case of the impedance analysis of those converters the difference is beside the point. The author states also that the most common grid model is *hybrid* system combining current and voltage sources (Figure II.4). Applying the *hybrid* model to the case of this study, then the wind turbine inverter is modelled as a current source while and the HVDC rectifier is modelled as voltage source.

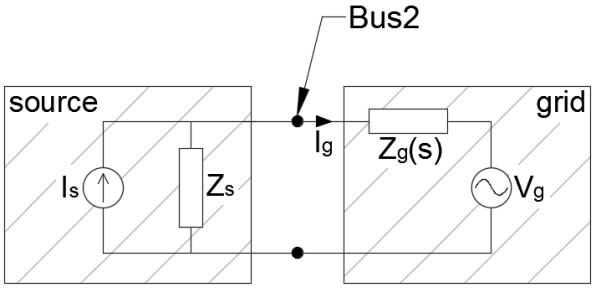

Figure II.4: Model for stability analysis consisting of current source with internal impedance (*source*) and voltage source with internal impedance (*grid*).

The assumptions of the stable system without the inverter and the stable inverter when grid impedance is zero are still applicable.

In this model, the current in the system is:

$$I_g(s) = \left[I_s(s) - \frac{V_g(s)}{Z_s(s)}\right] \cdot \frac{1}{1 + Z_g(s)/Z_s(s)} \tag{II.3}$$

and the Nyquist stability criterion of this system is analogous to the previous models i.e.: $Z_g(s)/Z_s(s)$.

II.2.3 Stability assessment

As stated in the previous sections the stability assessment comes down to the evaluation Nyquist stability criterion of the impedance ratio. In our study, the results of those impedances will be

analysed in the Bode diagrams due to the ease of resonance frequency identification. Bode diagrams combine all necessary data including information about frequency which is missing in the Nyquist plots.

The evaluation of the Nyquist stability criterion in the Bode diagram depends on two crucial points of the Bode curves: the zero-dB crossing point and -180°crossing point.

Zero-dB crossing point is the point when the Bode magnitude curve crosses the 0 dB value. In our case, we evaluate the ratio of grid and source impedances. Since the ratio of two values in logarithmic scale (dB) is subtraction in the linear scale, the zero-dB crossing occurs when the values are the same (subtraction of two equal numbers gives zero). Therefore, in our case, the zero-dB crossing points are when the impedances are the same i.e. at the intersection points of *source* impedance magnitude curve and *grid* impedance magnitude curve.

The second crucial point for stability evaluation is the -180°crossing point which is the point when the Bode angle curve crosses -180°. Once again, due to the same reason as for zero-dB crossing, the curve that crosses the level of -180°is the result of *grid* and *source* impedance angles subtraction. Since the real system model of the study case is based on linearisation and assumptions, the calculated angle do not reach the value of -180°, therefore for stability analysis the *safety margin* of 30° is introduced. To evaluate this condition, the concept of *phase margin* is introduced. It is well-known idea of the Nyquist stability criterion that offers the possibility of more practical assessment of the system quality of stability. From control theory: the larger the distance of the locus from the critical point, the farther is the closed loop system from the stability. As the measure of this distance the *phase margin* is evaluated. In our case, the phase margin will be calculated according to following equation [6]:

$$\phi_m = 180° - \Delta\phi \tag{II.4}$$

where $\Delta\phi$ is the phase difference between considered curves in degrees. If the phase margin calculated in such a way is below 30° the system is assumed to be possibly instable [6].

To sum up, as the result of stability assessment, we obtain, for each intersection, phase margin corresponding to the either stable or unstable operation. As aforementioned, the stability assessment is performed for specified point of division and specified *source* and *grid* sides.

Chapter III

Modelling of elements

III.1 Transformers

For harmonic modelling of transformers in electrical grid models for very high frequencies a generally not necessary. For higher frequencies resistance increases, while the leakage inductance reduces [7]. In this study, two- and three- winding transformers impedances will be represented simply by its resistance and inductance as follows:

$$Z_{tr}(j\omega_f) = R_{tr} + jX_{tr}(\omega_f/\omega_1) \tag{III.1}$$

where R_tr and X_tr correspond to fundamental frequency resistance and reactance. The skin effect and eddy currents effect the resistance at higher frequencies, therefore we do not consider these effects.

III.2 Cables

Modelling of cables is important in harmonic analysis since they are very significant source of capacitance in considered grids. For harmonic frequencies up to 3000Hz the resistance of cables will increase. The slight effect of decrease in inductance and shunt capacitance can be ignored [7]. PI models are considered as appropriate for frequency scan analysis, but not for transient analysis. Usually, exact frequency-dependent model is obtained by Finite Element analysis [7], however in this study exact methods of cable models are not considered. Elements of Pi model of the cables is described by:

$$\begin{aligned} Z_{cable}(j\omega_f) &= R_{cable} + j(\omega_f/\omega_1)L_{cable} \\ Y_{cable}(j\omega_f) &= j(\omega_f/\omega_1)C_{cable} \end{aligned} \tag{III.2}$$

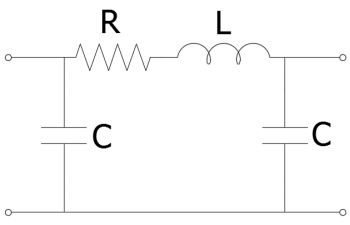

Figure III.1: PI circuit for modelling cables.

III.3 Filter reactors

Filter reactors modelling is important since it significantly affects the tuning of whole system. Resistance of the filters at high frequencies can be calculated as follows [8]:

- For aluminium reactors: $R_h = \left[\frac{0.115h^2+1}{1.15}\right] R_f$
- For copper reactors: $R_h = \left[\frac{0.015h^2+1}{1.055}\right] R_f$

In the models presented, series resistance of LCL filters and resistance of phase reactor is neglected (equals zero).

III.4 Power converters

Modelling of power converters is the most crucial and challenging within all elements. Power converters devices are very nonlinear and their impedance behaviour strongly depends on many factors. The exact model should be derived on the basis of control codes, ideally also on the basis of measurements on the real device.

Control codes are very unique and never published by the manufacturers. Control codes are considered their intellectual property and thus the determination of the exact frequency is very difficult [6]. There are also more simple approaches to face the problem of converter modelling. The principles presented below are considered for frequency domain analysis. EMT (electromechanical transient) analysis is not considered.

III.4.1 Voltage Source (VS) and Current Source (CS) models

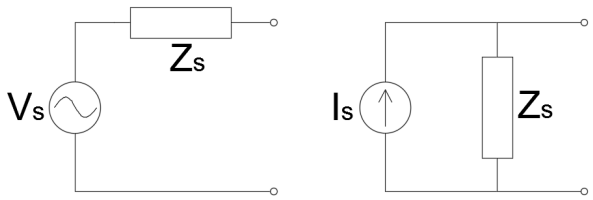

Figure III.2: Ideal voltage source and current source models.

It is common to approach modelling of converters as either current or voltage source. As stated in [6], current sources should be only used if the grid impedances are similar. Otherwise it leads to very inaccurate harmonic current values and wrong results. Therefore, voltage sources should be modelled instead and the input impedance should be considered.

There is very important fact to be considered for both approaches in frequency domain analysis. According to circuit theory, ideal voltage source internal resistance is zero (short-circuit). On the other hand, the ideal current source internal resistance is infinite (open-circuit).

In this study, models with either ideal current source or voltage sources are considered for comparison in FS method and HRMA method. For those models, internal impedance of source (VS or CS) Z_s is zero or infinite, respectively. The third model of converter is described in the following section and is based on either voltage or current source with nonzero, nonlinear internal impedance Z_s (nonideal VS or CS). For stability study the principles of converters modelling and stability assessment are described in Sections II.2.2-II.2.3.

III.4.2 Frequency dependent impedance model Z(s)

The models of either ideal voltage source or ideal current source described in the previous section are very important, however for the resonance analysis the value of series impedance (in case of voltage source) or parallel impedance (in case of current source) is crucial. The voltage and current sources themselves should be open-circuited or short-circuited, respectively. The approach developed in [18] and [21] of frequency dependent impedance of converters is introduced to this study and described below.

The authors, by applying appropriate modelling method, such as harmonic linearization presented in [22, 23], obtain impedance models valid below and above the fundamental frequency [18]. Each converter is described by positive- and negative-sequence impedances without cross coupling [24]. The Park's transformation, described in Section I.3.6 is also crucial to derive the converters impedances equations.

The assumed converters modelled are [18]: 2-level VSC Wind Turbine DC/AC inverter and the same type of HVDC AC/DC rectifier. Models of these converters are then used in the simulation.

III.4.2.1 Wind turbine converter (inverter)

For the control purposes, wind turbine converter is controlled as current source. Due to this fact, the device behaves more like current source and the control will be modelled in this way. Reactive power supply and voltage regulation of the model is not considered. A phase-locked loop (PLL) is included in the model for AC bus synchronisation [18].

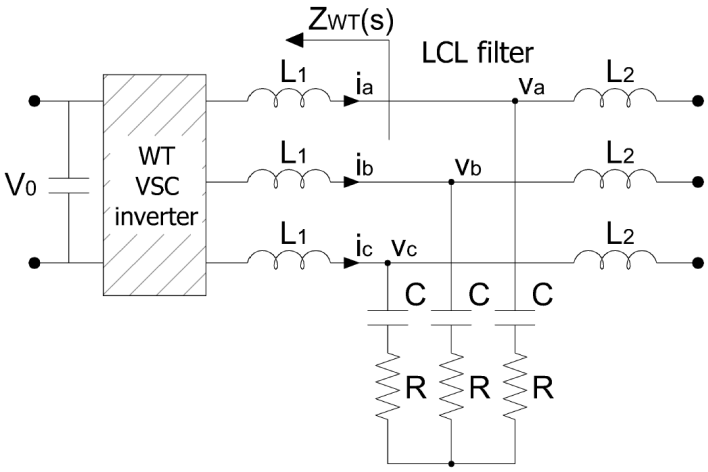

Figure III.3: Simplified diagram of aggregated wind turbine converter (inverter) with LCL filter.

The wind turbine model is described in *dq*-frame. As mentioned, the current control scheme is used. The reference value is the current provided be the DC link voltage regulator. The current compensator transfer function is given:

$$H_i(s) = K_p + \frac{K_i}{s} \tag{III.3}$$

The PLL is implemented using PI regulator. Including the integrator to convert frequency into angle, the PLL compensation transfer function becomes:

$$H_p(s) = \left(K_p + \frac{K_i}{s}\right)\frac{1}{s} \tag{III.4}$$

The values of parameters are specified in Chapter V.

For the stability study, the wind turbines are lumped into one device (one impedance). The output impedance of WT inverter is developed using the harmonic linearization method described in [23]. As the result, converters are represented by positive-sequence and negative-sequence impedances without cross coupling [24]. Providing constant DC bus voltage (as the reference) the impedances become:

$$\begin{aligned} Z_p(s) &= \frac{H_i(s-j\omega_1)V_0 + (s-j\omega_1)L_1}{1 - T_{pll}(s-j\omega_1)[1 + H_i(s-j\omega_1)I_1V_0/V_1]} \\ Z_n(s) &= \frac{H_i(s-j\omega_1)V_0 + (s-j\omega_1)L_1}{1 - T_{pll}(s-j\omega_1)[1 + H_i(s-j\omega_1)I_1V_0/V_1]} \end{aligned} \tag{III.5}$$

where ω_1 is fundamental angular frequency, $T_pll(s)$ is the loop gain of dq-frame PLL defined by:

$$T_{pll}(s) = \frac{V_1 H_p(s)}{2[1 + V_1 H_p(s)]} \tag{III.6}$$

and H_i and H_p are the current an PLL compensator transfer functions, as defined before.

III.4.2.2 HVDC link converter (rectifier)

In case of HVDC converter, the device is controlled to behave as a voltage source at the ac terminals [25]. Figure III.4 demonstrate the model for HVDC converter impedance calculation.

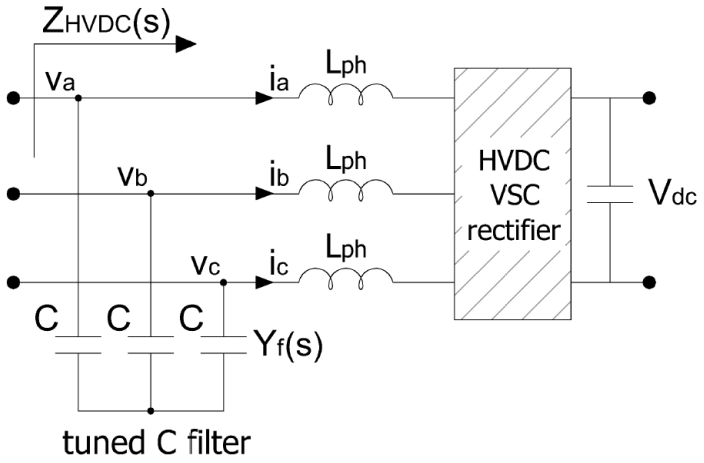

Figure III.4: Simplified diagram of HVDC-link VSC converter (rectifier) tuned C filter and phase reactor.

The HVDC rectifier voltage control is performed by a PI regulator in the dq-reference frame [18]:

$$H_v(s) = K_p + \frac{K_i}{s} \tag{III.7}$$

A current loop is embedded within the voltage loop and the current compensator transfer function is defined as:

$$H_i(s) = K_p + \frac{K_i}{s} \tag{III.8}$$

Other control approaches could be incorporated but are not considered. The values of parameters are included in Chapter V.

Again, the assumption of constant DC-link voltage (V_dc) is made. The resulting positive- and negative-sequence input impedance are given by:

$$\begin{aligned} Z_p(s) &= \frac{H_i(s - j\omega_1)V_{dc} + sL_{ph}}{1 + Y(s)[H_i(s - j\omega_1)V_{dc} + sL_{ph}] + T_p(s)} \\ Z_n(s) &= \frac{H_i(s + j\omega_1)V_{dc} + sL_{ph}}{1 + Y(s)[H_i(s + j\omega_1)V_{dc} + sL_{ph}] + T_n(s)} \end{aligned} \tag{III.9}$$

where ω_1 is fundamental angular frequency, $Y(s)$ is admittance of the ac filter, in our case equals $Y(s) = sC$. $T_p(s)$ and $T_n(s)$ are defined as:

$$\begin{aligned} T_p(s) &= [H_i(s - j\omega_1) + jK_{id}]H_v(s - j\omega_1)V_{dc} \\ T_n(s) &= [H_i(s + j\omega_1) - jK_{id}]H_v(s + j\omega_1)V_{dc} \end{aligned} \tag{III.10}$$

and $H_i(s)$ and $H_v(s)$ are the current and voltage compensator transfer functions defined before.

Implementation of equations above is described in Section V.1.3, where we present necessary data and evaluate results.

Chapter IV

Harmonics and power quality regulations

In this chapter the harmonic distortion limitations according to some standards are described. It is worth of mentioning that harmonics are not the only problem of power quality in power system. Power quality includes more electromagnetic phenomena which are categorized on the basis of duration (from nanoseconds, like lightning strokes) to steady state disturbances (e.g. harmonics and interharmonics) [7].

One of the standard that provides information about harmonics and interharmonics and is internationally accepted is [26] IEC Standard Series 61000. Moreover, there are EN standards like [27] EN 50160 approved by European standardization body CENLEC. EN standards are official standards for European Union. In North America, the harmonic limits are described in [28] IEEE 519. All three mentioned standard are internationally accepted [7]. These standards establish emission requirements such as harmonics, voltage fluctuations, radio frequency disturbance, immunity requirements etc. For example, the standard IEEE 519 standard ([28]) provides the harmonic limits for current waveforms presented in the Table IV.1. The ratio I_{sc}/I_L is the ratio of short-circuit current available at the point of common coupling (PCC) to the maximum fundamental frequency load current at PCC. The ratio is calculated on the basis of the average maximum demand of previous 12 months. Moreover, [28] all power generation equipment is limited to these values of current distortion regardless that ratio and the even harmonics are limited to 25% of the odd harmonic limits presented in the table.

Table IV.1: Current distortion limits for general transmission system $U > 161$kV [28].

	Dispersed Generation and Cogeneration Maximum Harmonic Current Distortion in % of Fundamental Harmonic Order (Odd Harmonics)					
I_{sc}/I_L	<11	$11 \leq h < 17$	$17 \leq h < 23$	$23 \leq h < 35$	$35 \leq h$	TDD
<50	2.0	1.0	0.75	0.3	0.15	2.5
>50	3.0	1.5	1.15	0.45	0.22	3.75

Most of the information included in the mentioned standards would not be utilized in further analysis, even if applicable to the inner WPP networks, since the EMT simulations are not performed in this study. In other words the waveforms in the time domain, for which the harmonic content is assessed, do not appear in this study.

Chapter V

Simulations

V.1 System description

In most of the simulations for harmonic resonance study we consider offshore wind power plant with VSC-HVDC connection to the onshore grid. Total amount of installed wind turbines power is 400MW. The WPP considered has a radial topology consisting of four-branch network. It is assumed that each string (branch) of wind turbines has the same parameters. The layout of the 400MW WPP is presented in the Figure V.1.

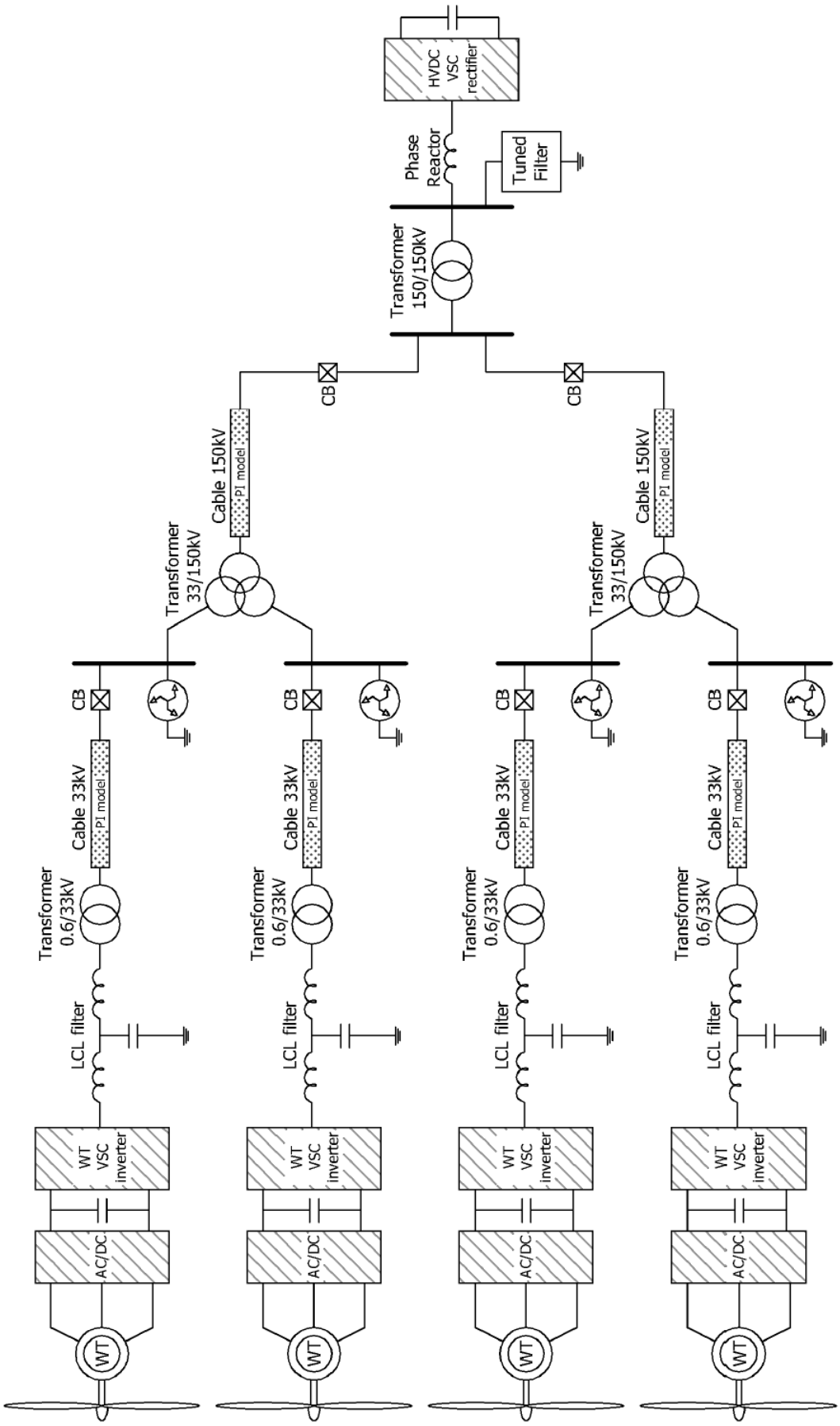

Figure V.1: Wind Power Plant of 400 MW considered in the study.

Each of four branch is formed by ten 10-MW wind turbines with a terminal voltage of 690V. The aggregated model of each branch is used where each set of ten turbines is lumped and modelled as a single aggregated turbine, represented by a 100 MW turbine. Each aggregated turbine is connected to the LCL filter. Behind the LCL filter there are elements of collection grid: 690V/33kV transformer and an 8km underground collector cable (33kV). 33kV cable is linked to the 150kV transmission cable with a length of 58km via a 150kV/33kV/33kV three winding transformer with YN-dd configuration. The 150kV transmission cable is tied to the VSC-HVDC rectifier through a 150kV/150kV transformer and a phase reactor with an tuned shunt capacitor filter.

V.1.1 Network impedance model

Equivalent impedance diagram of WPP AC system is shown in the Figure V.2. All of the parameters are converted to the 150kV equivalent voltage level. Table V.1 presents the values of parameters in the network. The impedances of VSC-WT inverters and VSC-HVDC rectifier are calculated on the basis of three different methods presented in Section III.4. The resulting impedances are presented in Section V.1.3.

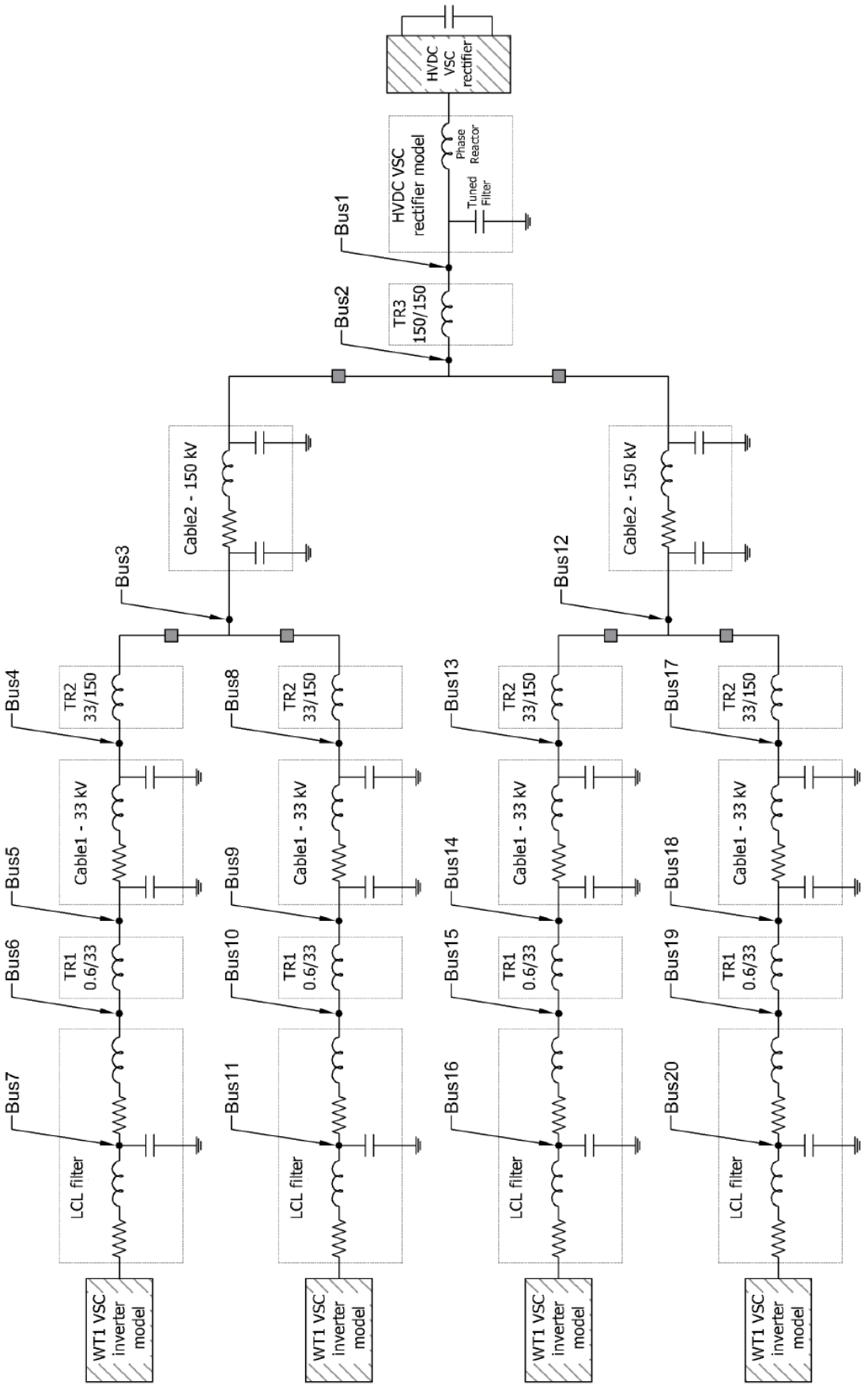

Figure V.2: Impedance diagram of the whole WPP network.

Table V.1: Data of the WPP network elements converted into the equivalent voltage level of 150 kV.

Component	Symbol	Value at 150 kV
Phase reactor	L_{ph}	19.3 mH
Tuned C filter	C_f	5.658 μF
Converter transformer	L_{tr3}	19.338 mH
Cable 150 kV	R_{cab2}	0.056 Ω
	L_{cab2}	1 mH
	C_{cab2}	0.52 μF
MV/HC three-winding transformer	L_{tr2}	38.676 mH
Cable 33 kV	R_{cab1}	0.372 Ω
	L_{cab1}	18.181 mH
	C_{cab1}	57.09 nF
LV/MV wind turbine transformer	L_{tr1}	51.568 mH
LCL filter	L_{LCL1}	1.2 H
	L_{LCL2}	149.1 nF
	C_{LCL}	0.641 H

V.1.2 Topology cases

In the study, we approach comparison between different topologies. There are three topology cases examined. In principle, the difference between three topology depends on the number of included branches with aggregated wind turbines (1, 2 or 4 branches). The buses in the figures have assigned numbers which we employ in further analysis.

- Case 1 model consist of one aggregated WT. In this case only one out of four branches is connected. The other three branches are disconnected by circuit breakers at the lower side of the three-winding transformers. Both branches connected to the lower other 150kV cable are disconnected, therefore this line is also disconnected. The topology of this system is presented in the Figure V.3.

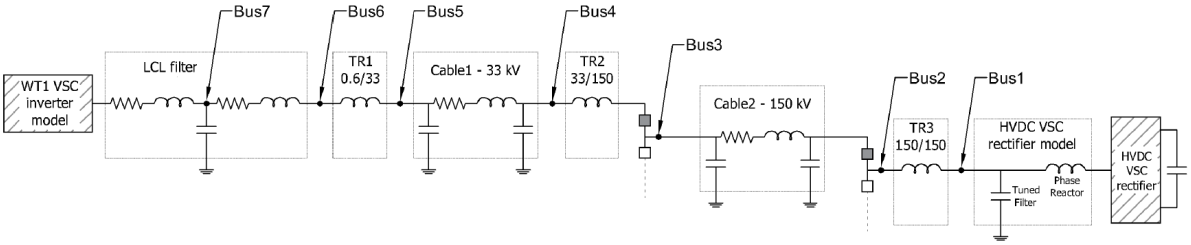

Figure V.3: Impedance diagram for Case 1 (only one aggregated wind turbine branch connected).

- Case 2 includes one more aggregated turbine branch than Case 1. The second WT branch is connected to the first three-winding transformer. The second 150kV line is still disconnected. The topology of this system is presented in the Figure V.4.

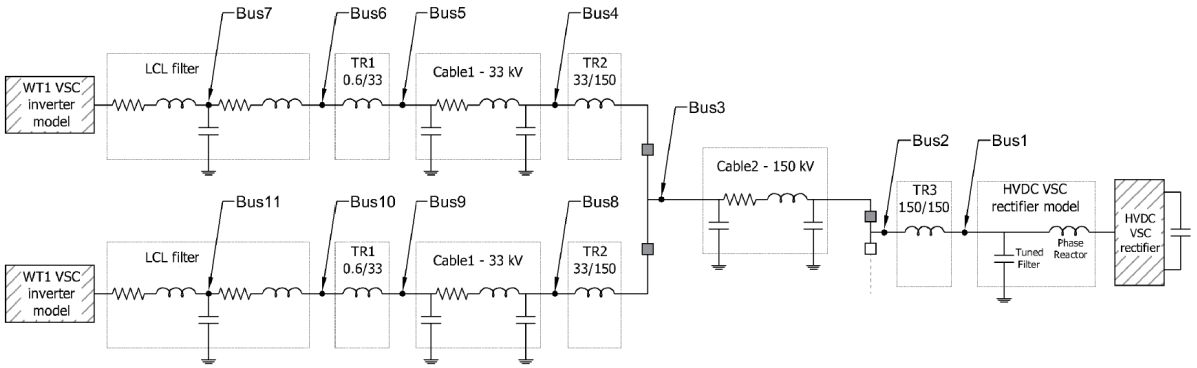

Figure V.4: Impedance diagram for Case 2 (two aggregated wind turbine branches connected).

- Case 3 consists of all elements in the networks. All branches are activated, therefore all elements are included in analysis. This topology is presented in the previous section, in the Figure V.2.

V.1.3 Power converters models

All of the elements excluding converters are modelled as the RLC elements. The principles of modelling of the elements are described in Section III. This section explains also the three different approaches to model converters (Section III.4). In whole Chapter V of the thesis containing results of simulation, for simplicity, we refer to the different models of converters as follows: VS the model where both WT and HVDC converters are modelled as voltage sources (Section III.4.1), $CS-WT$ or CS where WT converter is modelled as a current source and HVDC converter is still represented by voltage source (Section III.4.1), $Z(s)$ where both converters are represented by non-linear impedance models (Section III.4.2).

Following tables (Table V.2 and Table V.3) present the values of parameters which are implemented to the models described by Equations (III.5) and (III.9). The values of these parameters are obtained from [18], however we rescale the resulting impedance into the 150kV equivalent circuit level. These changes are vital in order to align the impedance to further analysis where we combine the converter models with the other elements of the network. The values of other network elements are also at the equivalent 150kV voltage level (Table V.1).

Table V.2: Numerical data necessary for calculation of aggregated WT converter model (inverter).

Parameter	Symbol	Value
DC Bus Voltage	V_0	$1500\,V$
Phase Voltage Amplitude	V_1	$563\,V$
Phase Current Amplitude	I_1	$236\,kA$
Phase LCL Inductance	L_1	$25.3\,\mu H$
Current Control Compensator $H_i(s)$	K_p	$0.44 \cdot 10^{-6}$
	K_i	$0.55 \cdot 10^{-3}$
PLL Compensator $H_p(s)$	K_p	0.239
	K_i	45

Table V.3: Numerical data necessary for calculation of HVDC-link converter model (rectifier).

Parameter	Symbol	Value
HVDC Link DC Voltage	V_{dc}	300 kV
Phase Inductance	L_{ph}	19.3 mH
AC Tuned Filter Capacitance	C	5.658 μF
Current Control Compensator $H_i(s)$	K_p	$0.075 \cdot 10^{-3}$
	K_i	0.094
Voltage Control Compensator $H_v(s)$	K_p	$11.1 \cdot 10^{-3}$
	K_i	8.388

The results of impedance for both Z(s) modek converters are demonstrated in the Figure V.5 for WT-converter and in the Figure V.6 for HVDC converter. Both plots include curves of impedance magnitude and impedance angle for positive-sequence and negative-sequence in the domain of frequency.

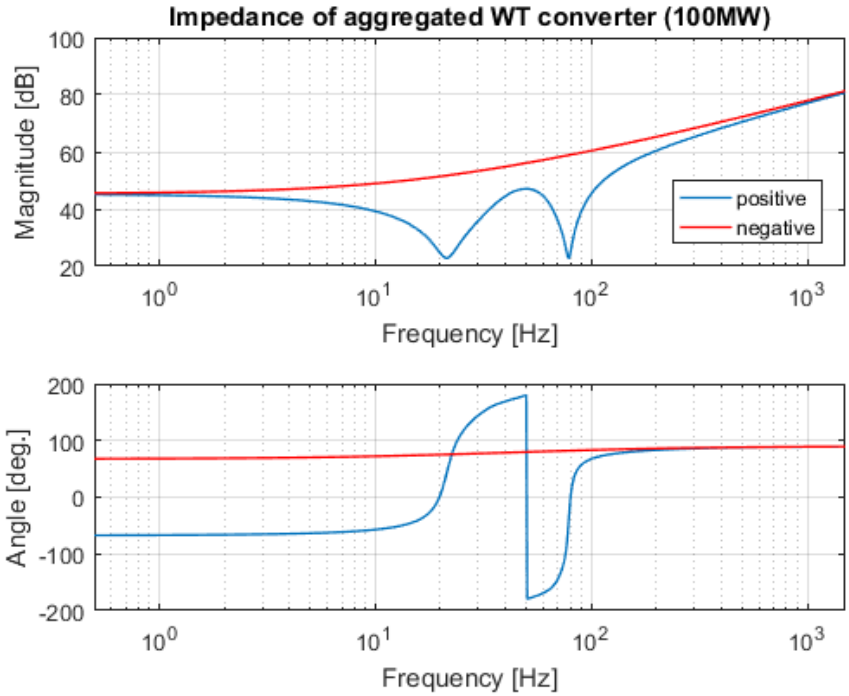

Figure V.5: Results of the WT converter nonlinear impedances in frequency domain (positive- and negative-sequences of impedance).

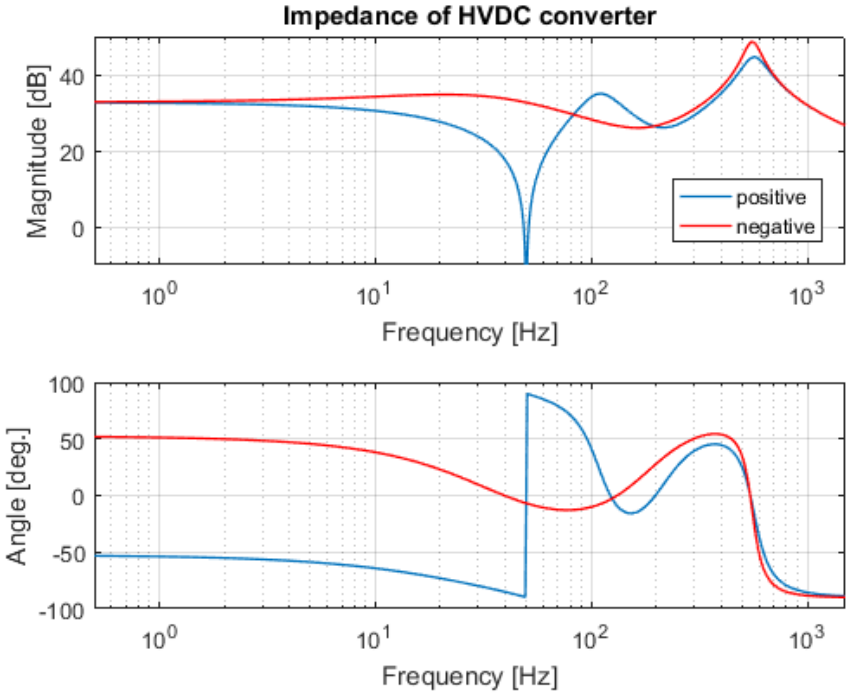

Figure V.6: Results of the HVDC-link converter nonlinear impedances in frequency domain (positive- and negative-sequences of impedance).

For both converters, we note sharp changes in the values of positive-sequence impedance angle at the fundamental frequency. On the other hand, the values of magnitudes and angles of negative-sequence are quite smooth for both converters. Moreover, we observe that above approximately second frequency order the curves of positive- and negative-sequences are very close to each other for all four plots.

Having in mind the different voltage level, thus different values of impedance, the outcome obtained correspond to the results from [18].

V.2 Comparison of resonance frequencies between different topology cases and converter models

The first objective of this section is to compare results of resonance frequencies for three topology cases (Section V.1.2) in utilizing different converter models: VS, CS and Z(s). The description of modelling converter as VS, CS and Z(s) can be found in Section III.4. The comparison is performed based on two methods: Frequency Sweep (Section I.4.1) and Harmonic Resonance Modal Analysis (Section I.4.2). Secondly, on the basis of HRMA we spot the buses that have the most significant influence on the particular resonance frequencies. This identification is very useful for further study of implementation of filters, however filters are not investigated deeply in this study.

V.2.1 Case 1

Frequency Sweep

Figure V.7 presents implementation of the frequency sweep method. All three converter models are included. The frequency sweep always refers to the particular node in the network. For this study, the bus number 7 (see Figure V.3) is the bus of observation. In other words, the impedance is seen from that point of the network.

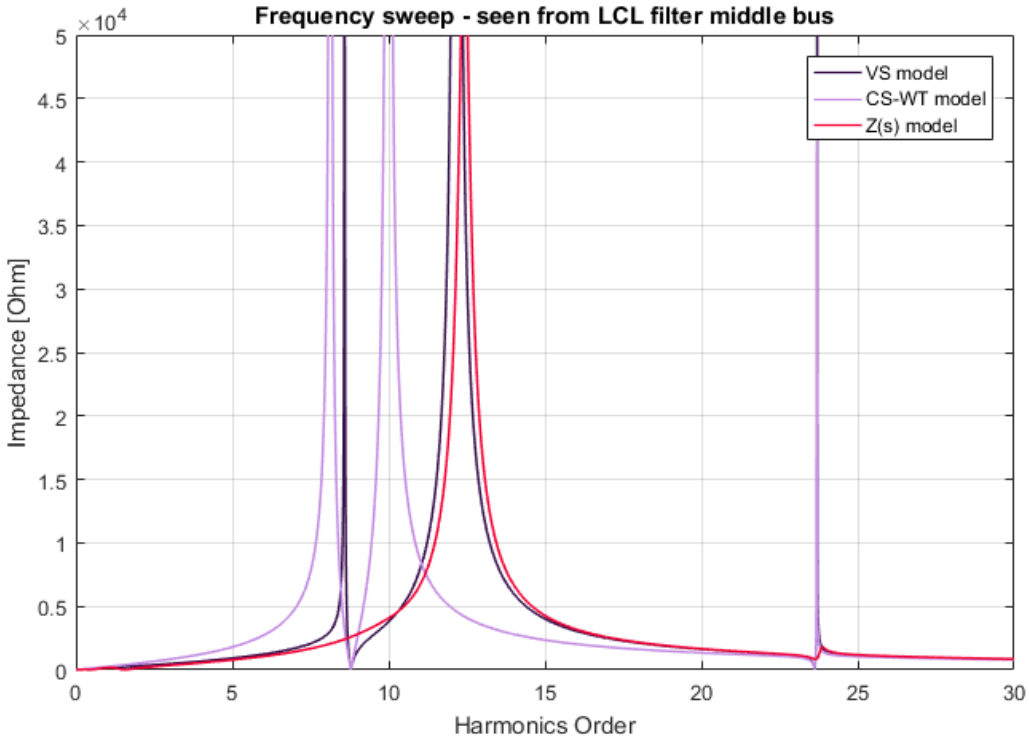

Figure V.7: Case 1: Frequency sweep curves (1) for three models (seen from bus 7).

For easier analysis, the Figure V.8 presents the same data but with logarithmic vertical axis.

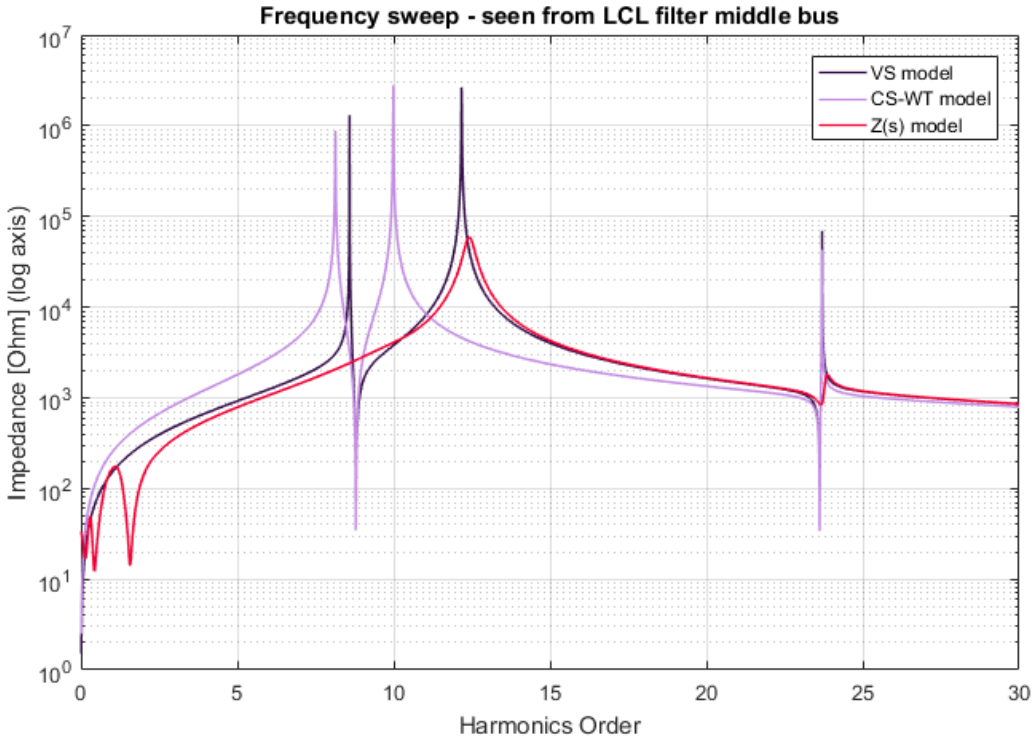

Figure V.8: Case 1: Frequency sweep curves (2) for three models (seen from bus 7).

We can clearly see that the resonance frequencies alter for different models of converters. Table V.4 presents resonance frequencies values obtained from this analysis. The values of frequencies are identified in the points where the impedance curves reach local extreme values.

Table V.4: Case 1: Frequency sweep numerical results of resonant frequencies and corresponding peak impedance values for three models.

Converter model	Frequency order [-]	Peak impedance [Ω]
VS	8.59	1304 k
	12.17	2655 k
	23.7	69 k
CS-WT	8.14	880 k
	9.99	2787 k
	23.69	43 k
Z(s)	12.42	59 k
	23.87	2 k

First of all, discover some peaking values of impedance for very low frequency orders (around fundamental frequency) in Z(s) model. These peaks are at much lower impedance level than the other values for higher orders. We exclude these peaks from our further analysis, reasoning that such a phenomenon needs more detailed research focused mainly on that problem and it won't be an issue in this study.

For VS model (within the examined frequency range) we observe three resonance frequencies. Similarly, in case of CS model there are three resonance frequencies. For the Z(s) model of converters only two resonance frequencies are noted (as aforementioned, the low peaks around fundamental frequency are ignored).

Moreover, the values of impedance for Z(s) model are significantly reduced comparing to the

VS and CS models. We can mark that the principles of modelling converters by this method leads to higher values of damping than by modelling as voltage or current source. The detailed description is provided in Section III.4.2 and in [18, 21].

Harmonic Resonance Modal Analysis

In this section we compare the results of frequency sweep to the results of Harmonic Resonance Modal Analysis. As mentioned in Section I.4.2, with HRMA method we also gain values of participation factors which suggest buses and elements which influence resonance more than others buses/elements. The Figures V.9, V.10 and V.11 present the curves of modal impedance in domain of harmonic order.

The Figure V.9 illustrates the modal impedance for three models. Only maximum modal impedance for each frequency order is selected and plotted.

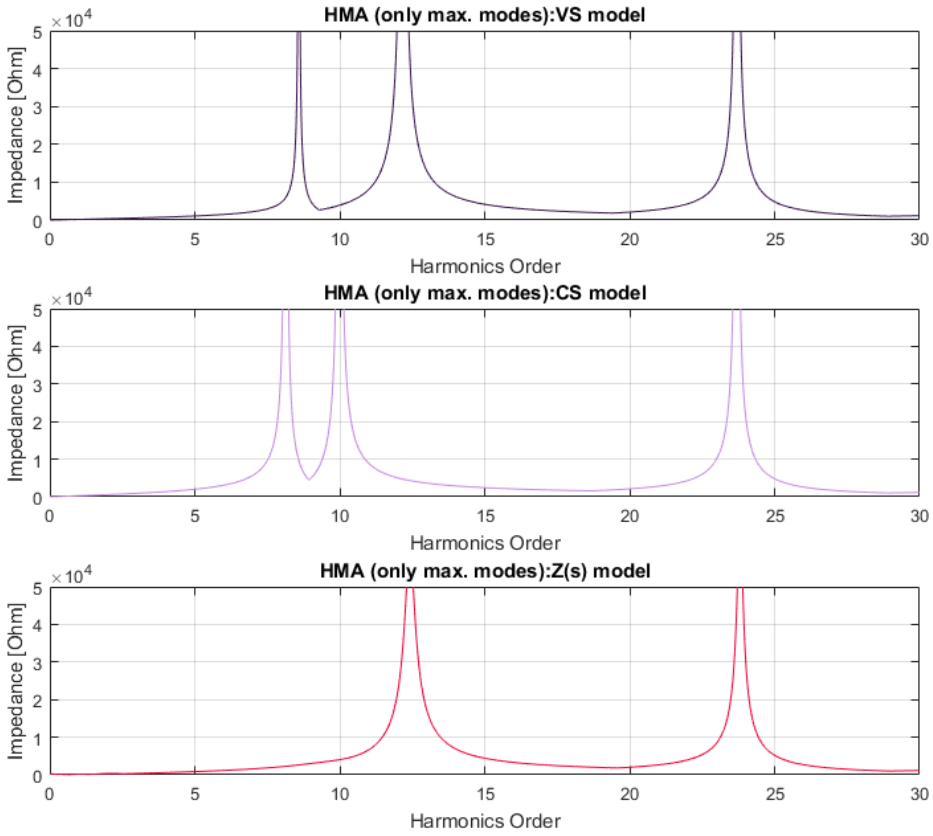

Figure V.9: Case 1: HRMA method *maximum modes only* impedance curves for three models.

In the Figure V.10, we observe the very similar shapes of curves, however, this time all the modes are drawn. Most of the modes are barely visible since they equals zero or very small values for whole range of frequencies.

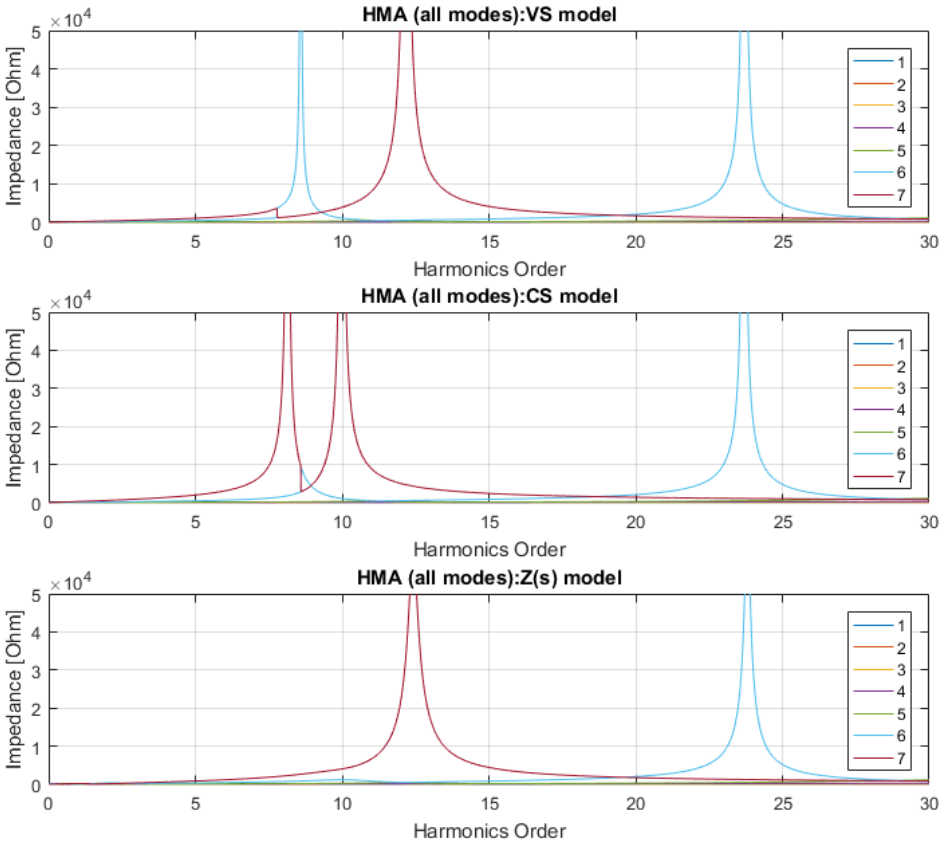

Figure V.10: Case 1: HRMA method *all modes* impedance curves for three models.

The graphs above distinguish two modes which are peaking for all thre models - mode 6. and 7. Modal impedance for these modes reaches much higher value at the frequencies of resonance. The modes that determine the resonances are called critical modes. The critical modes impedances only, with full range of impedance, are plotted in the Figure V.11.

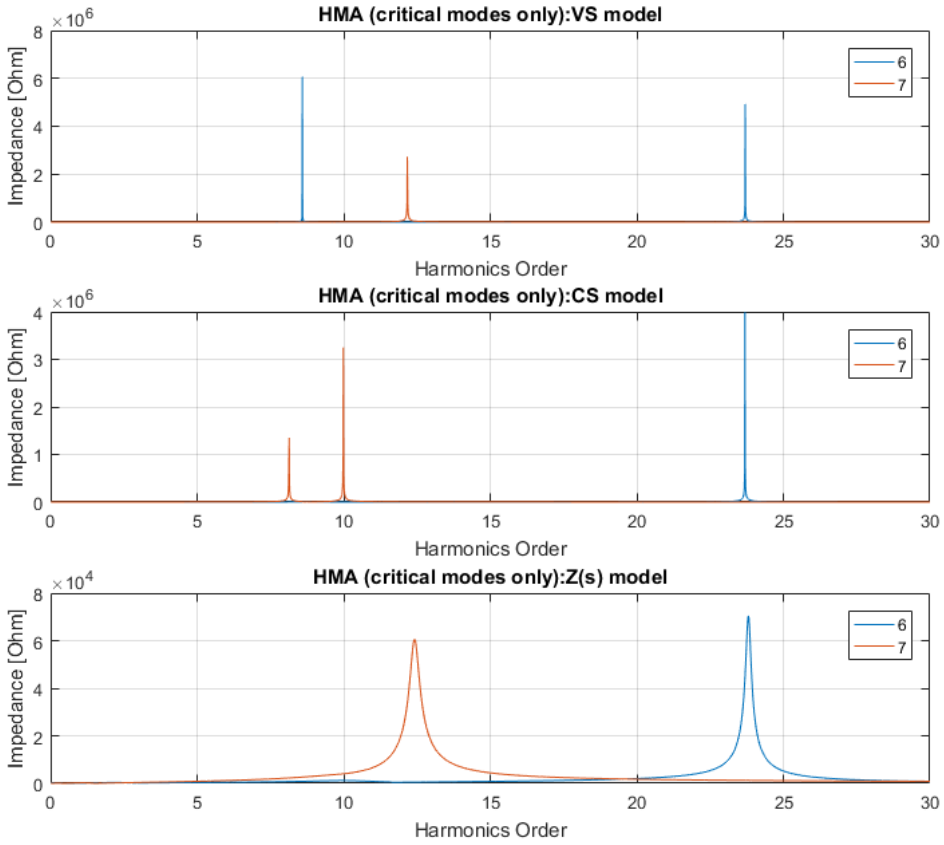

Figure V.11: Case 1: HRMA method *critical modes* impedance curves for three models.

As explained in Section I.4.2, even though the total number of modes equals the number of buses in the network, these modes do not correspond to the network buses exactly. Their correlation is reported by the participation factors presented in Table V.6. Before, Table V.5 presents the critical modal impedance values and the harmonic orders for frequencies when the critical modal impedances occur.

Table V.5: Case 1: HRMA numerical results of resonant frequencies and corresponding peak impedances for three models.

Order	Critical mode	Critical impedance magnitude [Ω]	Angle [°]
VS model			
8.59	6	6072 k	-79.9
12.17	7	2727 k	-81.3
23.7	6	4928 k	-20.5
CS-WT model			
8.14	7	1351 k	84.6
9.99	7	3252 k	74.5
23.69	6	3992 k	-40.5
Z(s) model			
12.42	7	61 k	5.5
23.81	6	70 k	2.0

Table V.6: Case 1: HRMA numerical results of resonant frequencies and participation factors for three models.

Frequency order [-]	Participation factors [%] for the buses						
	1	2	3	4	5	6	7
VS-model							
8.59	8.8	12.8	13.0	14.2	14.6	15.1	**21.5**
12.17	0.1	0.0	0.0	0.2	0.4	1.8	**97.4**
23.7	0.9	14.6	15.7	**23.1**	**24.3**	20.0	1.4
CS-WT model							
8.14	2.6	4.4	4.4	6.2	7.0	9.3	**66.0**
9.99	1.1	1.0	0.9	0.2	0.0	0.3	**96.5**
23.69	0.9	14.6	15.6	**23.2**	**24.4**	20.2	1.1
Z(s) model							
12.42	0.2	0.1	0.1	0.2	0.5	1.8	**97.1**
23.81	1.0	14.5	15.6	**23.1**	**24.3**	20.1	1.4

The study of participation factors is very relevant for localization of the best nodes in a network for filter implementation. The participation factors express the significance of a bus in resonance emission. Therefore, the modification of capacitance/inductance at the point of the network with the highest participation factor should trigger to the most powerful change of the resonance frequency. The details about participation factors in Section I.4.2 and [13].

In the study of Case 1, from the values of participation factors, one can easily recognize that the buses number 5 and 7 are the two buses which contribute to the resonance frequencies more than the others. As we can see, these two buses play the lead role in all three different models what indirectly confirms the consistency of three approaches. We also observe only two resonant frequencies for Z(s) model. From the values of the participation factors, we also derive some conclusions. Since the two resonance frequencies from the first two models are mostly correlated to the bus 7 and similarly for the one of the resonance frequencies from the Z(s) model, the two resonance frequencies from VS and CS models could have been merged into one resonance frequency from Z(s) model. Otherwise, due to the higher resistance of the Z(s) model, one of the resonance frequency could have been smoothed down to the insignificant value.

DIgSILENT Power Factory model

In this simulation, we use the Power Factory model presented in the Figure V.12. The model is combined of basic RLC elements.

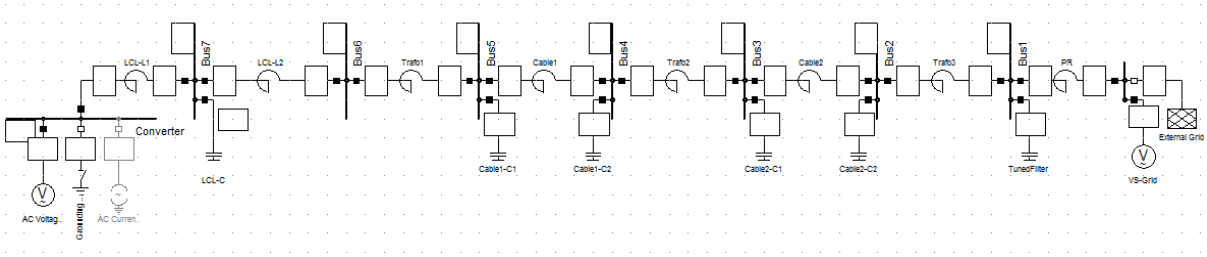

Figure V.12: Case 1: DIgSILENT Power Factory model.

Only two models: VS and CS-WT are simulated. We perform so-called *Impedance Frequency Characteristic* calculation in the software. Figures V.13 and V.14 show the results of frequency sweep for VS and CS-WT model, respectively.

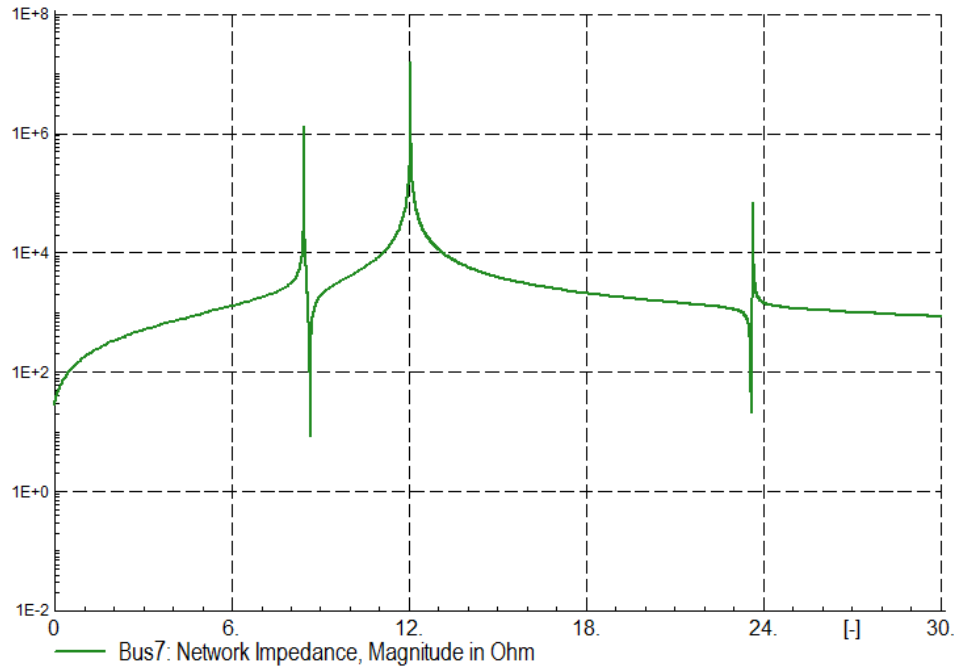

Figure V.13: Case 1: Power Factory impedance curves for VS model (seen from bus 7).

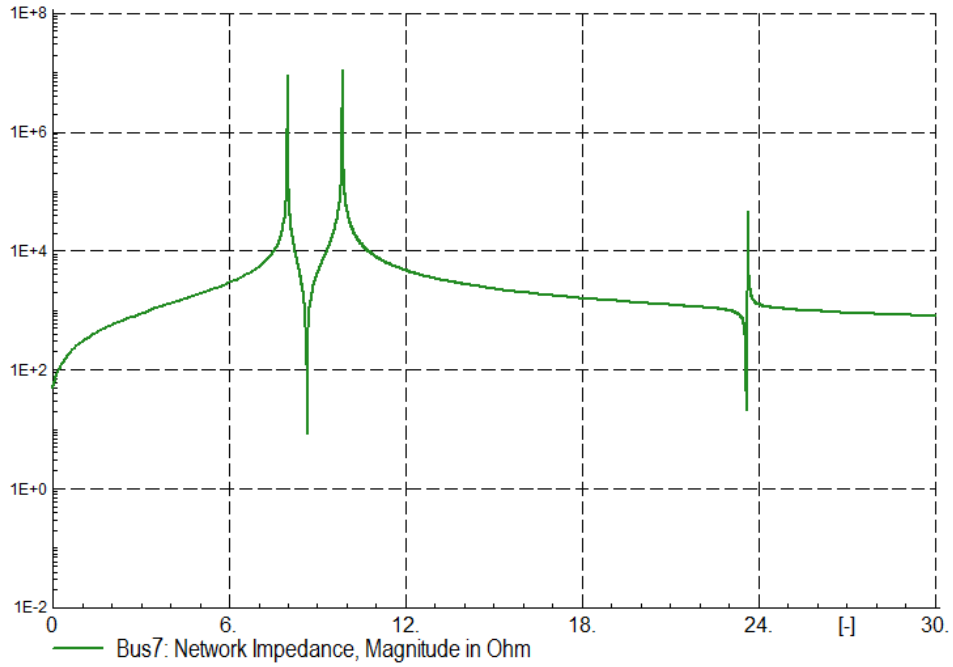

Figure V.14: Case 1: Power Factory impedance curves for CS-WT model (seen from bus 7).

We can examine the figures obtained from the Power Factory software and conclude that, regarding resonant frequency values, they are definitely coincident with the ones received from detail analysis in MATLAB. However, the peak values of impedances are different. The differences probably source in the settings of *Impedance Calculation* for frequency sweep analysis. The step size of the simulation was set to the value of 0.1 Hz; furthermore the *Automatic Step Size Adaptation* was selected. Hence, difference in the values of impedance occurs. The dependence of the peak values from the value of step size was checked through similar simulation with different step sizes. The observation confirms that the step size influences peak impedance values.

What is more important in this study are the values of the resonance frequencies. The values obtained by Power Factory confirms the values gained from MATLAB analysis of both frequency sweep and modal analysis.

Table V.7: Case 1: Power Factory resonant frequencies values for two models.

	Order [-]		
VS model	8.59	12.17	23.7
CS-WT model	8.14	9.99	23.69

As aforementioned, the observation of network impedance (frequency sweep) is performed from the specified bus in the network (bus 7). Due to the Power Factory software, we can performed the observation of impedance from each of the bus in the considered case. The results of frequency sweep seen from all 7 buses is presented in the Figure V.15 and V.16, for VS model and CS model, respectively.

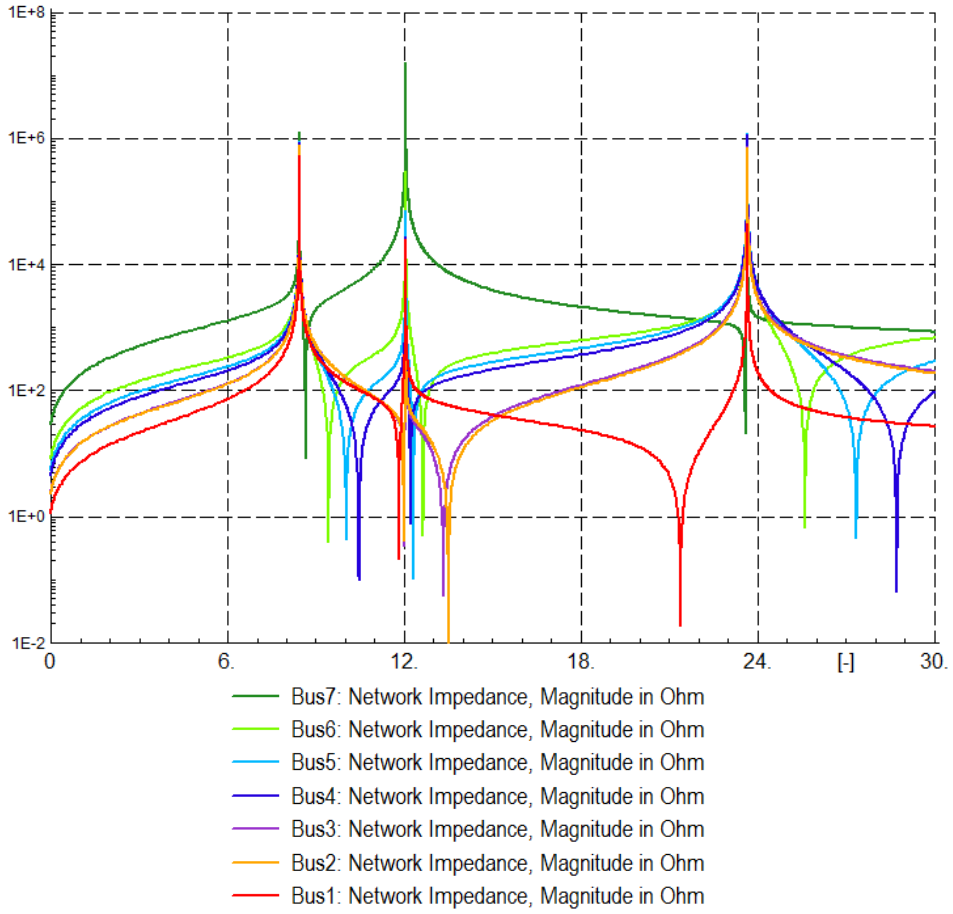

Figure V.15: Case 1: Power Factory impedance curves for VS model (seen from buses 1-7).

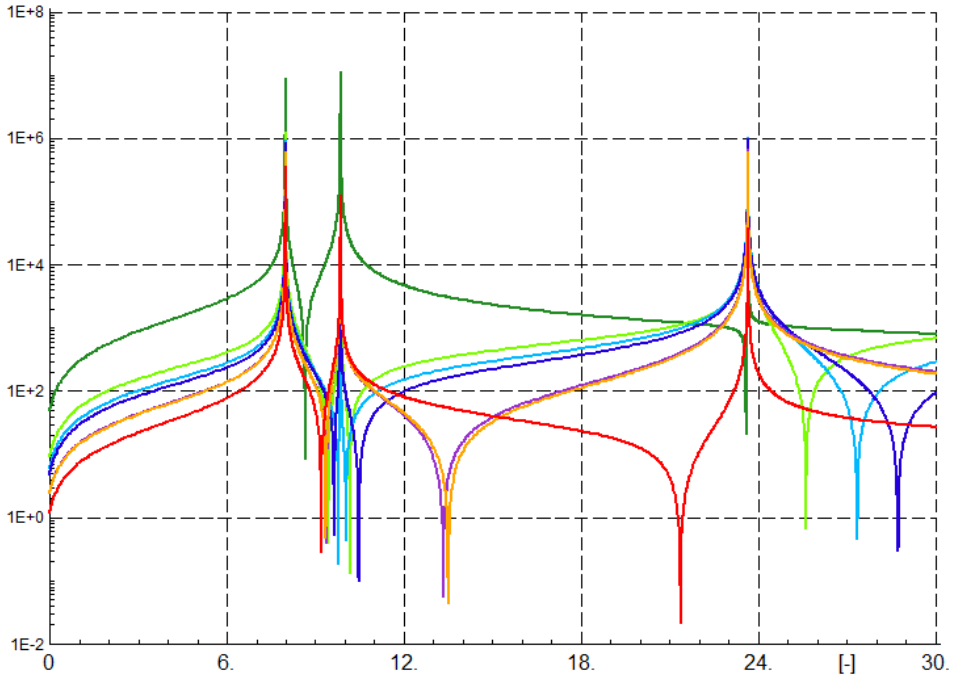

Figure V.16: Case 1: Power Factory impedance curves for CS-WT model (seen from buses 1-7).

The examination of the curves above demonstrates that the peaking impedances for both models occur at the same frequencies, regardless the bus of observation. On the other hand, the dips of impedance undoubtedly depend on the bus where the observation is performed from. Coupling with the principles of parallel and series resonance, we can draw the two conclusions. Firstly, the series resonance frequency depends on the bus in the network i.e. series resonance frequency is different at the different points in the network. Secondly, since the peaks of the impedance, so the parallel resonance frequencies, are the same regardless the bus of observation, we conclude that the parallel resonance frequencies do not depend on the point of observation. The confirmation of the latter statement we recognize in the HRMA method. As described in Section I.4.2, the method is utilized in order to investigate the parallel resonance and is not performed for particular bus, but for entire network. The frequencies collected from that method are exactly the frequencies obtained for every different case of observation bus in the frequency sweep method.

Results comparison

In the three previous paragraphs the results of frequency sweep analysis, harmonic resonance modal analysis, both performed in MATLAB were presented. Moreover, these results we couple with frequency sweep tool in Power Factory software. The values of resonance frequencies obtained ambiguously confirms the correspondence of these three approaches to each other. The values of parallel resonant frequencies are the same for the considered accuracy.

The difference of the impedance peak values are not considered very deeply in this study. However, as aforementioned, these values very often depends on the step size of the calculation. Moreover, the threshold impedance values above which the impedance level is defined as dangerous should be assigned individually for each particular case of a network. Furthermore, the values of modal impedance from HRMA method does not exactly correspond to the real impedance value and should not be compared directly to the values of impedances obtained from frequency sweep or Power Factory tool.

V.2.2 Case 2

The topology Case 2 was presented in Section V.1.2. In this case, the Wind Power Plant consists of two branches. There is one aggregated Wind Turbine in each branch. The total power of connected Wind Turbines is 200 MW.

Frequency Sweep

In the Figures V.17 and V.18 the results of frequency sweep method are presented with linear and logarithmic impedance scale, respectively. Again, all three models of converters are included. The impedance of the grid is seen again from the bus number 7 i.e. middle bus of LCL filter in the first branch. Since the branch 1 is the same the branch 2, we could collect the same curves for impedance observed from bus 11.

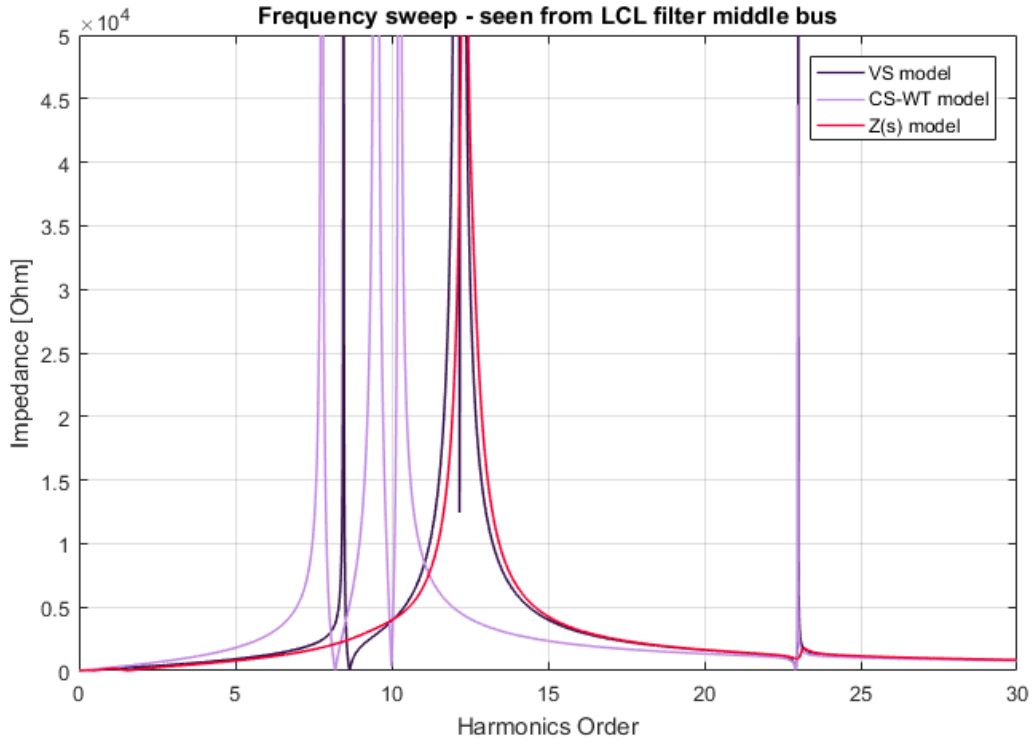

Figure V.17: Case 2: Frequency sweep curves (1) for three models (seen from bus 7).

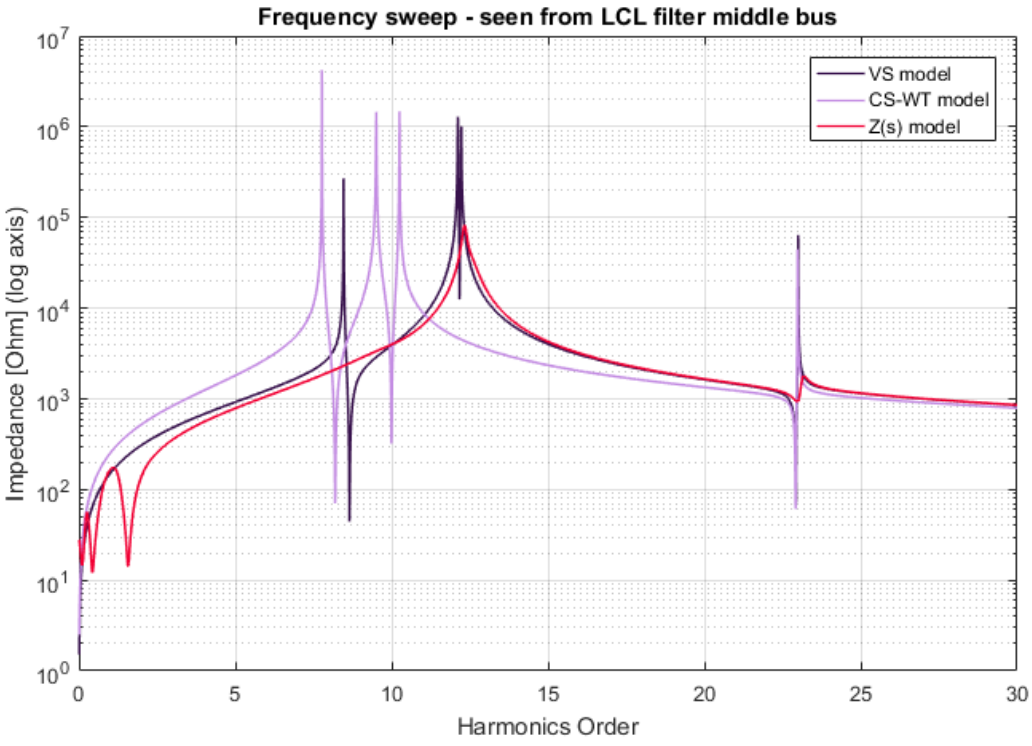

Figure V.18: Case 2: Frequency sweep curves (2) for three models (seen from bus 7).

Table V.8 presents resonance frequencies values from the graphs above. The values of frequencies are identified when impedance reaches local extreme values (parallel resonance). This time again, the results of resonance frequencies around fundamental value are ignored.

Table V.8: Case 2: Frequency sweep numerical results of resonant frequencies and corresponding peak impedance values for three models.

Converter model	Frequency order [-]	Peak impedance [Ω]
VS	8.46	269 k
	12.12	1289 k
	12.23	1007 k
	23.00	64 k
CS-WT	7.77	4217 k
	9.51	1455 k
	10.25	1475 k
	22.98	45 k
Z(s)	12.33	82 k
	23.18	2 k

We can note that undoubtedly this time there are four resonant frequencies for Current Source model. The curve of VS model consists surely of three peaks, however, looking at the values, the fourth one is very close to the other around 12^{th} order. Therefore, it is harder to notice it from the graph. The Z(s) model comprises two impedance rises, excluding ones around fundamental frequency. The value of impedance of Z(s) model is significantly lower than in other models, similarly to the Case 1. We carry on further conclusions and contemplations about the resonant frequencies after presenting HRMA results for this case.

Harmonic Resonance Modal Analysis

The Figures V.19-V.21 illustrate the HRMA result curves. Similarly to the previous topology case, the following graphs shows the curves of maximum modal impedances for each harmonic order, than modal impedances with respect to the each mode separately and finally, critical modes only i.e. the modes that are assigned to the modal impedance peaks.

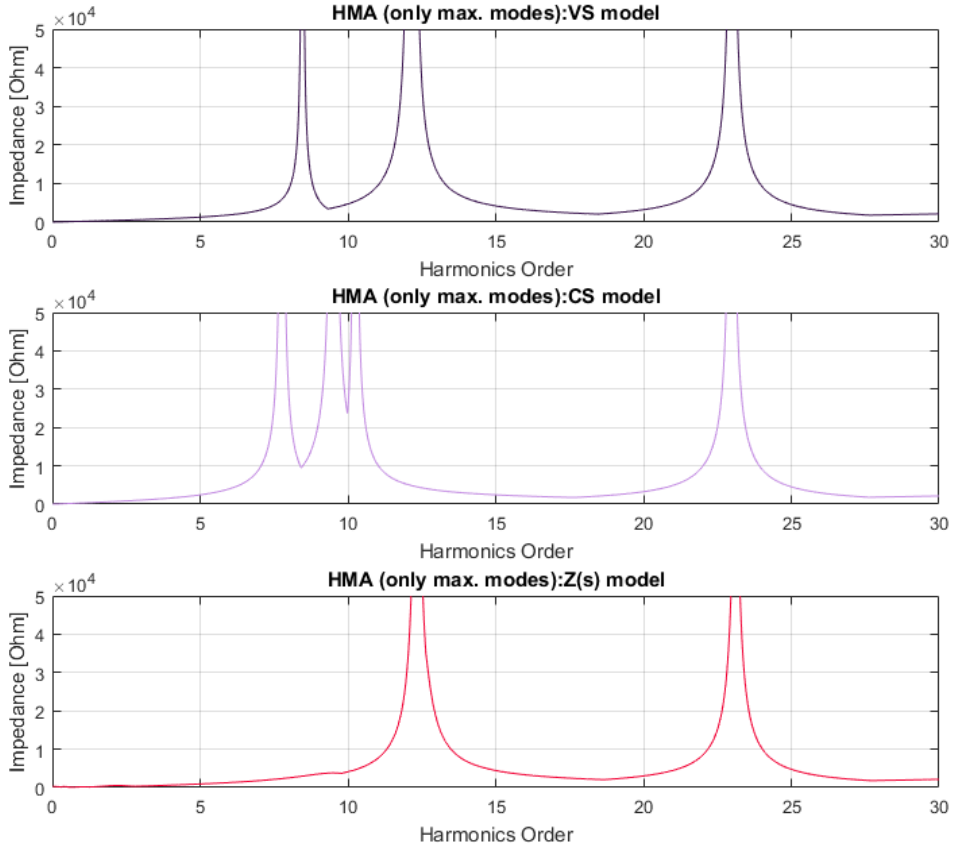

Figure V.19: Case 2: HRMA method *maximum modes only* impedance curves for three models.

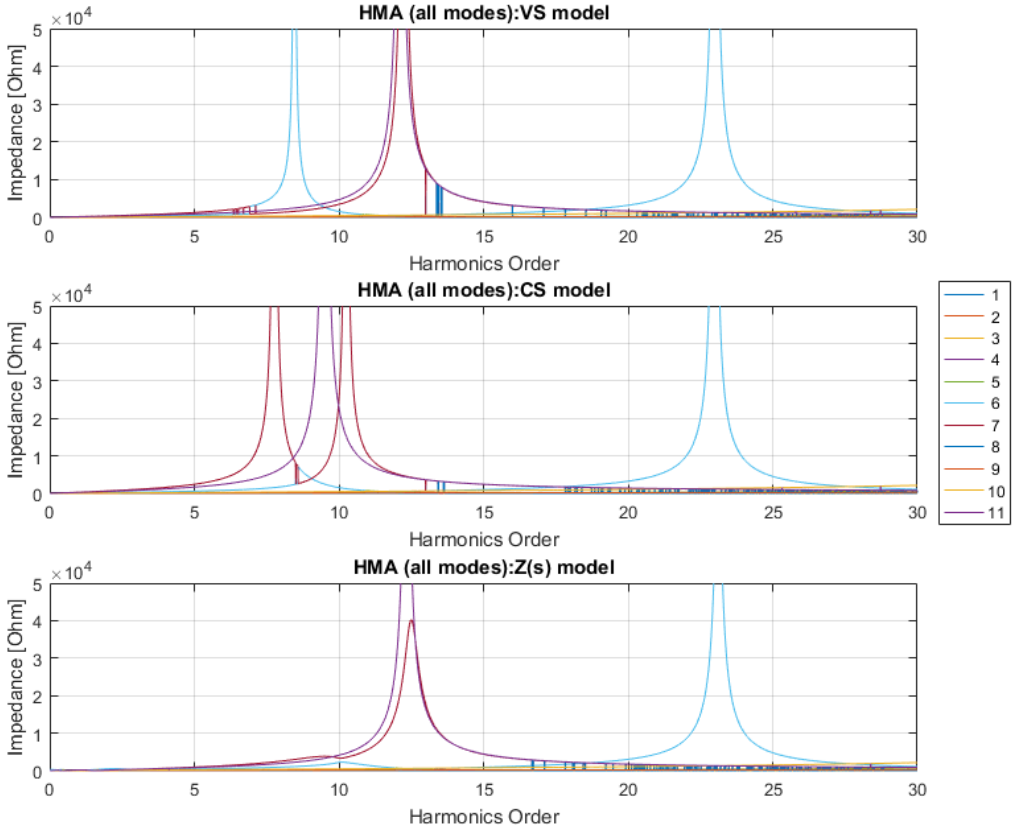

Figure V.20: Case 2: HRMA method *all modes* impedance curves for three models.

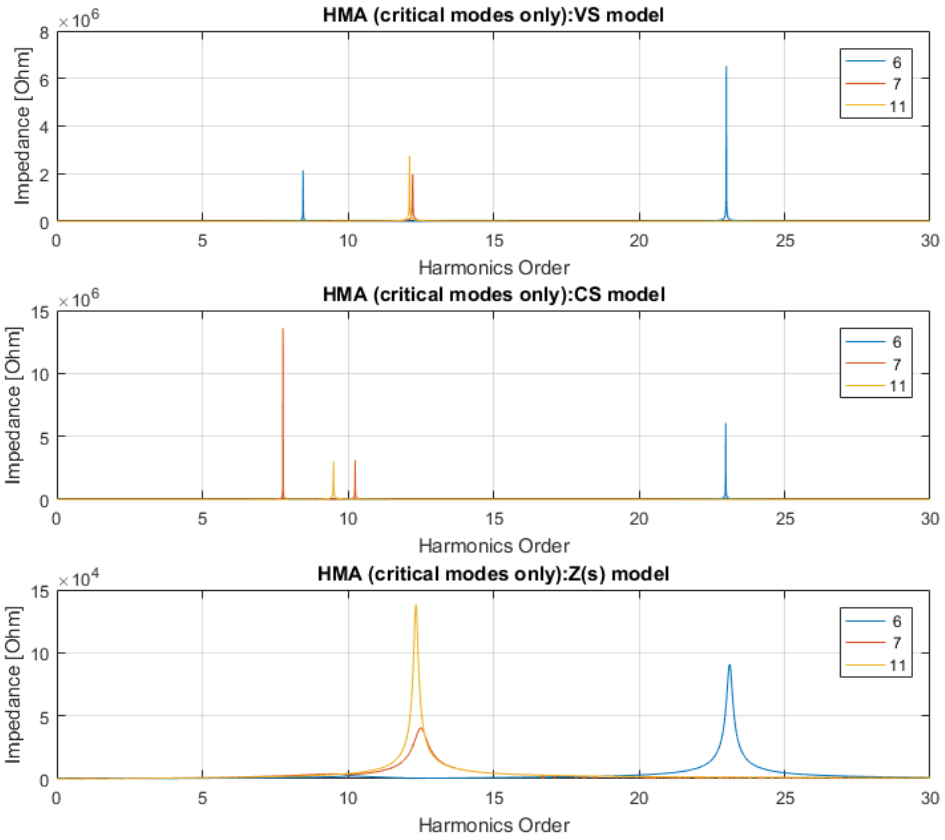

Figure V.21: Case 2: HRMA method *critical modes* impedance curves for three models.

Again, the participation factors point out the connotation of each mode to the real buses in the network. Table V.10 presents the participation factors for the detected resonant frequencies i.e. frequencies at which the modal impedance rises occur. The values of critical impedances and critical modes for each of them are gathered in Table V.9.

Table V.9: Case 2: HRMA numerical results of resonant frequencies and corresponding peak impedances for three models.

Order	Critical mode	Critical impedance magnitude [Ω]	Angle [°]
VS model			
8.46	6	2140 k	-86.7
12.12	11	2753 k	82.4
12.23	7	1965 k	83.0
23	6	6517 k	20.3
CS-WT model			
7.77	7	13.6 M	10.6
9.51	11	3008 k	76.8
10.25	7	3098 k	74.2
22.98	6	6062 k	-28.5
Z(s) model			
9.51	7	4 k	-52.3
12.34	11	138 k	3.3
23.11	6	91 k	-1.5

Table V.10: Case 2: HRMA numerical results of resonant frequencies and participation factors for three models.

Frequency order [-]	Participation factors [%] for the buses										
	1	2	3	4	5	6	7	8	9	10	11
VS-model											
8.46	5.3	7.9	8.0	8.7	9.0	9.2	**12.5**	8.7	9.0	9.2	**12.5**
12.12	0.0	0.0	0.0	0.2	0.3	1.1	**48.4**	0.2	0.3	1.1	**48.4**
12.23	0.3	0.0	0.0	0.0	0.1	0.8	**48.9**	0.0	0.1	0.8	**48.9**
23	0.6	8.9	9.6	**13.6**	**14.2**	11.7	1.0	**13.6**	**14.2**	11.7	1.0
CS-WT model											
7.77	1.7	3.2	3.2	4.2	4.6	5.8	**31.3**	4.2	4.6	5.8	**31.3**
9.51	0.0	0.0	0.0	0.1	0.3	1.1	**48.5**	0.1	0.3	1.1	**48.5**
10.25	1.5	1.1	1.1	0.4	0.2	0.0	**47.4**	0.4	0.2	0.0	**47.4**
22.98	0.6	8.9	9.6	**13.7**	**14.3**	11.8	0.7	**13.7**	**14.3**	11.8	0.7
Z(s) model											
9.51	1.8	3.5	3.6	4.6	5.1	6.1	**29.7**	4.6	5.1	6.1	**29.7**
12.34	0.0	0.0	0.0	0.2	0.3	1.1	**48.4**	0.2	0.3	1.1	**48.4**
23.11	0.7	8.8	9.5	**13.6**	**14.2**	11.7	1.0	**13.6**	**14.2**	11.7	1.0

This time we observe one significant difference between the frequency sweep curves and HRMA curves. For Z(s) model, one of the frequency that is missing in the frequency sweep method appears in the HRMA curves. To interpret this we look at the value of the modal impedance for this resonant frequency or at the figures. The value of critical impedance of critical module is much smaller than the other modal critical impedances (for other resonant frequencies). Since the resonant frequencies are recognized as the extreme points of impedance curves, peak value are identified in this way. However, in order to exclude this frequency from the results, further investigation of for example minimum dangerous impedance would be necessary.

Besides this difference, the results of frequencies converge completely.

From the values of participation factors we derive couple of conclusions. First of all, the values of participation factors for buses of branch 1 (4-7) correspond to the buses of branch 2 (8-11) with the same values. It shows that from the modal analysis point of view the wind turbine branches are the same and the participation factor is distributed symmetrically to the two analogous buses of both branches. Secondly, comparing the results of participation factors for Case 1 and Case 2 we can observe some similarities in apparition of the new resonant frequency. For both VS and CS-WT model, the lowest resonant frequency stays approximately at the same level, to be more precise is slightly shifted down to the lower value. The value of participation factor is divided equally into two analogous buses. The second frequency from Case 1 seems to appear in Case 2 as two resonant frequencies, one greater and the other less than the frequency from Case 1. The values of participation factors for both cases for these frequencies appear to confirm this assumption since their values are again distributed equally and the values are very similar for the new two frequencies.

On the contrary, in the Z(s) model, the two frequencies stay at approximately the same level and the new resonance frequency appears *independently* after adding new branch. As stated before, the value of critical impedance is very low.

From the curves of modal impedances with regards to each single node (Figure V.20), we observe that for resonance around 12^{th} order, the values of two modes are at the similar level of modal impedance for this value of resonance mode 7 and mode 11. This condition disturbs the assumption settled in Section I.4.2 and [13] that only one within the modal impedances is much greater than the others.

DIgSILENT Power Factory model

Furthermore, the results of FS and HRMA are compared with the curves acquired from Power Factory software. Figure V.22 presents the diagram of the network used for calculation.

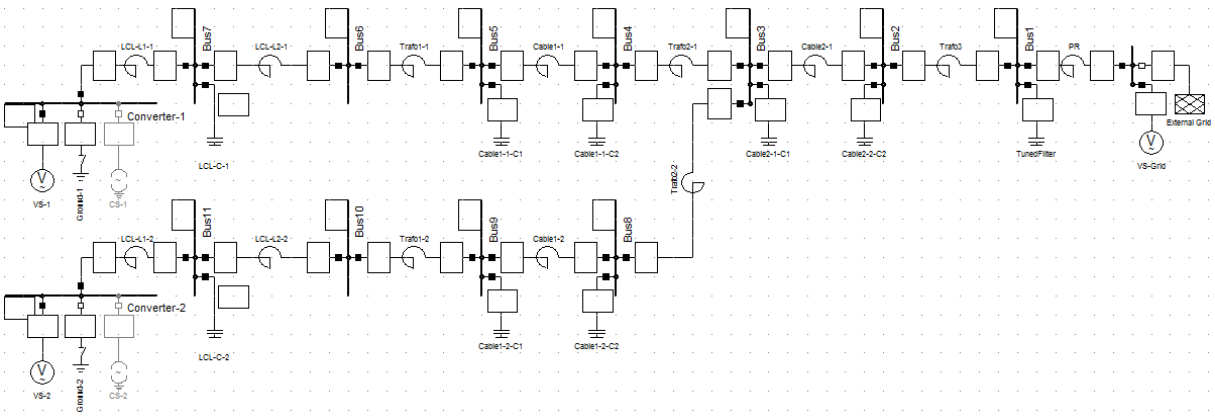

Figure V.22: Case 2: DIgSILENT Power Factory model.

Again, the models of VS and CS-WT are simulated for *Impedance Frequency Characteristic* calculations. Figures V.23 and V.24 present the results of frequency sweep for VS and CS-WT models, seen from the middle LCL filter bus i.e. the same bus as for MATLAB model bus 7.

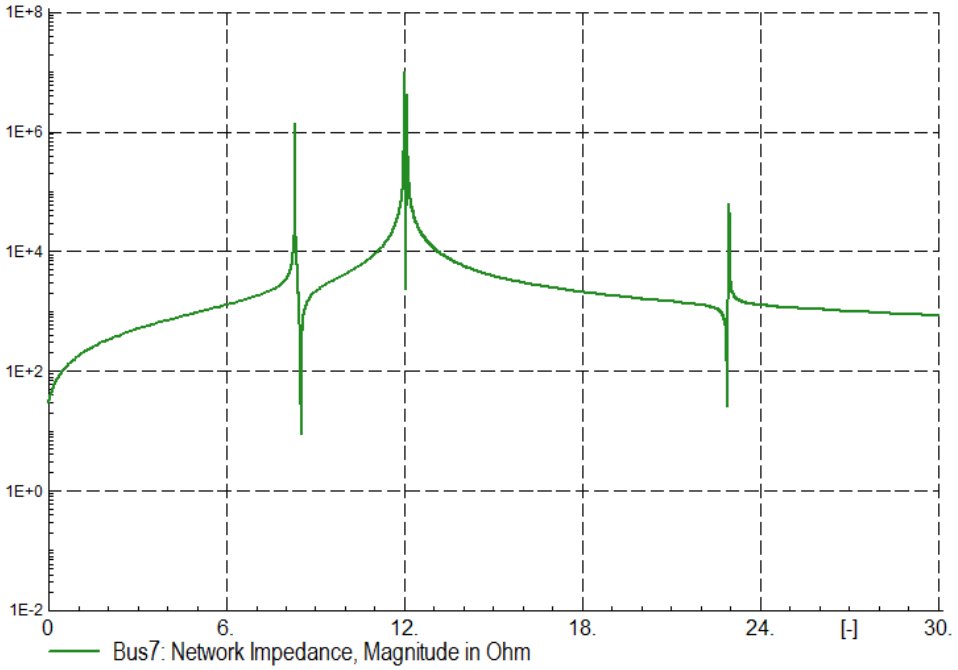

Figure V.23: Case 2: Power Factory impedance curves for VS model (seen from bus 7).

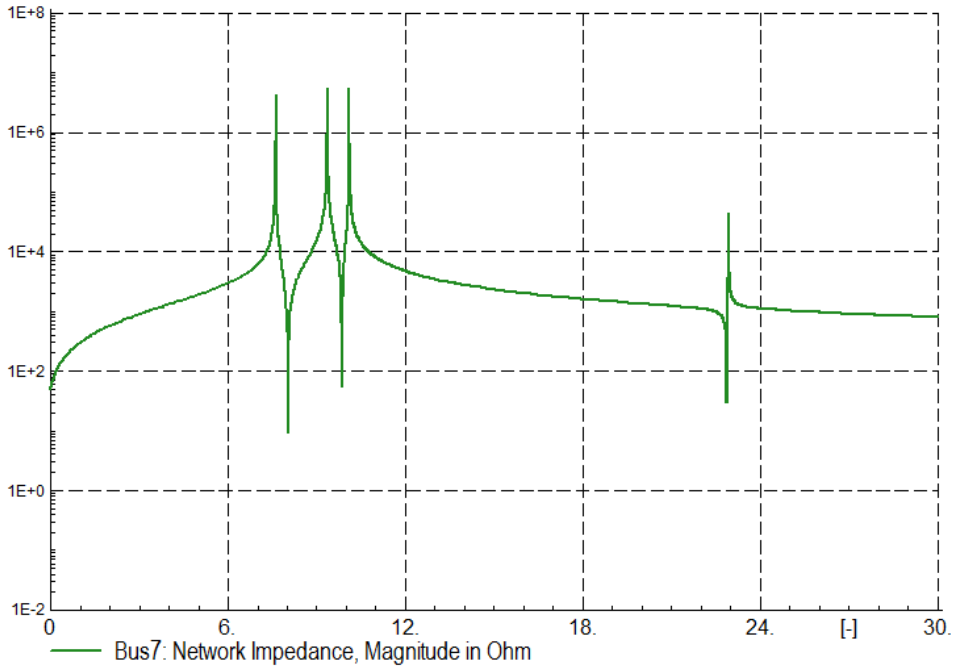

Figure V.24: Case 1: Power Factory impedance curves for CS-WT model (seen from bus 7).

The resonant frequencies for peak impedances are measured by the software tool and presented in the Table V.11.

Table V.11: Case 2: Power Factory resonant frequencies values for two models.

	Order [-]			
VS model	8.46	12.12	12.23	23.00
CS-WT model	7.77	9.51	10.25	22.98

The values of resonant frequencies are consistent with the values obtained both in FS and HRMA in MATLAB. Again, we present the impedance curves seen from other buses. The buses where the impedance is observed are buses 1-7. Since the two branches with wind turbines are the same, we know that the impedance curves seen from buses 4-7 are the same as seen from respective buses 8-11. Therefore the impedance curves for only one branch are sufficient. The Figure V.25 shows the curves for buses 1-7 for the VS model, while the Figure V.26 illustrate the same curves but for model CS-WT.

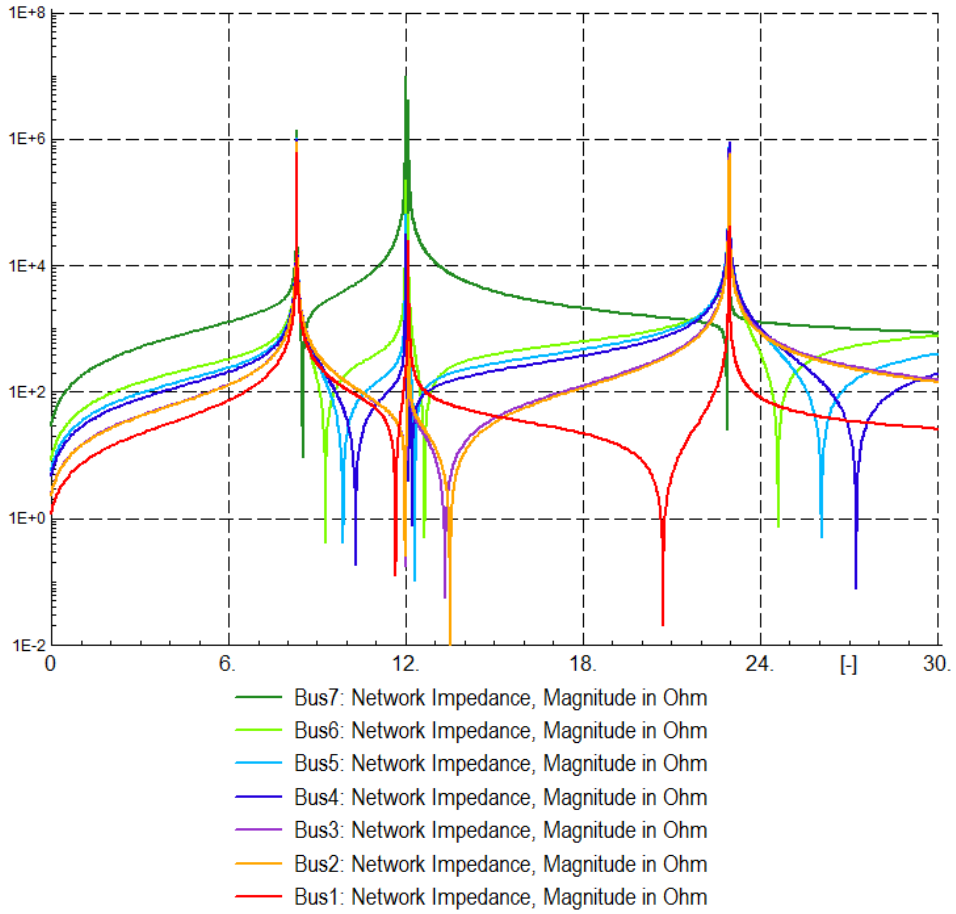

Figure V.25: Case 2: Power Factory impedance curves for VS model (seen from buses 1-7).

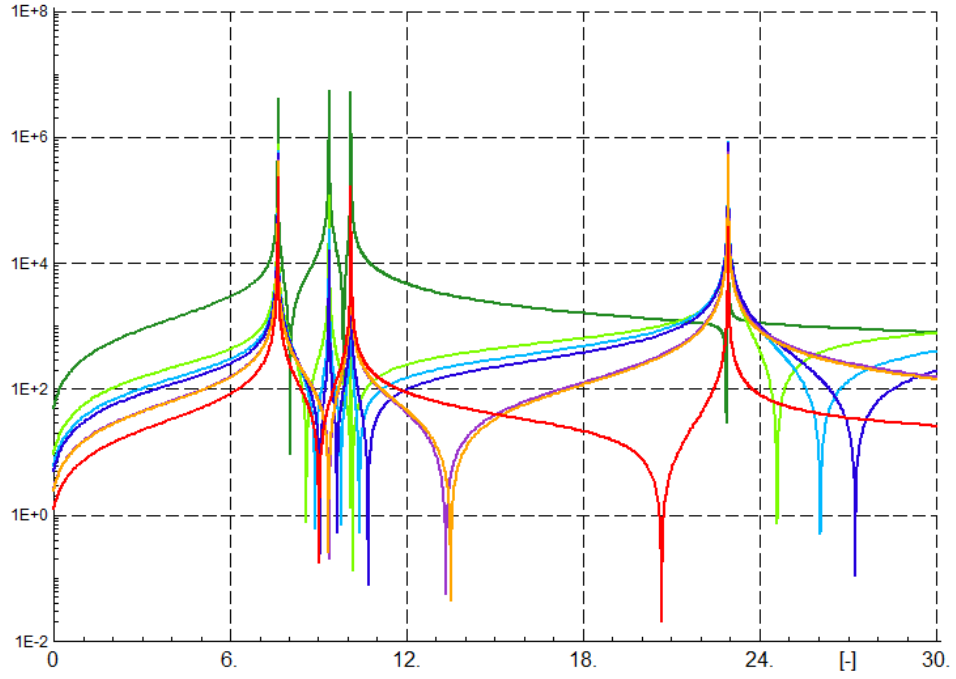

Figure V.26: Case 2: Power Factory impedance curves for CS-WT model (seen from buses 1-7).

The shapes of the curves indicate the same conclusions like for Case 1 i.e. the series and parallel resonance does depend on and does not depend on the point in the network, respectively. The previous section presenting results of Case 1 describes these principles in details.

Results comparison

Similarly to the first case, the results of FS, HRMA and from Power Factory are very similar. For the considered accuracy, the values of corresponding frequencies are exactly the same. The important fact to highlight is that we obtain one resonance frequency more for HRMA comparing to FS in the Z(s) model. Even though the value of modal impedance is quite low comparing to the other resonance points, the level of impedance dangerous for the network is not identified and could apparently be already dangerous for the network. The situation suggests the conclusion that we should always consider both methods together and compare their outputs. Since the amount of data necessary for both methods is very similar, this does not pose a problem during analysis.

V.2.3 Case 3

The last topology case is described in Section V.1.2. All installed power (400 MW) and all elements of Wind Power Plant are considered.

Frequency Sweep

Figures V.27 and V.28 present the frequency sweep curves for linear and logarithmic scales, respectively. All three models are included. The bus of observation is again bus 7. All four wind turbine branches are equal therefore the features of those branches are symmetrical to each other. The groups of equal bus numbers at the wind turbine branches are: (4, 8, 13, 17), (5, 9, 14, 18), (6, 10, 15, 19), (7, 11, 16, 20). Moreover bus 3 and bus 12 are also symmetrical, installed at the end of two symmetrical cables connecting pairs of wind turbine branches.

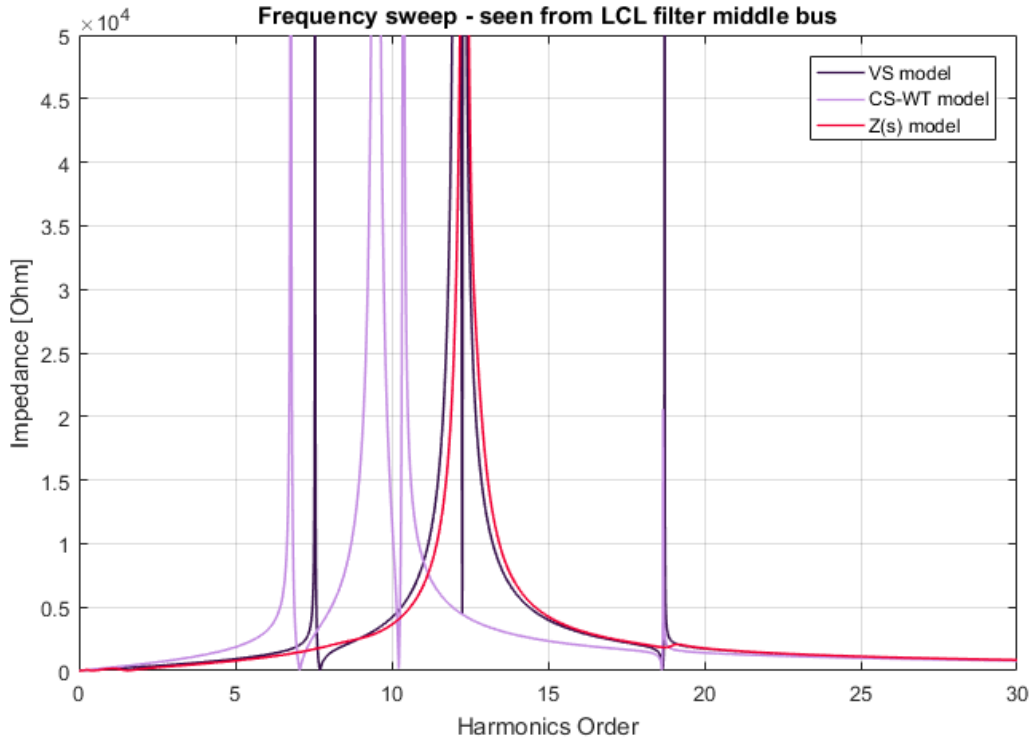

Figure V.27: Case 3: Frequency sweep curves (1) for three models (seen from bus 7).

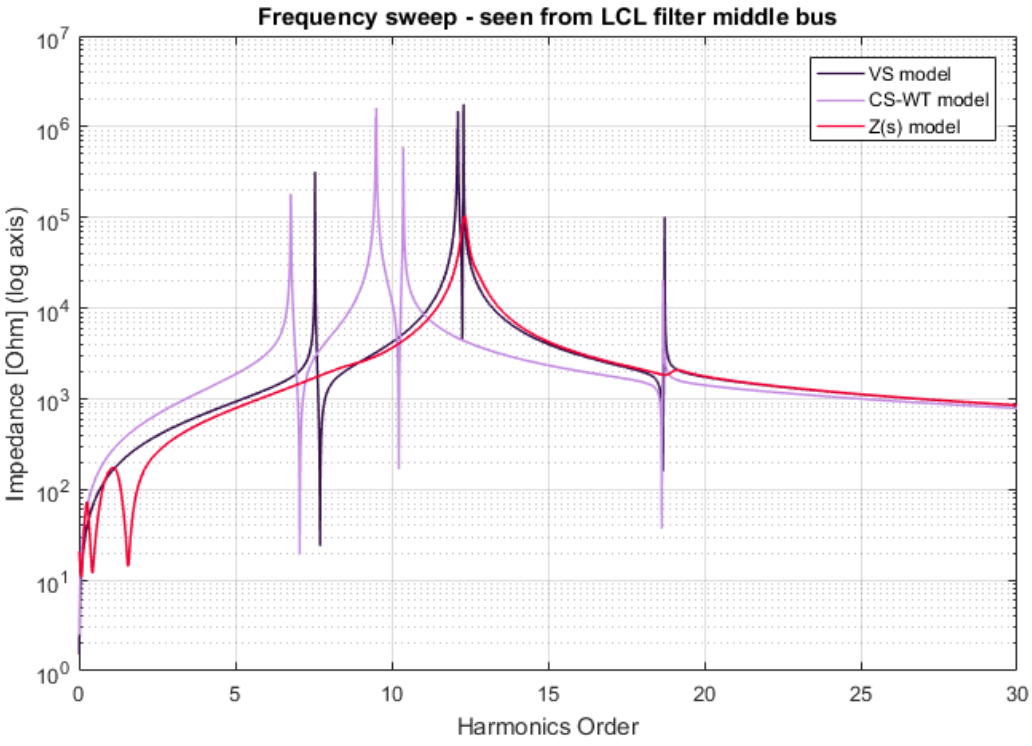

Figure V.28: Case 3: Frequency sweep curves (2) for three models (seen from bus 7).

Table V.12 presents resonance frequency values and the peak values of corresponding impedances. The values around the fundamental frequency for Z(s) model are ignored.

Table V.12: Case 3: Frequency sweep numerical results of resonant frequencies and corresponding peak impedances for three models.

Converter model	Frequency order [-]	Peak impedance [Ω]
VS	7.55	318 k
	12.1	941 k
	12.12	1491 k
	12.3	1769 k
	18.73	102 k
CS-WT	6.78	180 k
	9.49	1288 k
	9.51	1606 k
	10.37	595 k
	18.68	21 k
Z(s)	12.33	104 k
	19.13	2 k

We can observe one additional resonance frequency for each of the VS and CS-WT models comparing to Case 2. However, pair of frequencies for each model have very similar values therefore, from the figure, could be considered as the one resonant frequency. Further examination and comparison of the frequency sweep results for all considered topology cases is presented in Section V.2.4.

Harmonic Resonance Modal Analysis

Following Figures V.29, V.30 and V.31 shows the HRMA results. Again, the graphs present maximum modal impedances, modal impedances curves for all modes separately and critical modes curves alone.

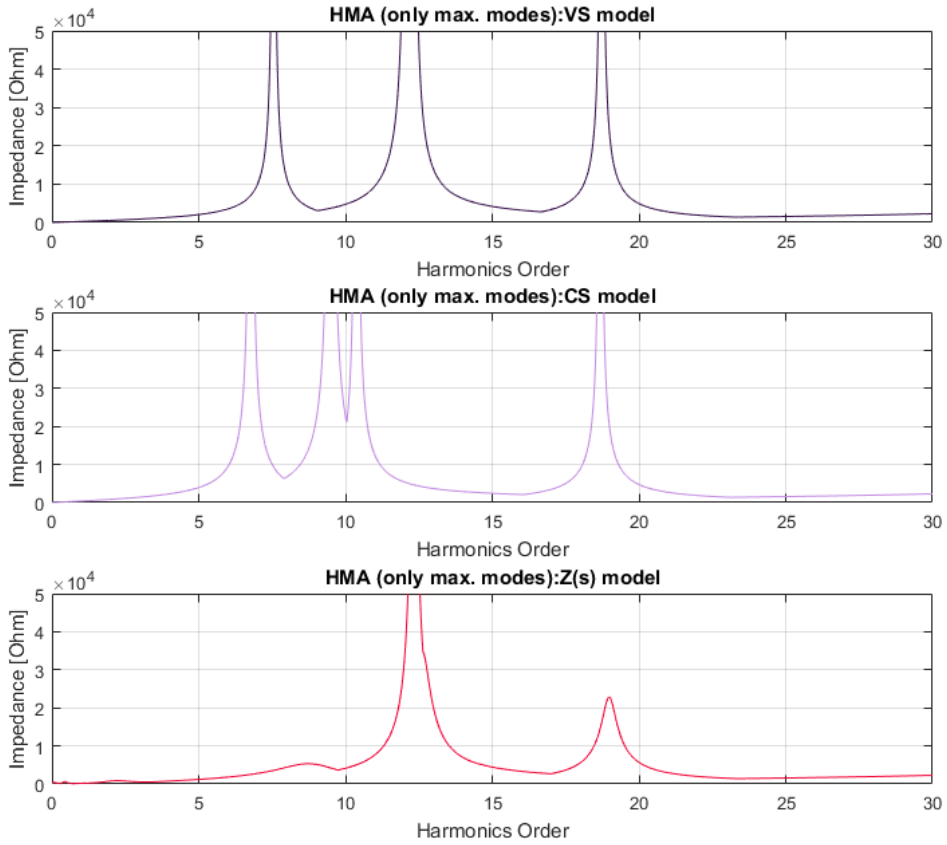

Figure V.29: Case 3: HRMA method *maximum modes* only impedance curves for three models.

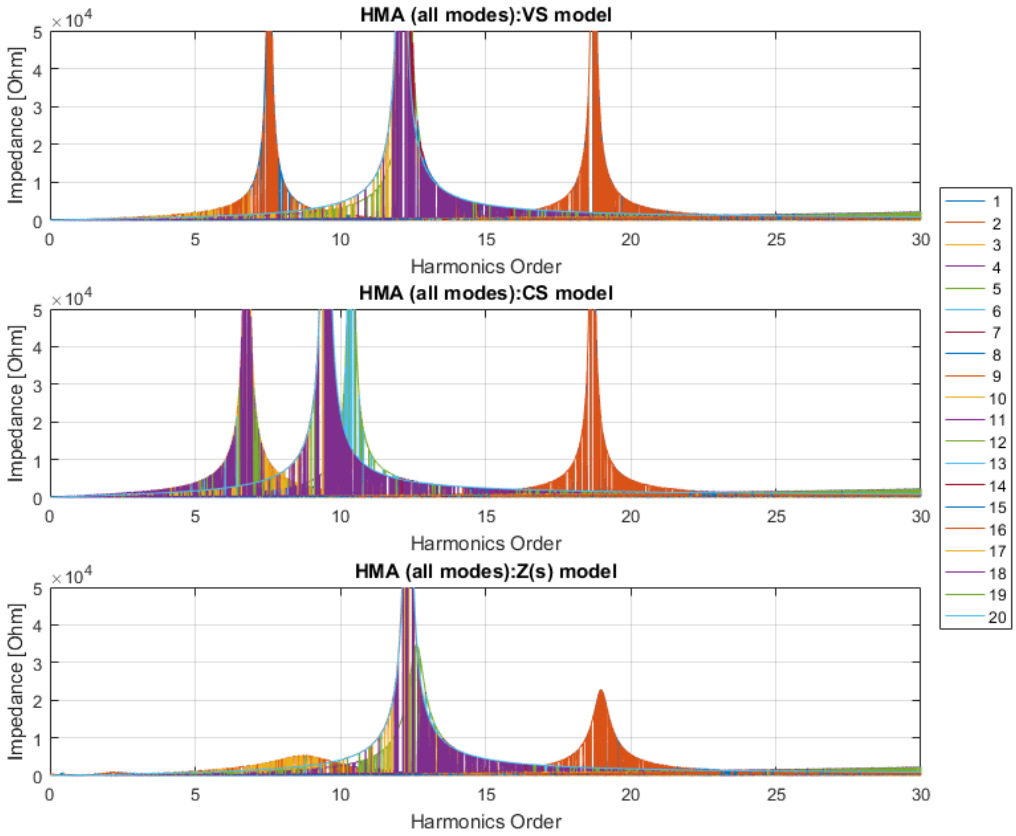

Figure V.30: Case 3: HRMA method *all modes* impedance curves for three models.

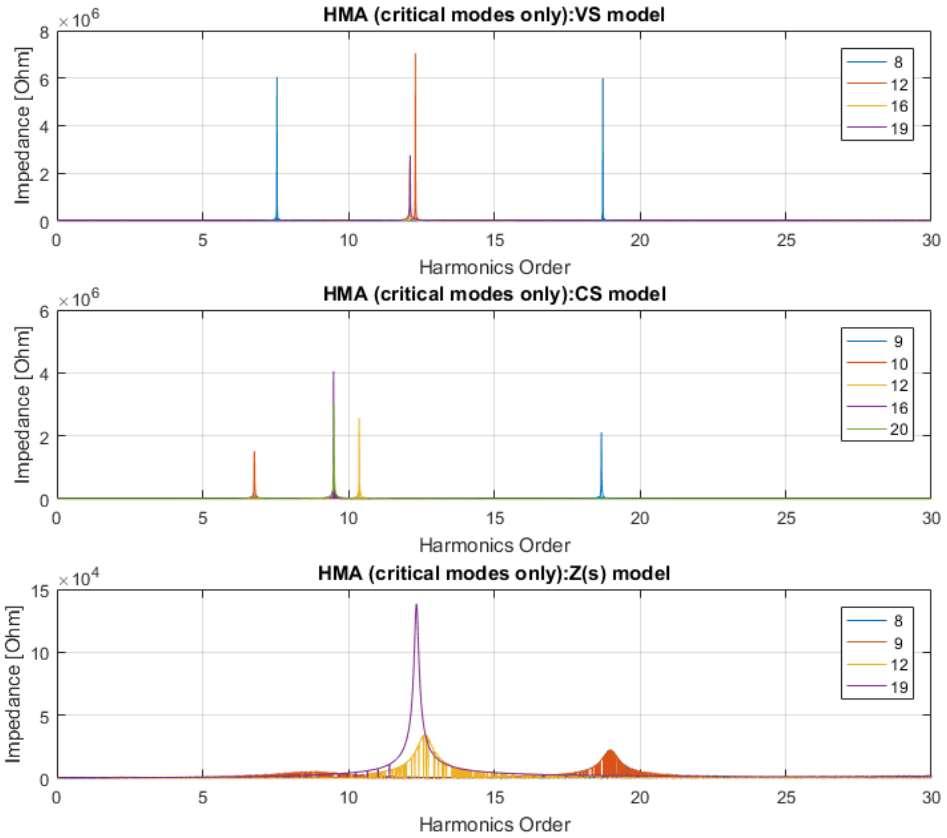

Figure V.31: Case 3: HRMA method *critical modes* impedance curves for three models.

With these results in mind, the values of critical impedances and values of participation factors for Case 3 are presented for each resonance frequency in Table V.13 and V.14, respectively.

Table V.13: Case 3: HRMA numerical results of resonant frequencies and corresponding peak impedances for three models.

Order	Critical mode	Critical impedance magnitude [Ω]	Angle [°]
VS model			
7.55	8	6050 k	-83.4
12.1	16	2484 k	-80.8
12.12	19	2753 k	82.4
12.3	12	7050 k	64.5
18.73	8	5997 k	57.5
CS-WT model			
6.78	10	1511 k	85.4
9.49	16	4054 k	-66.1
9.51	20	3008 k	76.8
10.37	12	2567 k	-77.3
18.68	9	2114 k	-78.7
Z(s) model			
8.73	9	5 k	-13.6
12.34	19	138 k	3.3
18.98	9	23 k	4.0

Table V.14: Case 3: HRMA numerical results of resonant frequencies and participation factors for three models.

Frequency order [-]	Participation factors [%] for the buses									
VS-model										
	1	2	3	4	5	6	7	8	9	10
7.55	2.5	**4.8**	**4.9**	**5.1**	**5.2**	**5.2**	**5.2**	**5.1**	**5.2**	**5.2**
12.1	0.0	0.0	0.0	0.1	0.2	0.6	**24.2**	0.1	0.2	0.6
12.12	0.0	0.0	0.0	0.2	0.3	1.0	**46.6**	0.2	0.3	1.0
12.3	0.4	0.1	0.1	0.0	0.0	0.3	**24.5**	0.0	0.0	0.3
18.73	1.7	5.6	5.8	**6.7**	**6.7**	5.2	1.7	**6.7**	**6.7**	5.2
	11	12	13	14	15	16	17	18	19	20
7.55	**5.2**	**4.9**	**5.1**	**5.2**	**5.2**	**5.2**	**5.1**	**5.2**	**5.2**	**5.2**
12.1	**24.2**	0.0	0.1	0.2	0.6	**24.2**	0.1	0.2	0.6	**24.2**
12.12	**46.6**	0.0	0.0	0.0	0.0	1.8	0.0	0.0	0.0	1.8
12.3	**24.5**	0.1	0.0	0.0	0.3	**24.5**	0.0	0.0	0.3	**24.5**
18.73	1.7	5.8	**6.7**	**6.7**	5.2	1.7	**6.7**	**6.7**	5.2	1.7
CS-WT model										
	1	2	3	4	5	6	7	8	9	10
6.78	1.2	2.8	2.8	3.2	3.4	3.9	**12.1**	3.2	3.4	3.9
9.49	0.0	0.0	0.0	0.1	0.2	0.5	**24.2**	0.1	0.2	0.5
9.51	0.0	0.0	0.0	0.0	0.0	0.1	4.3	0.0	0.0	0.1
10.37	1.1	0.8	0.8	0.4	0.2	0.0	**23.6**	0.4	0.2	0.0
18.68	1.8	5.6	5.9	**6.8**	**6.8**	5.5	1.0	**6.8**	**6.8**	5.5
	11	12	13	14	15	16	17	18	19	20
6.78	**12.1**	2.8	3.2	3.4	3.9	**12.1**	3.2	3.4	3.9	**12.1**
9.49	**24.2**	0.0	0.1	0.2	0.5	**24.2**	0.1	0.2	0.5	**24.2**
9.51	4.3	0.0	0.1	0.3	1.0	**44.2**	0.1	0.3	1.0	**44.2**
10.37	**23.6**	0.8	0.4	0.2	0.0	**23.6**	0.4	0.2	0.0	**23.6**
18.68	1.0	5.9	**6.8**	**6.8**	5.5	1.0	**6.8**	**6.8**	5.5	1.0
Z(s) model										
	1	2	3	4	5	6	7	8	9	10
8.73	1.7	**4.3**	**4.3**	**4.8**	**4.9**	**5.0**	**6.7**	**4.8**	**4.9**	**5.0**
12.34	0.0	0.0	0.0	0.1	0.3	1.1	**47.3**	0.1	0.3	1.1
18.98	2.0	5.5	5.8	**6.7**	**6.7**	5.3	1.6	**6.7**	**6.7**	5.3
	11	12	13	14	15	16	17	18	19	20
8.73	**6.7**	**4.3**	**4.8**	**4.9**	**5.0**	**6.7**	**4.8**	**4.9**	**5.0**	**6.7**
12.34	**47.3**	0.0	0.0	0.0	0.0	1.2	0.0	0.0	0.0	1.2
18.98	1.6	5.8	**6.7**	**6.7**	5.3	1.6	**6.7**	**6.7**	5.3	1.6

Similarly to the Case 2, for Z(s) model we obtain one more resonance frequency from HRMA comparing to frequency sweep. Besides this frequency, the values of equivalent ones are the same or very similar. Again, the modal impedance value of critical mode for new frequency is very low.

Finally, we note that the participation factors are not completely symmetrical in some cases. The symmetry remains between the pair of branches 1 and 2 or 3 and 4 (the pairs connected to the same three-winding transformer) but symmetry of participation factors between pair branches connected to different three-winding transformers fades away for some cases.

DIgSILENT Power Factory model

Analogously, we compare the results of FS and HRMA with the curves from Power Factory model. The model used in this case is presented in the Figure V.32.

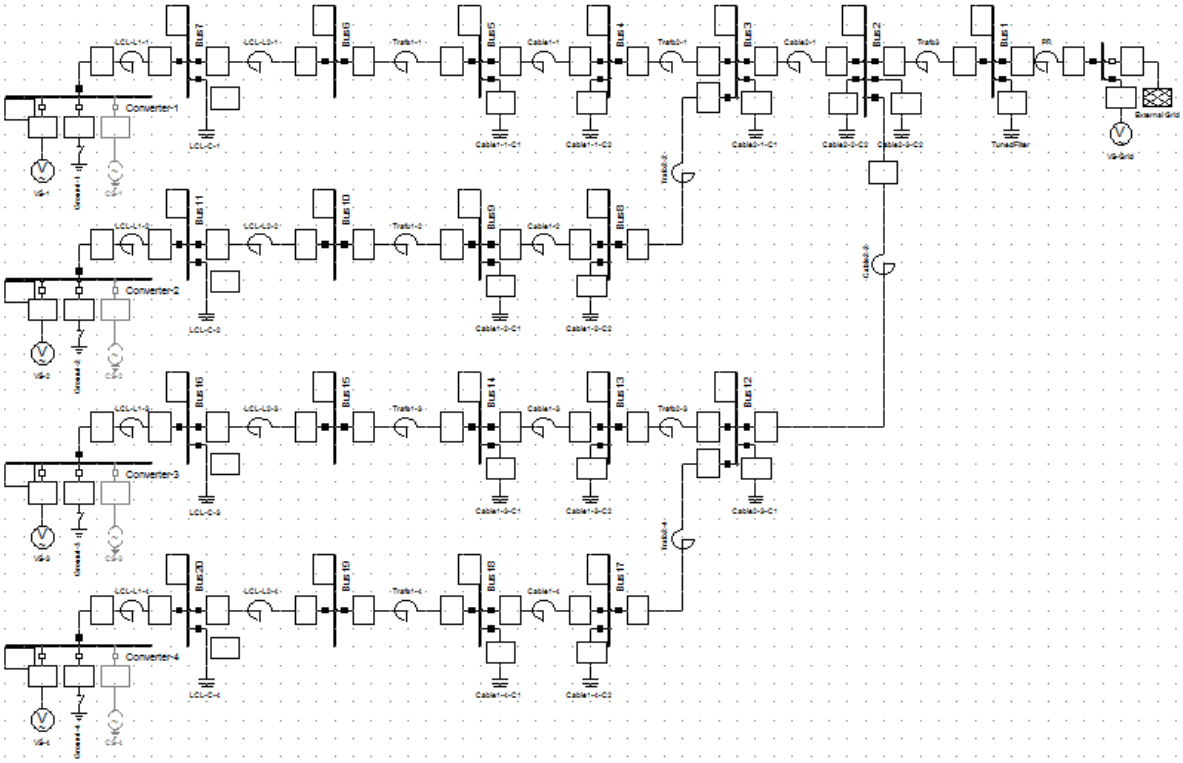

Figure V.32: Case 3: DIgSILENT Power Factory model.

The models of VS and CS-WT are simulated for Impedance Frequency Characteristic calculations. Figures V.33 and Figures V.34 present the results of frequency sweep for VS and CS-WT model, seen from the middle LCL filter bus i.e. the same bus as for MATLAB model bus 7.

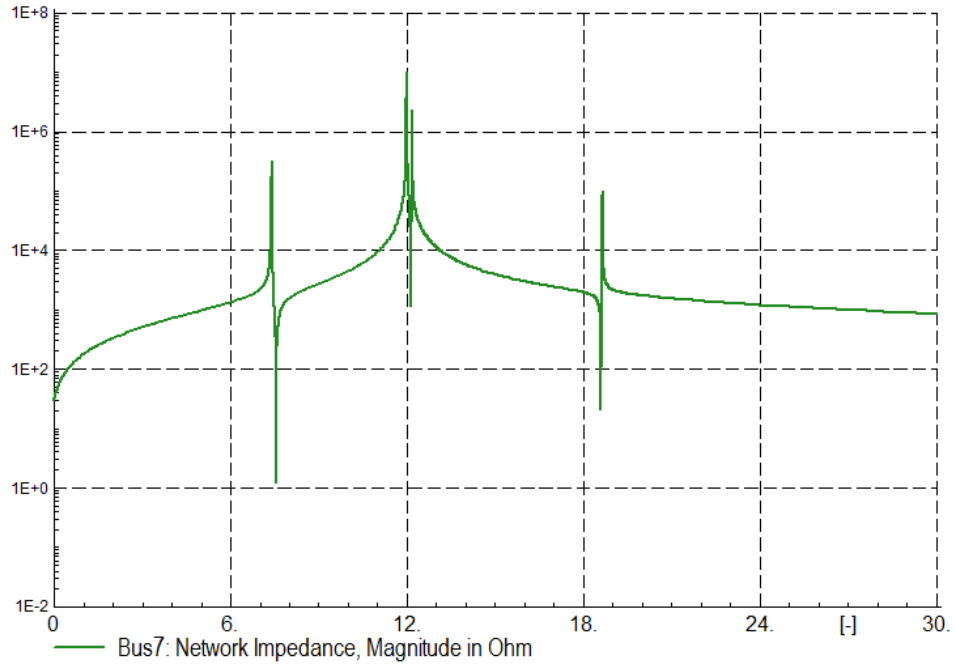

Figure V.33: Case 3: Power Factory impedance curves for VS model (seen from bus 7).

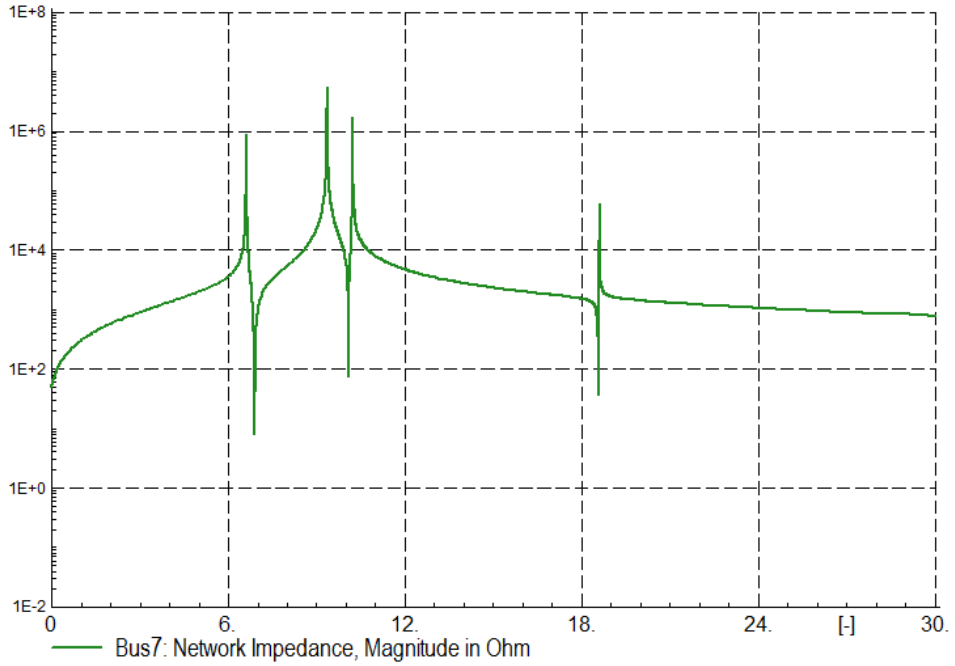

Figure V.34: Case 3: Power Factory impedance curves for CS-WT model (seen from bus 7).

The resonant frequencies for peak impedances are measured in the software tool and presented in the Table V.15.

Table V.15: Case 3: Power Factory resonant frequencies values for two models.

	Order [-]				
VS model	7.55	12.10	12.12	12.30	18.73
CS-WT model	6.78	9.49	9.51	10.37	18.68

One more time, the values obtained from Power Factory converge with those we collected from frequency sweep analysis in MATLAB. Similarly to the Case 2 analysis, the Figures V.35 and V.36 show the curves for buses 1-7 for the VS model and CS-WT model, respectively.

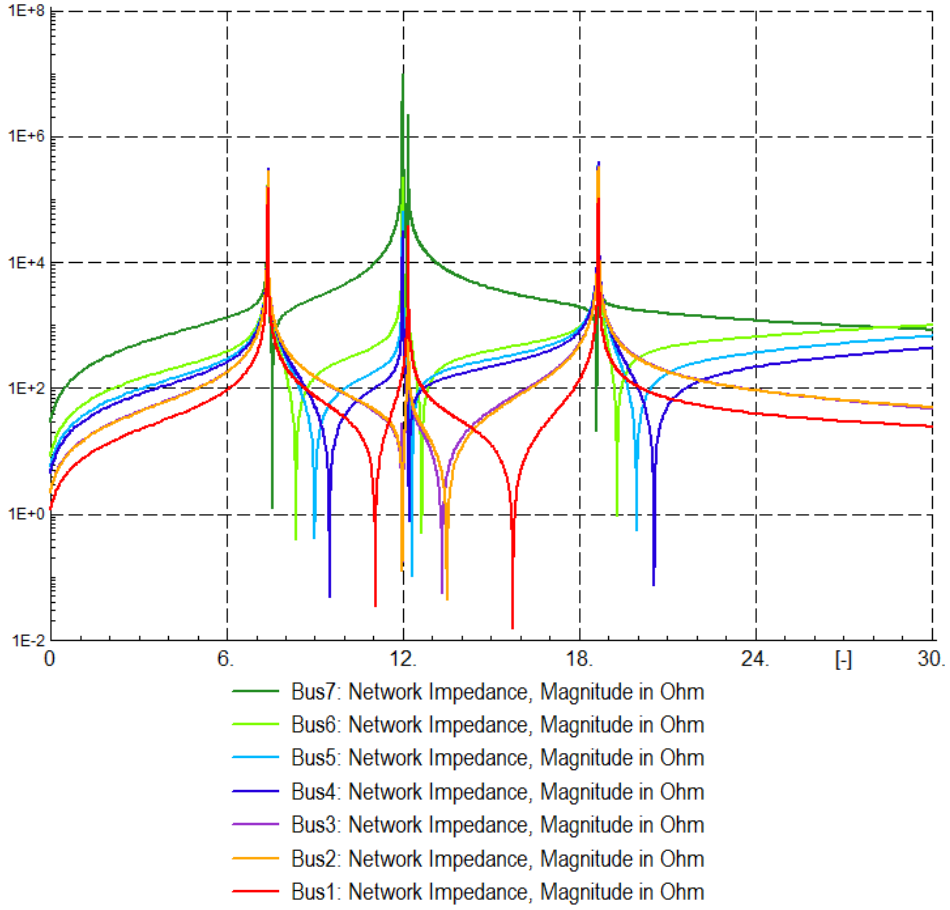

Figure V.35: Case 3: Power Factory impedance curves for VS model (seen from buses 1-7).

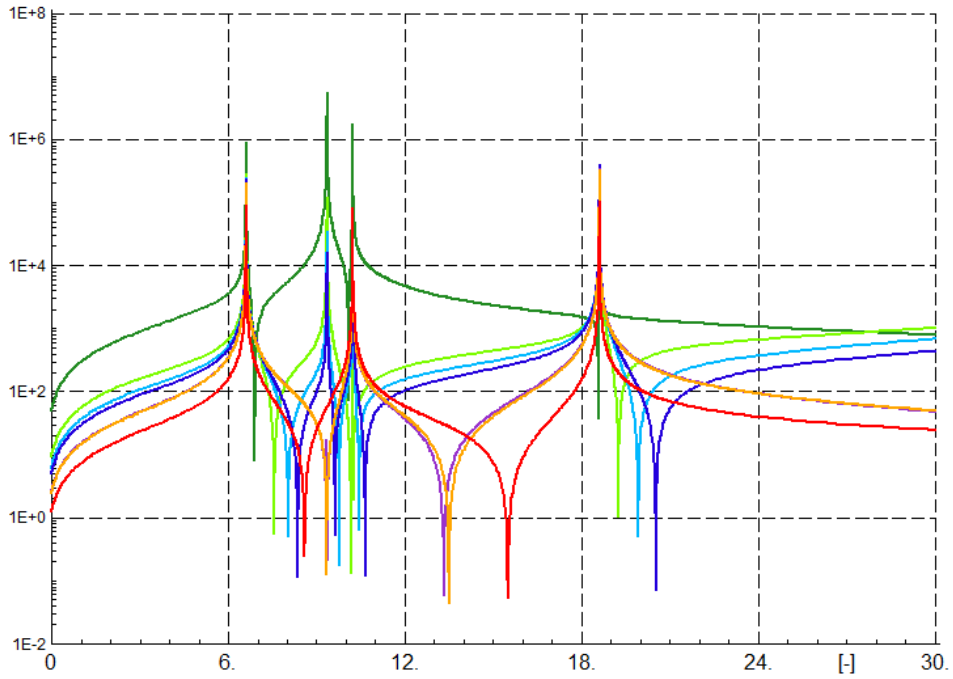

Figure V.36: Case 3: Power Factory impedance curves for CS-WT model (seen from buses 1-7).

The shapes of the curves indicate the similar conclusions like for Case 1 and Case 2.

Results comparison

Similarly to the first and second topology case, the values of received frequencies from all three approaches are very similar. Once again, we obtain one more resonant frequency from HRMA comparing to frequency sweep. Also, we observe similar behaviour of resonances with regard to the bus of observation.

V.2.4 Comparison between models

In this section we compare the results obtained in three previous sections jointly. The following figures and tables demonstrate the behaviour of frequency sweep curves for VS model, CS-WT model and Z(s) model. Each model is considered separately but for all three topology cases. In tables the results of resonance frequencies for all topology cases are gathered. The aim of this section is to identify patterns and any similarities between the topology cases within the three models.

V.2.4.1 VS model

Frequency sweep

The following figure presents the frequency sweep curves for all three topology cases. We had a try to group the frequencies in the three groups like indicated in the figure.

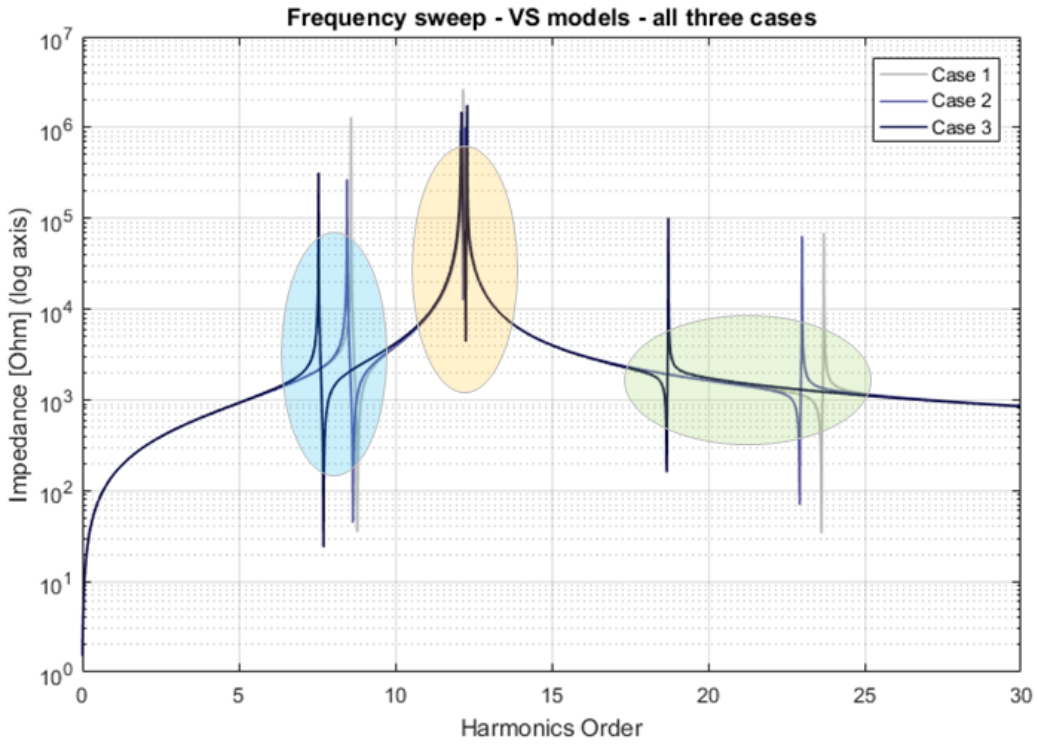

Figure V.37: Frequency sweep curves for VS model in three topology cases (seen from bus 7).

Table V.16: Frequency sweep numerical results of resonant frequencies and corresponding peak impedances for VS model in three topology cases.

Method / model	Frequency order [-]		
	Case 1	**Case 2**	**Case 3**
FS / VS	8.59	8.46	7.55
	12.17	12.12	12.1
		12.23	12.12
			12.3
	23.7	23.00	18.73

We observe clearly that in each next case, the frequencies of first and third group are shifted downward. This shifting occurs due to the increasing amount of capacitive power in the network. In Case 2, 33kV cable with significant amount of capacitance is connected to the grid. In Case 3, three additional cables are connected i.e. one 150kV and two 33kV collection cables. Thus, we can mark more significant shift between Case 2 and Case 3 than between first two. The second group (around 12th harmonic order) is becoming more numerous for the cases with multiple branches, whereas the values stay at the similar level.

Harmonic Resonance Modal Analysis

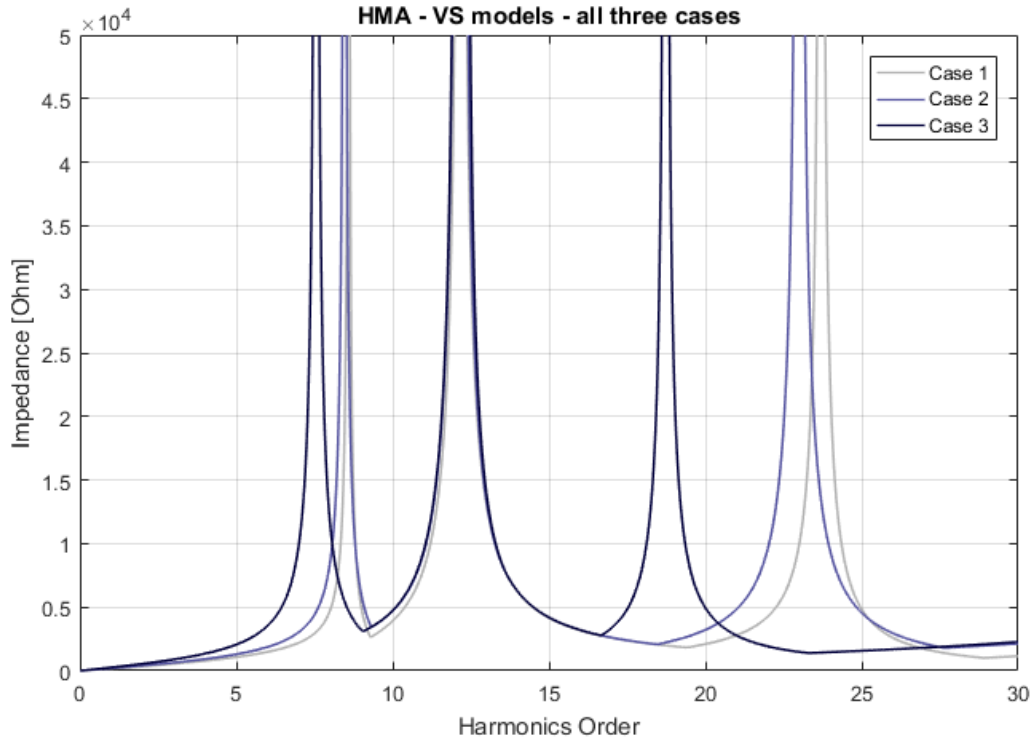

Figure V.38: HRMA method *maximum modes* impedance curves for VS model in three topology cases.

Since the frequencies calculated in HRMA are the same to those obtained from frequency sweep, we do not draw more observations. However, we also have at our disposal the values of participation factors indicating the excitability and observability of the buses in the network. The values of PFs for three topology cases for VS mode are gathered in the Table V.17.

Table V.17: HRMA numerical results of resonant frequencies and participation factors for VS model in three topology cases.

Frequency order [-]	Participation factors [%] for the buses										
Case 1											
	1	2	3	4	5	6	7				
8.59	8.8	12.8	13.0	14.2	14.6	15.1	**21.5**				
12.17	0.1	0.0	0.0	0.2	0.4	1.8	**97.4**				
23.7	0.9	14.6	15.7	**23.1**	**24.3**	20.0	1.4				
Case 2											
	1	2	3	4	5	6	7	8	9	10	11
8.46	5.3	7.9	8.0	8.7	9.0	9.2	**12.5**	8.7	9.0	9.2	**12.5**
12.12	0.0	0.0	0.0	0.2	0.3	1.1	**48.4**	0.2	0.3	1.1	**48.4**
12.23	0.3	0.0	0.0	0.0	0.1	0.8	**48.9**	0.0	0.1	0.8	**48.9**
23	0.6	8.9	9.6	**13.6**	**14.2**	11.7	1.0	**13.6**	**14.2**	11.7	1.0
Case 3											
	1	2	3	4	5	6	7	8	9	10	
7.55	2.5	**4.8**	**4.9**	**5.1**	**5.2**	**5.2**	**5.2**	**5.1**	**5.2**	**5.2**	
12.1	0.0	0.0	0.0	0.1	0.2	0.6	**24.2**	0.1	0.2	0.6	
12.12	0.0	0.0	0.0	0.2	0.3	1.0	**46.6**	0.2	0.3	1.0	
12.3	0.4	0.1	0.1	0.0	0.0	0.3	**24.5**	0.0	0.0	0.3	
18.73	1.7	5.6	5.8	**6.7**	**6.7**	5.2	1.7	**6.7**	**6.7**	5.2	
	11	12	13	14	15	16	17	18	19	20	
7.55	**5.2**	**4.9**	**5.1**	**5.2**	**5.2**	**5.2**	**5.1**	**5.2**	**5.2**	**5.2**	
12.1	**24.2**	0.0	0.1	0.2	0.6	**24.2**	0.1	0.2	0.6	**24.2**	
12.12	**46.6**	0.0	0.0	0.0	0.0	1.8	0.0	0.0	0.0	1.8	
12.3	**24.5**	0.1	0.0	0.0	0.3	**24.5**	0.0	0.0	0.3	**24.5**	
18.73	1.7	5.8	**6.7**	**6.7**	5.2	1.7	**6.7**	**6.7**	5.2	1.7	

From the values of PFs we can see the pattern that confirms our assumption created with respect to resonant frequencies from frequency sweep only. The first group of harmonics seems to mark the bus 7 (and symmetrical buses within other branches) as the source of this group of resonances. It touches all topology cases. We have to notice that the values of the PFs could be also considered as spread quite evenly between the buses. In case of the second group of resonant frequency (around 12th harmonic order), the bus that is surely indicated by the PFs is the bus 7 (and symmetrical ones). Moreover, the more symmetrical branches in the network, the more numerous the number of resonant frequencies in this group. Further connection of analogous branches apparently gives more resonant frequencies around 12^{th} frequency order. For the third group of resonances, we identify two buses (bus 4 and bus 5) indicated by PFs as the two buses participating the most in the excitation of the resonance. Bus 4 and bus 5 are the terminals of 33 kV collection cable. The observations described above are encapsulated in the Table V.18.

Table V.18: HRMA numerical results of resonant frequencies for VS model in three topology cases with the dominant bus(es) assigned.

Method / model	Frequency order [-]			Dominant bus
	Case 1	**Case 2**	**Case 3**	
HRMA / VS	8.59	8.46	7.55	Middle LCL buses (7) or evenly
	12.17	12.12	12.1	Middle LCL buses (7)
		12.23	12.12	
			12.3	
	23.7	23.00	18.73	Cable 33 kV terminal buses (4, 5)

V.2.4.2 CS-WT model

Frequency sweep

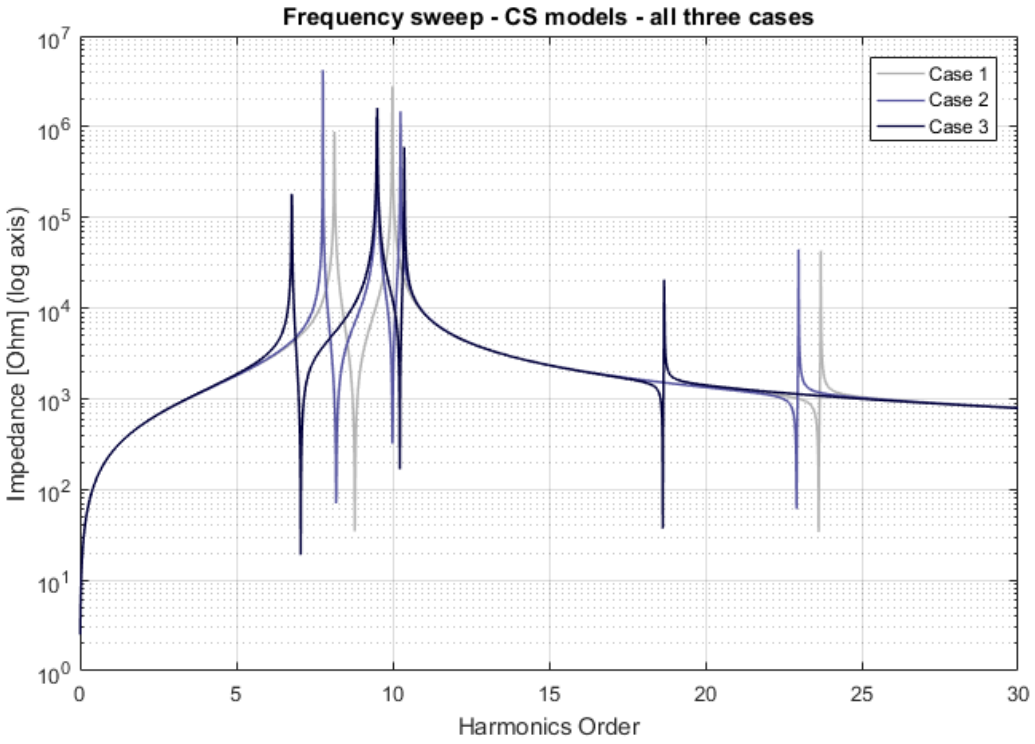

Figure V.39: Frequency sweep curves for CS-WT model in three topology cases (seen from bus 7).

Table V.19: Frequency sweep numerical results of resonant frequencies and corresponding peak impedances for CS-WT model in three topology cases.

Method / model	Frequency order [-]		
	Case 1	**Case 2**	**Case 3**
FS / CS-WT	8.14	7.77	6.78
	9.99	9.51	9.49
		10.25	9.51
			10.37
	23.69	22.98	18.68

Similarly to the observations drawn for the Voltage Source model we can conclude for the model with aggregated WT converters modelled as Current Sources. On the basis of FS results only, we divide the values of resonance frequencies into three groups. Again, we detect that the values of each group are shifted downwards when the number of branches is increased, it happens more significantly for between second and third case. Second group of frequencies becomes more numerous, same as for VS model. All the values of the second group are around 10^{th} order. Generally for CS-WT model, all of the values of the frequencies are lower comparing o the first topology case. For each group, these changes differ.

Harmonic Resonance Modal Analysis

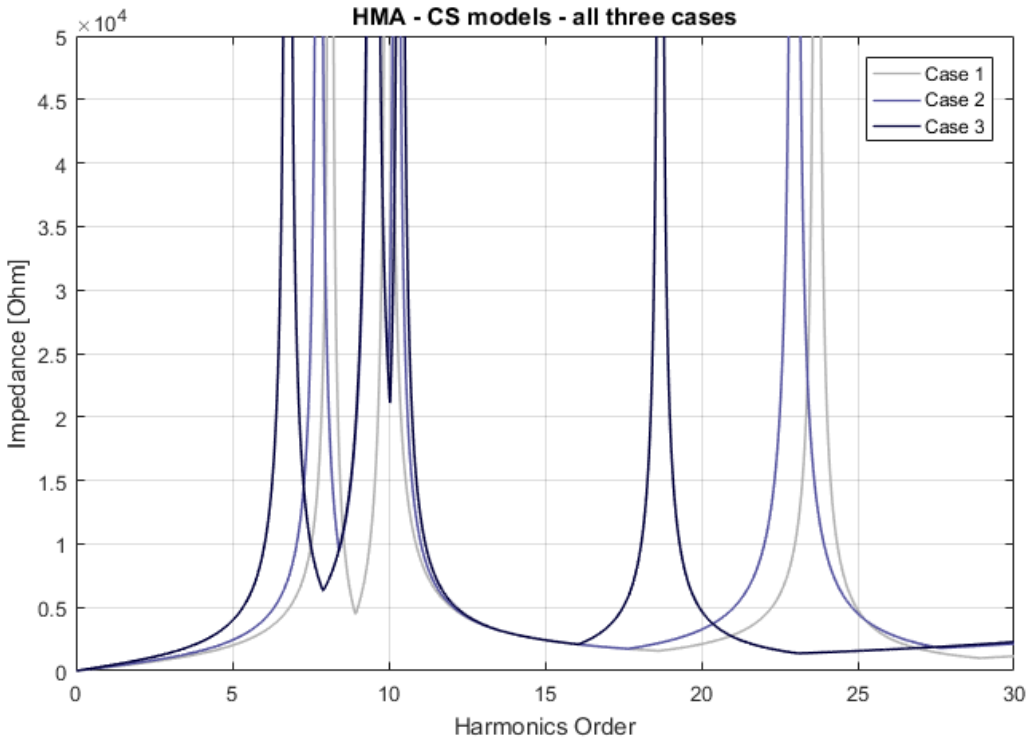

Figure V.40: HRMA method *maximum modes* impedance curves for CS-WT model in three topology cases.

The values of frequency orders are the same for FS and HRMA. Again, we include participation factors to our conclusions and try to identify some patterns. The values of PFs for all cases are presented first in Table V.20.

Table V.20: HRMA numerical results of resonant frequencies and participation factors for CS-WT model in three topology cases.

Frequency order [-]	Participation factors [%] for the buses										
Case 1											
	1	2	3	4	5	6	7				
8.14	2.6	4.4	4.4	6.2	7.0	9.3	**66.0**				
9.99	1.1	1.0	0.9	0.2	0.0	0.3	**96.5**				
23.69	0.9	14.6	15.6	**23.2**	**24.4**	20.2	1.1				
Case 2											
	1	2	3	4	5	6	7	8	9	10	11
7.77	1.7	3.2	3.2	4.2	4.6	5.8	**31.3**	4.2	4.6	5.8	**31.3**
9.51	0.0	0.0	0.0	0.1	0.3	1.1	**48.5**	0.1	0.3	1.1	**48.5**
10.25	1.5	1.1	1.1	0.4	0.2	0.0	**47.4**	0.4	0.2	0.0	**47.4**
22.98	0.6	8.9	9.6	**13.7**	**14.3**	11.8	0.7	**13.7**	**14.3**	11.8	0.7
Case 3											
	1	2	3	4	5	6	7	8	9	10	
6.78	1.2	2.8	2.8	3.2	3.4	3.9	**12.1**	3.2	3.4	3.9	
9.49	0.0	0.0	0.0	0.1	0.2	0.5	**24.2**	0.1	0.2	0.5	
9.51	0.0	0.0	0.0	0.0	0.0	0.1	4.3	0.0	0.0	0.1	
10.37	1.1	0.8	0.8	0.4	0.2	0.0	**23.6**	0.4	0.2	0.0	
18.68	1.8	5.6	5.9	**6.8**	**6.8**	5.5	1.0	**6.8**	**6.8**	5.5	
	11	12	13	14	15	16	17	18	19	20	
6.78	**12.1**	2.8	3.2	3.4	3.9	**12.1**	3.2	3.4	3.9	**12.1**	
9.49	**24.2**	0.0	0.1	0.2	0.5	**24.2**	0.1	0.2	0.5	**24.2**	
9.51	4.3	0.0	0.1	0.3	1.0	**44.2**	0.1	0.3	1.0	**44.2**	
10.37	**23.6**	0.8	0.4	0.2	0.0	**23.6**	0.4	0.2	0.0	**23.6**	
18.68	1.0	5.9	**6.8**	**6.8**	5.5	1.0	**6.8**	**6.8**	5.5	1.0	

On the basis of PF's, we gather similar conclusions for CS-WT model than for VS model. The PF's for the first two groups of harmonic orders indicates bus 7 (and symmetrical buses at other branches) as the bus with highest participation to the harmonic excitation. This time, PF's of first group of the lowest frequencies are not distributed evenly and mark bus 7 as dominant bus, similarly to second group of frequencies. In the same manner as for VS model, the PF's of harmonic orders of third group mark the buses 4 and 5 as the buses exciting the resonance. These observations are gathered in the Table V.21.

Table V.21: HRMA numerical results of resonant frequencies for CS-WT model in three topology cases with the dominant bus(es) assigned.

Method / model	Frequency order [-]			Dominant bus
	Case 1	**Case 2**	**Case 3**	
HRMA / CS-WT	8.14	7.77	6.78	Middle LCL bus (7)
	9.99	9.51	9.49	
		10.25	9.51	
			10.37	
	23.69	22.98	18.68	Cable 33 kV terminal buses (4, 5)

V.2.4.3 Z(s) model

Frequency sweep

Figure V.41 shows the FS curves for all topology cases derived for Z(s) model.

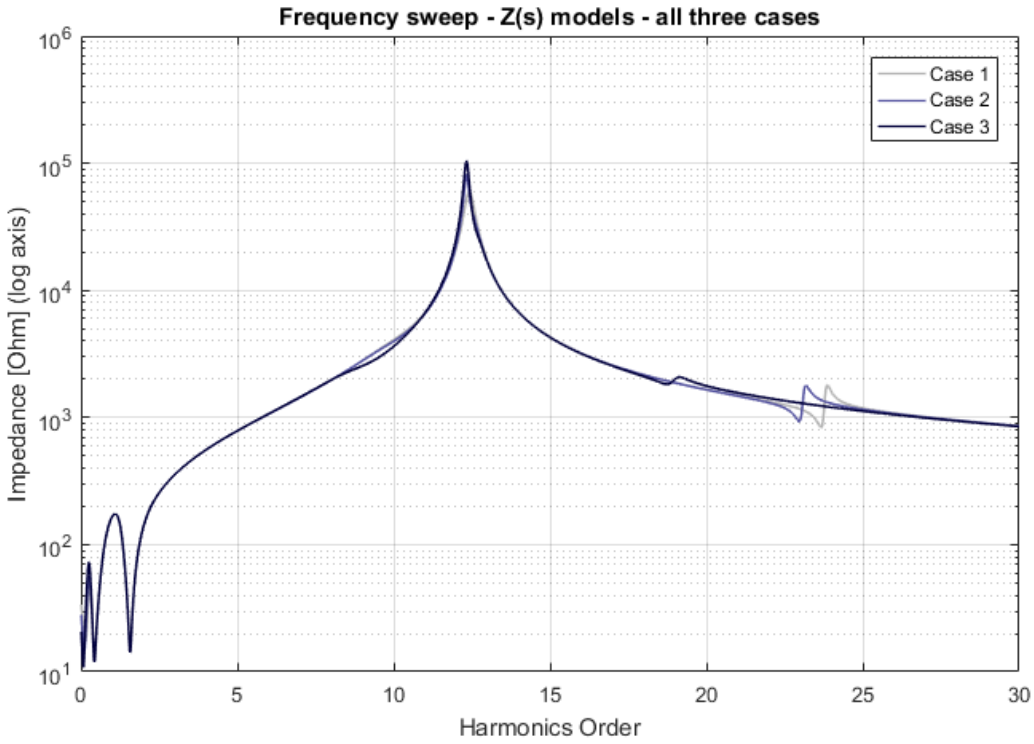

Figure V.41: Frequency sweep curves for Z(s) model in three topology cases (seen from bus 7).

Table V.22: Frequency sweep numerical results of resonant frequencies and corresponding peak impedances for Z(s) model in three topology cases.

Method / model	Frequency order [-]		
	Case 1	**Case 2**	**Case 3**
FS / Z(s)	12.42	12.33	12.33
	23.87	23.18	19.13

This time, FS method does not detect resonance frequencies analogous to the lowest orders group for VS and CS-WT model, therefore whole that group does not exist in the Table V.22. The number of peaking impedance points around 12th order also does not increase for multiple branches cases. However, we observe the equivalent resonances for two groups with values very close to the VS model. Similarly to both VS and CS-WT models, we mark the downward shift of frequencies for analogous group of highest frequencies for each next topology case.

Harmonic Resonance Modal Analysis

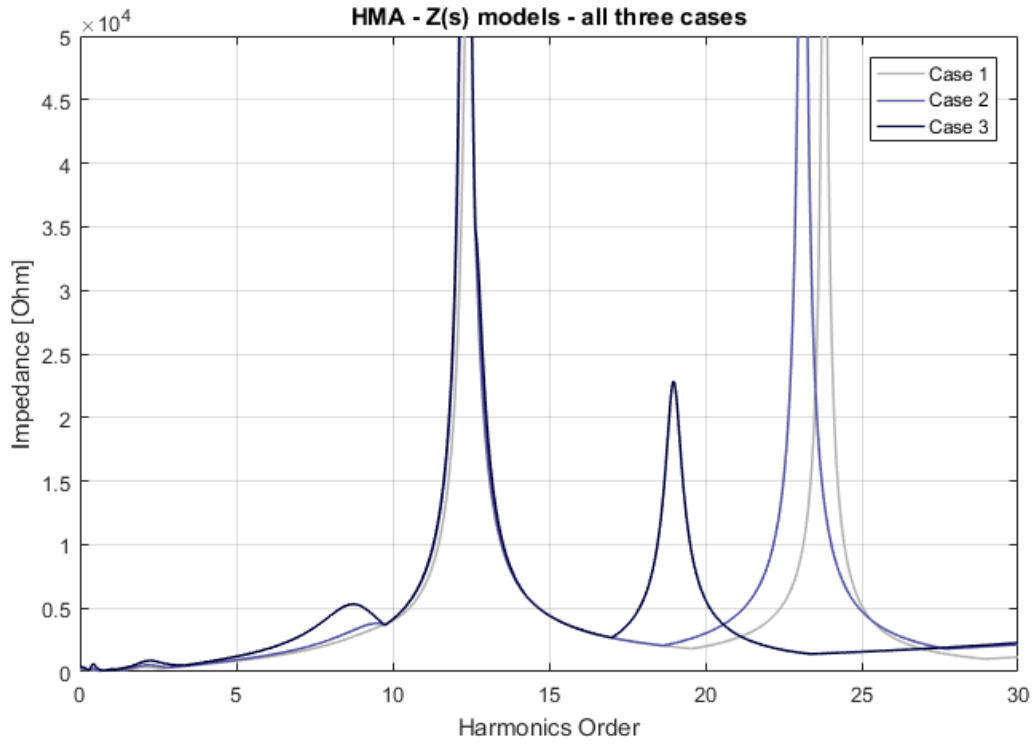

Figure V.42: HRMA method *maximum modes* impedance curves for Z(s) model in three topology cases.

As pointed out in Section V.2, for Z(s) model HRMA detects additional resonant frequency comparing to FS, but at the low level (relatively to the other critical impedances). These new frequencies corresponds accurately to the first group of frequencies detected in VS and CS-WT model.

Again, we include PFs in the analysis and we identify the buses with the highest values of PFs. The Table V.23 presents PFs values for all topology cases.

Table V.23: HRMA numerical results of resonant frequencies and participation factors for Z(s) model in three topology cases.

Frequency order [-]	Participation factors [%] for the buses										
	Case 1										
	1	2	3	4	5	6	7				
12.42	0.2	0.1	0.1	0.2	0.5	1.8	**97.8**				
23.81	1.0	14.5	15.6	**23.1**	**24.3**	20.1	1.4				
	Case 2										
	1	2	3	4	5	6	7	8	9	10	11
9.51	1.8	3.5	3.6	4.6	5.1	6.1	**29.7**	4.6	5.1	6.1	**29.7**
12.34	0.0	0.0	0.0	0.2	0.3	1.1	**48.4**	0.2	0.3	1.1	**48.4**
23.11	0.7	8.8	9.5	**13.6**	**14.2**	11.7	1.0	**13.6**	**14.2**	11.7	1.0
	Case 3										
	1	2	3	4	5	6	7	8	9	10	
8.73	1.7	4.3	4.3	4.8	4.9	5.0	**6.7**	4.8	4.9	5.0	
12.34	0.0	0.0	0.0	0.1	0.3	1.1	**47.3**	0.1	0.3	1.1	
18.98	2.0	5.5	5.8	**6.7**	**6.7**	5.3	1.6	**6.7**	**6.7**	5.3	
	11	12	13	14	15	16	17	18	19	20	
8.73	**6.7**	4.3	4.8	4.9	5.0	**6.7**	4.8	4.9	5.0	**6.7**	
12.34	**47.3**	0.0	0.0	0.0	0.0	1.2	0.0	0.0	0.0	1.2	
18.98	1.6	5.8	**6.7**	**6.7**	5.3	1.6	**6.7**	**6.7**	5.3	1.6	

With respect to PF's, we notice the very similar observation to the models VS and CS-WT. The PF's of the first and second group of frequencies indicate bus 7 as the one participating the most in the resonances. For the highest order group, similarly, the buses 4 and 5 are identified. These observations are concluded in Table V.24.

Table V.24: HRMA numerical results of resonant frequencies for Z(s) model in three topology cases with the dominant bus(es) assigned.

Method / model	Frequency order [-]			Dominant bus
	Case 1	**Case 2**	**Case 3**	
HRMA / Z(s)		9.51	8.73	Middle LCL bus (7)
	12.42	12.34	12.34	
	23.81	23.11	18.98	Cable 33 kV terminal buses (4, 5)

V.3 Stability study with respect to topology cases

This section presents the results of stability analysis for the three different already described topology cases. The principles of stability analysis are described in Section II.2.2 in the theoretical part of the thesis. Only the last model of the network is used i.e. the model containing the nonlinear impedances of the converters Z(s) model - described in Section III.4.2. This model is considered as the more accurate than two others (VS and CS-WT) presented in the thesis. In short, the stability is evaluated on the basis of phase margin plotted in the Bode diagrams

(Section II.2.3). This stability analysis method for WPP AC grid is considered as still under development [6]. The sections below present the results separately for each topology case, also comparing the values obtained to the previous results from FS and HRMA methods.

V.3.1 Case 1 stability

The Figure V.43 presents the Bode diagram of the considered model used for stability study. As described in detail in theoretical part, the network is divided into two limped impedances: the *source* and the *grid*. The point of division is behind the HV transformer, looking from the grid side. The positive and negative sequences of *source* and *grid* segments are plotted in domain of frequency in the Bode diagrams.

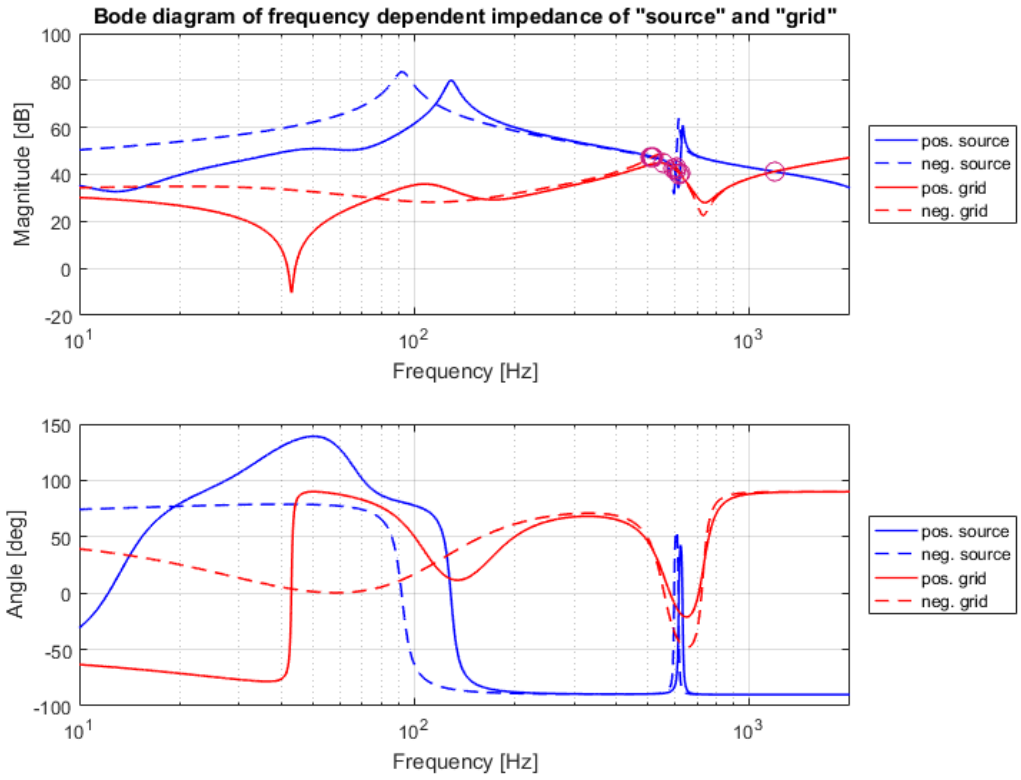

Figure V.43: Case 1: Bode diagram of frequency dependent positive- and negatice-impedances of *grid* and *source*.

The points of attention are the crossings of the grid and the source impedances magnitude (zero-dB crossings), regardless the positive or negative sequence. All of them are investigated with respect to phase difference of respective curves and the phase margin is calculated. In the Figure V.43 the intersections are marked with purple circles. Figure V.44 presents the source and grid curves zoomed in the area of high density of intersections.

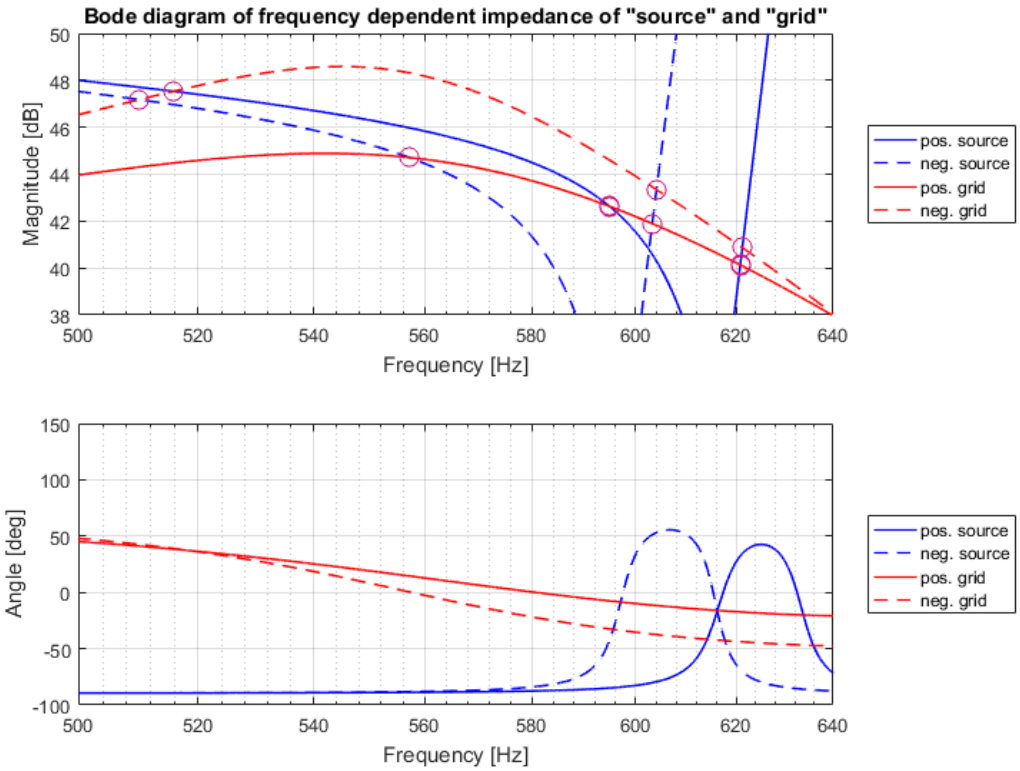

Figure V.44: Case 1: Bode diagram (zoomed) of frequency dependent positive- and negatice-impedances of *grid* and *source*.

For each intersection, the stability is assessed by the values of phase margins calculated in MATLAB as described in Section II.2.3. Table V.25 presents the values of frequency orders for which the crossings occur and the values of phase margins.

Table V.25: Case 1: Resonance frequencies and the phase margins assigned.

Frequency order [-]	Phase margin [deg]
Positive Grid – Positive Source	
11.90	102.61
12.42	130.28
23.81	**0.64**
Positive Grid – Negative Source	
11.14	77.25
12.07	117.44
23.81	**0.64**
Negative Grid –Positive Source	
10.32	51.66
12.43	101.61
23.81	**0.18**
Negative Grid – Negative Source	
10.20	48.01
12.08	89.40
23.81	**0.18**

First of all, we observe three points of intersections for each pair of sequence impedances of source and grid. Looking at the values of frequencies we obtain very similar values to the FS and HRMA results. Additionally to the frequency values, we obtain the stability assessment on the basis of phase margins at each intersection (Table V.25). We can see that the group of highest resonance frequencies could be marked as unstable due to very low values of phase margin which is very low. Thus, we conclude that unstable operation of this grid can occur if waveforms of frequency order around 23.81^{th} order appear in the network. For other resonant frequencies the stability margin is higher, therefore resonance at those frequencies is less exposed to unstable operation.

V.3.2 Case 2 stability

Similarly to the Case 1, the Bode diagram of the system is provided for Case 2 (Figure V.45 and Figure V.46). Regarding the additional branches connected in this topology case, the point of division for the stability study model is the same i.e. behind HV transformer.

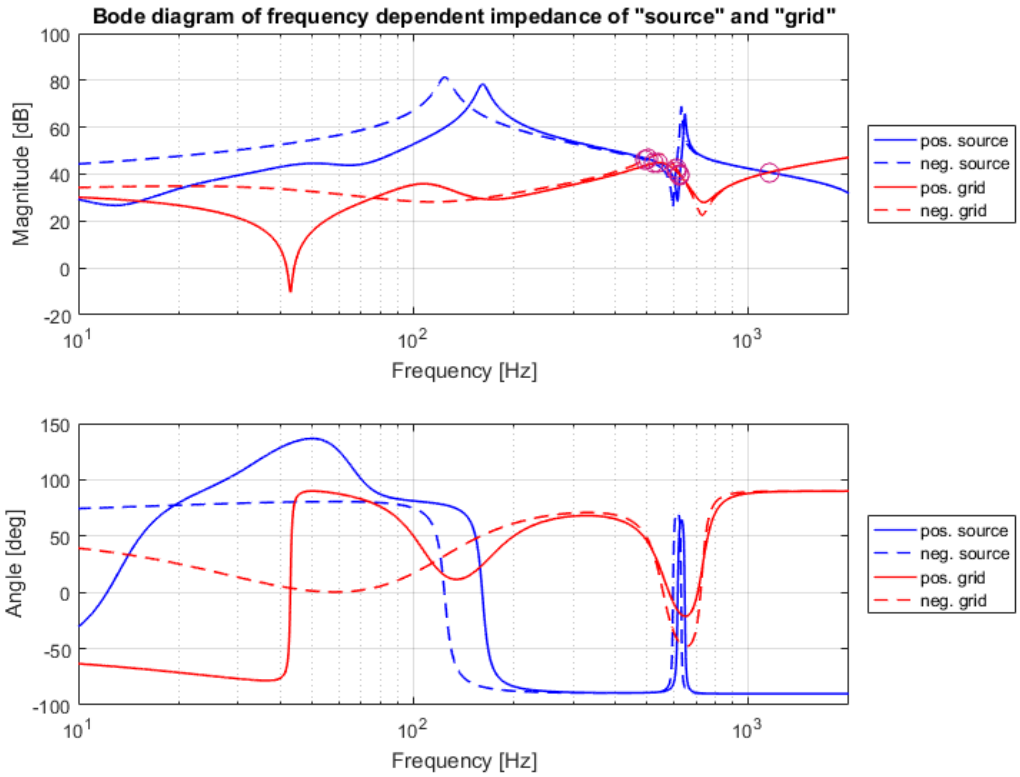

Figure V.45: Case 2: Bode diagram of frequency dependent positive- and negatice-impedances of *grid* and *source*.

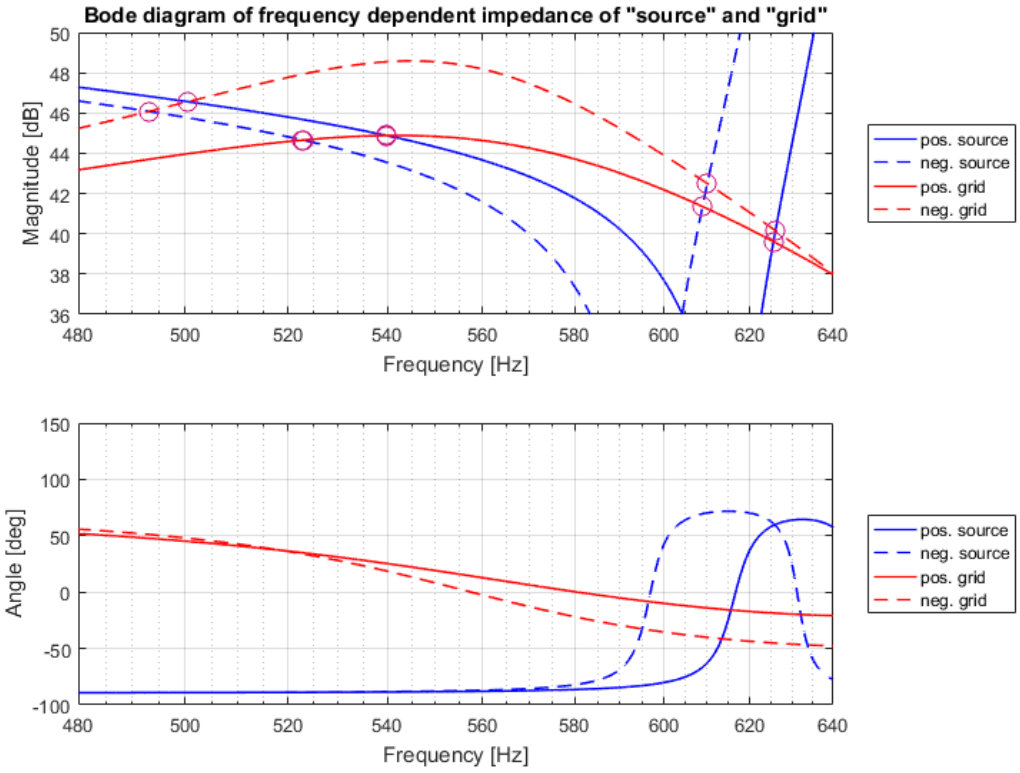

Figure V.46: Case 2: Bode diagram (zoomed) of frequency dependent positive- and negatice-impedances of *grid* and *source*.

In the Table V.26 the stability assessments by phase margins are gathered for all intersections.

Table V.26: Case 2: Resonance frequencies and the phase margins assigned.

Frequency order [-]	Phase margin [deg]
Positive Grid – Positive Source	
10.80	66.03
12.51	102.31
23.11	**0.78**
Positive Grid – Negative Source	
10.46	56.37
12.18	96.94
23.11	**0.78**
Negative Grid –Positive Source	
10.00	43.12
12.52	74.85
23.12	**0.26**
Negative Grid – Negative Source	
9.86	39.72
12.20	69.60
23.12	**0.24**

In Case 2, the values of frequencies at the intersections again correspond quite accurately to the values obtained in the FS and HRMA method. Regarding, the stability assessment base on the phase margins, we observe again the unstable operation for highest group of resonant frequencies. Moreover, we mark significant decrease of phase margins for resonances of lower and medium group of frequency orders.

V.3.3 Case 3 stability

Once again, the system impedance dynamics is plotted on the Bode diagram and the intersections of both sequences for grid and source are marked (Figure V.47 and Figure V.48). The point of division is the same as before.

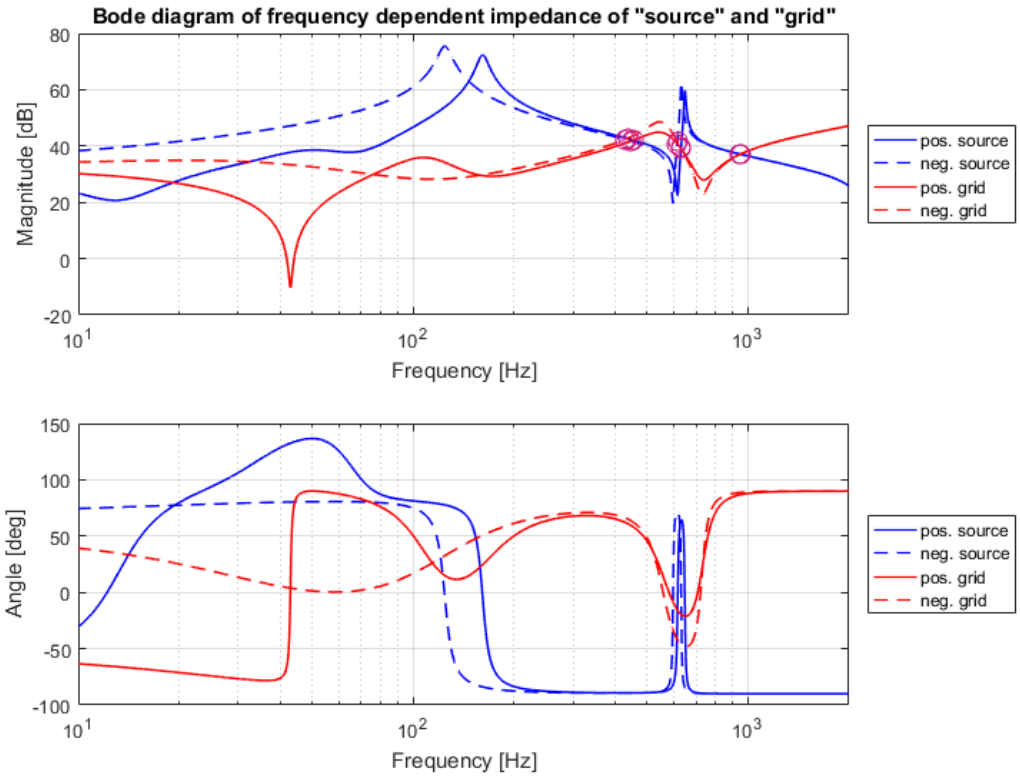

Figure V.47: Case 3: Bode diagram of frequency dependent positive- and negatice-impedances of *grid* and *source*.

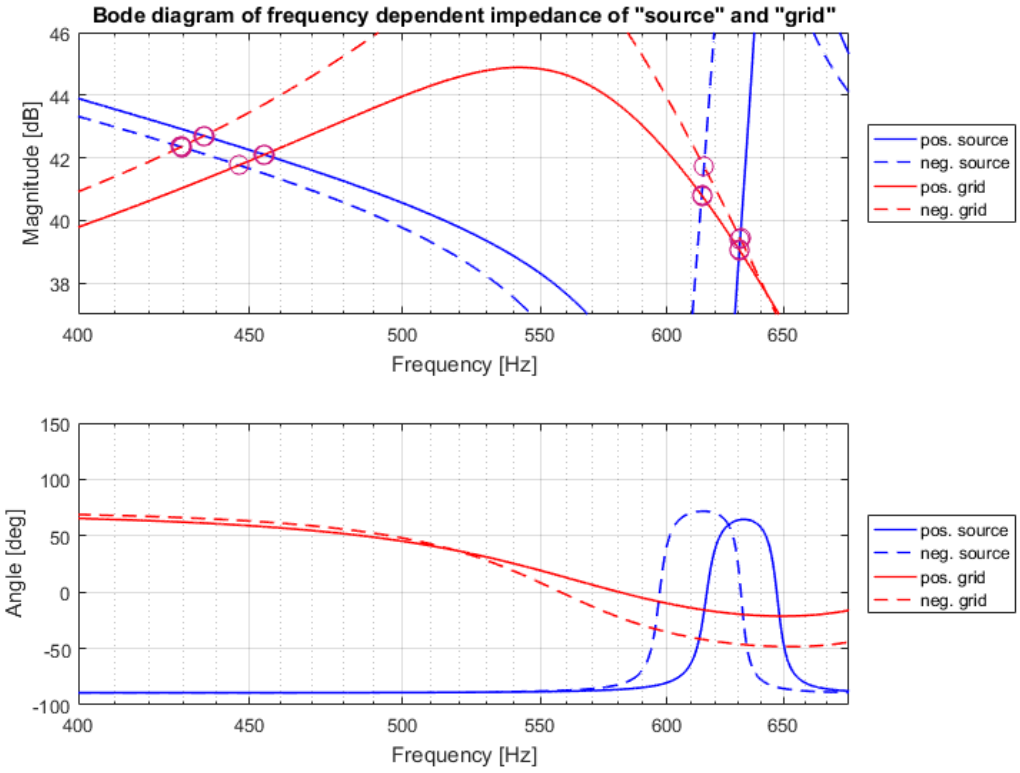

Figure V.48: Case 3: Bode diagram (zoomed) of frequency dependent positive- and negatice-impedances of *grid* and *source*.

The stability assessments by phase margins are gathered for all intersections in Table V.27.

Table V.27: Case 3: Resonance frequencies and the phase margins assigned.

Frequency order [-]	Phase margin [deg]
Positive Grid – Positive Source	
9.09	32.71
12.61	96.31
18.96	**3.28**
Positive Grid – Negative Source	
8.94	31.14
12.29	92.7
18.95	**3.29**
Negative Grid –Positive Source	
8.72	**25.45**
12.62	69.49
18.99	**1.29**
Negative Grid – Negative Source	
8.59	**24.47**
12.31	66.09
18.99	**1.29**

Once again, the values of frequencies where the intersections between curves occur correspond quite accurately to the values obtained from FS and HRMA methods. The phase margins of highest frequency is once again very low and marked as possibly unstable, similarly to the previous cases. The phase margin values of lowest and medium frequency groups are shifted down even more than in Case 1 and Case 2. While the phase margins of the medium frequency order group (around 12^{th} order) is still quite high, the phase margins of the resonance frequencies around 9^{th} order (negative grid - positive source and negative grid - negative source) become less than the safety margin of 30°assumed in Section II.2.3. The other two intersections around that order (positive grid - positive source and positive grid - negative source) are still above but only slightly above the safety margin. We conclude that in this case the resonance around 9^{th} order becomes possibly asymptotically stable (on the boundary of being stable and unstable) or even unstable.

V.3.4 Comparison to FS and HRMA

From the investigation of Bode diagrams we can compare the results to the ones obtained in both previous methods: FS and HRMA. The resonant frequencies are marked at the intersection of impedance curves. In this method we analyse both positive and negative impedances of converter models, therefore we obtain more resonant frequencies. In previous methods we did not divide the models into positive and negative sequences. In the following tables (Tables V.28 - V.30), for easy comparison, we can see once again the results of resonant frequency orders obtained from FS and HRMA methods presented in previous sections, as well as, the resonant frequency orders from Bode diagram analysis.

Table V.28: Comparison of three approaches (I). Frequency sweep.

Method / model	Frequency order [-]		
	Case 1	**Case 2**	**Case 3**
FS / Z(s)	12.42	12.33	12.33
	23.87	23.18	19.13

Table V.29: Comparison of three approaches (II). Harmonic Resonance Modal Analysis.

Method / model	Frequency order [-]			Dominant bus
	Case 1	**Case 2**	**Case 3**	
HRMA / Z(s)		9.51	8.73	Middle LCL bus (7)
	12.42	12.34	12.34	
	23.81	23.11	18.98	Cable 33 kV terminal buses (4, 5)

Table V.30: Comparison of three approaches (III). Resonant frequencies from Bode diagrams for all cases.

Method / model	Frequency order [-]		
	Case 1	**Case 2**	**Case 3**
Bode / Z(s)	11.90	10.80	9.09
	11.14	10.46	8.94
	10.32	10.00	8.72
	10.20	9.86	8.59
	12.42	12.51	12.61
	12.07	12.18	12.29
	12.43	12.52	12.62
	12.08	12.20	12.31
	23.81	23.11	18.96
	23.81	23.11	18.95
	23.81	23.12	18.99
	23.81	23.12	18.99

Comparing the results of frequency orders, we can clearly see that they are very similar, especially for higher orders where the values obtained are almost the same. In short, from all three approaches, we obtain very comparable results of resonant frequency. Additionally, from HRMA participation factors we identify the resonance source buses, while from Bode diagrams we conclude regarding the phase margins that correspond to stability issues in case of harmonic resonance.

Chapter VI

Approaches to resonance mitigation

To solve harmonic resonance problems the approaches are usually complicated. As described in Section I.3.4, the harmonic resonance depends on several factors and it may vary at different operational points or if any change in the network is performed (for example topology change or installation of new equipment). These facts make the mitigation of the resonance a complex issue. Proper preventive actions during designing phase seems easier to perform and more beneficial than facing the problem after commissioning through tuning or filtering.

If the network is already built, there are some approaches to limit the problem by additional assets like passive elements or active filters. In our study, we effectively identified the resonance frequencies. Moreover, we determined the main sources of resonances on the basis of participation factors from HRMA method. Thus, to solve the resonance problem, buses marked by participation factors are the candidates where passive or active elements may be installed. Additionally, if converters are present in the network, they may also be utilized, thought their control, to solve or mitigate the resonance problems. This could be especially applicable to the HVDC connected offshore wind farms grids where power converters dominate in the networks.

VI.1 Passive elements

The use of passive elements usually consists of addition of new resistive, inductive or capacitive element. Generally, passive elements (filters) are widely applied to limit harmonic propagation, improve power quality, reduce harmonic distortion and provide reactive power compensation simultaneously. Passive filters are still the first choice when it comes to high voltage or high current grids [7]. Limitations and concerns of passive filters includes [7]:

- They are not adaptable to the changing system conditions (tuned frequency or their size cannot be changed easily)
- Due to the network impedance in stiff systems very large filters may be required. This may bring overcompensation of reactive power or overvoltages on switching
- Power losses can be very significant
- The presence of new passive element (capacitive or inductinve) in a system may cause additional resonant frequency, therefore careful initial design is crucial
- The ageing, deterioration and temperature effects detune the filter in random manner, therefore the effect is difficult to predict
- Special protective and monitoring devices are required

In our case study of offshore WPP, the most straight-forward method for the resonance mitigation is to add a passive, resistive element to dissipate the energy of oscillations, in other words, to damp the resonance and increase stability margin. Other passive elements: inductance or capacitance are able shift the resonant frequencies away from the unwanted frequency level.

However, in the real offshore application, addition of new elements brings some problems. They require additional space in a substation which is apparently located on a offshore platform, therefore the cost of such an implementation is often very high. As aforementioned, new asset, especially resistive, always leads to increased power losses, which have to be effectively dissipated or cooled down. On the other hand, both capacitive and inductive elements, besides shifting of existing resonances, creates new resonance frequency to the offshore network what can cause additional problems. Due to the problems with offshore space for large passive elements and expected creation of new resonances by new asset, the solution of pure passive elements implementation is not recommended in our study case.

VI.2 Active filters, active damping

Generally, active filters can be classified according to the way these are connected in the circuit: series connection, parallel shunt connection and hybrid connections of active and passive filters. For general harmonics reduction, active filtering is usually incorporated with the harmonic producing equipment itself [7]. The active filters performance for harmonics mitigation is based on injecting a harmonic current of the same magnitude as that of the nonlinear load into the system, but of opposite polarity. Such an active filter is a harmonic current source and could be represented as a Norton equivalent circuit. The impedance of active filter influences aggregated network impedance, therefore the impedance resonant frequencies can be changed. However, for purely resonance mitigation, the following approaches of active filtering are proposed from the literature.

The implementation of hybrid filter (consisting of both passive and active elements) is presented in the paper [29]. The authors propose the solution for very similar offshore wind farm to the one presented in this study. The best location for placing the filters was chosen on the basis of power factors obtained harmonic resonance modal analysis. Moreover, the authors show how hybrid filter contributes positively in reducing the existing harmonics, while the risk of unwanted current magnification due to resonances is limited.

The active method of adding damping resistor is presented in [30]. The principle of the active damping is to implement damping resistor (in a virtual fashion) by inflicting changes in the controlled inductor current. In this way the presence of the resistor is emulated. As the result, virtual damping resistance is introduced to the equivalent control block diagram. It is stated that this type of active damping control scheme is much easier to be programmed and realized in digital control than conventional damping resistor in series with output capacitor. The authors also state that while designing a virtual parallel damping resistor limiting resonance, the issue of stability should be considered, especially in a weak grid. Therefore, consideration of active damping in this way has to be adopted according to the particular application.

In [31] the authors propose the active damping method for similar impedance model of HVDC converter to the one used in this study. The active damping [31] is based on injecting a voltage component of counter phase with detected oscillation in order to produce a cancellation effect. The active damping is implemented in the control structure. Three phase voltages are converted into d-q components and low pass filter version of measured voltage at PCC is subtracted from original signal. By that approach, the oscillatory phenomena is effectively damped.

VI.3 Tuning of converter control

As mentioned in the section above, we can influence the performance of a converter by introducing additional control elements i.e. adding additional function of active damping to converters.

Moreover, the tuning of controls which seems to be a very promising approach especially for islanded AC grids, provides other functionality. In principle, through the appropriate adjustment of control, converter should not be allowed to feed in active power above specified frequency. This frequency limit has to be predefined and should cover all undesired grid resonance frequencies, also regarding other possible operational topologies. This approach simply prevents the converter from feeding in active power at the frequencies higher than the limit. Therefore, the grid resonances will not be amplified and harmonic resonance interaction will not occur.

Additionally, the adjustment of converter control combined with the stability analysis approach enables assessment of the system stability. It can be assessed with respect to the changes of in the converter control and thus in converter impedance. From this, one can conclude how to tune the converter in order to provide stable system. The tuning has to be done with respect to detailed specifications and control codes which are the intellectual property of manufacturers and usually are not published.

Chapter VII

Conclusions

In the thesis we investigate the problem of resonance in offshore HVDC connected wind power plants. The analysis is performed on the basis of 400 MW wind park for three topology cases, for three models of converters and by different methods: frequency sweep, harmonic resonance modal analysis and stability analysis on the Bode plots. The results are also partially validated in DIgSILENT Power Factory software. We draw the conclusions step by step within the thesis, however in the following paragraphs the key outcome and observations are assembled.

The first conclusions we can draw having the results of frequency sweep method. The curves computed in MATLAB are confirmed by the Power Factory simulation results. The values of frequency are the same in both approaches. The values of impedance peaks are different, but because of the difference in step size, we do not consider it as inconsistency. From the results of FS only, we detect shifting of the resonance frequency in different topology cases. The shifting is expected and its reason is identified as amount of capacitance (capacitive power) in the network after new branches, including capacitive elements, are connected.

Secondly, the values of frequency resonance obtained in harmonic resonance modal analysis confirms the values obtained in frequency sweep method and in Power Factory software. However, for some cases, the HRMA method returns higher number of resonant frequency values than the number obtained from FS. Due to this, both methods should be considered jointly. Moreover, by decomposition of the resonances into different modes, we identify the critical modes responsible for each of resonance (in modal domain). Finally, the output of the method includes also participation factors.

On the basis of participation factors values, first of all, we can extend our conclusions regarding both methods. The values of participation factors indicate the buses which contribute more than others to excitement of particular resonance frequency. We identify those buses in each topology case for each model. In this way, we observe clear pattern with participation factors of new resonance frequencies which appear after connecting more branches to the model. For both approaches (FS and HRMA), connection of new branches is followed by appearance of new resonance frequencies (excluding Z(s) model). The new resonances are very close to one of existing resonance (emitted from previously connected branches) and have their origin in the newly connected branches. These observations also clearly tell us about the symmetry in the network.

From the results of frequency sweep analysis performed in Power Factory we can observe the difference between parallel and series resonance, by combining the impedance curves at the different buses along one branch. We recognize that the series resonance frequencies (marked by dips of impedance curves) depends on the bus which we observe the impedance from, while the parallel resonance frequencies (marked by peaks of impedance curves) are the same, regarding

the bus of observation. These features are confirmed for all topology cases as well as for both VS and CS-WT models.

Comparing the different converter models, we observe a lot of similarities but also slightly different behaviours for each of them. Generally, we detect lower values of resonance for CS-WT model than for VS model. In Z(s) model the changes in resonant frequencies for different topology cases are less significant than for both VS and CS-WT models. In terms of participation factors analysis, we draw very similar conclusions about the buses participating the most in the resonances. Even though the levels of frequencies are sometimes considerably different, the participation factors indicate the same buses as the sources of respective resonance. Hence, the comparison of frequencies between the models gives clear results in terms of emission of resonances.

The non-linear model of converter impedance Z(s) also provides some interesting outcome. Fist of all, the obtained curves shapes of positive and negative sequences of impedance for both converters are consistent with the models found in the literature, often verified by real converters. With Z(s) converter impedances implemented, we obtain similar values of resonant frequencies which have the origins in the same buses like in the VS and CS-WT models. From HRMA method we collect the similar number of resonant frequencies, while from FS the lowest frequencies are not detected in this model. Moreover, we observe interesting phenomenon of resonance (peaking impedance curves) below the fundamental frequency (subsynchronous resonance), which is not the subject of the thesis. What is more, for different topology cases, the downward shifting of the resonant frequencies is very small for the resonances emitted from the WT-converters buses. The other resonance frequencies are not constant and behave similarly as in VS and CS-WT models.

The stability analysis were performed to assess the harmonic stability of each topology case. On the basis of aggregated model (*source* and *grid*) and Nyquist stability criterion interpreted on Bode diagram, we identify resonance frequencies and we asses the quality of stability by phase margin for each identified resonance frequency. The Bode diagram is utilized instead of Nyquist diagram in order to easily find the intersections and the values of resonant frequencies. First of all, the frequencies correspond quite accurately to the resonant frequencies obtained from the FS and HRMA methods. This confirms the consistency of all approaches. Due to the consideration of positive and negative sequences we obtain more intersections (more resonance frequencies) than in previous methods, however once again, the values coincide very accurately to the previous methods. The additional information of phase margins tells us about the quality of stability for each intersection, in other words - the quality of stability for each resonant frequency. From this analysis, we gain information about possible unstable operation of the network in case of presence of harmonics waveforms at the resonant frequencies (harmonic resonances). For all three topology cases, group of highest frequency orders are marked unstable while having non-sufficient phase margins, thus being exposed to unstable operation hazard in the network. Additionally, for topology cases with more branches, we observe the significant decrease in the phase margin for the all frequencies above safety margin. This change leads, in topology Case 3, to the decrease of the phase margin below the safety margin of 30°for lowest group of frequencies. Thus, we conclude that, for our model, highest number of branches (highest number of aggregated wind turbines) can lead to the problems with stability, which are less probable for lower number of branches.

Application of the methods brings crucial information for further steps of such an analysis like resonance mitigation. The results obtained are sufficient for further implementation of different approaches to mitigate the resonance phenomenon. In this thesis, we discuss and propose some exemplary methods presented in the literature. The active methods of damping and the appropriate tuning of converters control are considered as relevant in the case of considered offshore wind farm network. Finally, we can highlight very promising, currently developed approach

of resonance mitigation by inverters and rectifiers. Since converters nonlinear impedance can be influenced by their control, by relevant altering of control we should be able to regulate output impedance curves and in this way influence resonances in the system without installing additional devices.

Chapter VIII

Related environmental impact and costs of the thesis development

VIII.1 Environmental impact of offshore WPP

This section treats about general concerns within environmental impact of offshore wind farms. Since, from environmental point of view, there is almost no difference between AC of DC connected wind farms, they are not distinguished. This section gathers some potential impacts of offshore farms, paying attention only to direct environmental impact pathways, excluding positive aspects of renewable energy production.

The first commercial scale offshore wind farm (Horns Rev 1, installed power of 160 MW) was commissioned in 2002. Since then, rapid growth of offshore wind energy generation is observed, particularly in northern European waters. As stated in I.2, average capacity of turbines has been increasing since then and wind farms are being installed further from the coasts. It is expected that the size of offshore wind project will continue increase [32] affecting different environment (further from shores). The relative novelty of the technology makes it difficult to identify all of the impacts on environment and effects of those activities.

The most studied impact of offshore wind farms is the impact on marine mammals and seabirds. It is usually of concerns for stakeholders because of legal protection of those spacies [33]. Construction of such a wind farm has the greatest impact on marine spacies because of the noise, vessel traffic and pile driving [34]. Those activities could potentially cause hearing damages, spatial displacement to avoid noise or collisions and disturbances from vessels movements [35]. During operation of wind farms, underwater sound levels also can reach dangerous levels, disturbing acoustic communication of marine mammals [36] and fishes [37].

Of greatest concern is also the impact of seabirds. Mortality can be caused by collision with blades. This may affect birds migrating through the area as well as those that breed or forage in the vicinity [38].

Another issue to look at is the emission of electromagnetic field by submarine cables transmitting the electricity onshore. This can also affects the movements and navigation of spacies that are sensitive to electromagnetic fields (mainly fishes and sea turtles) [39].

The species of concern will of course differ among regions depending on climate, occurrence of those species or regulations and protection statuses.

VIII.2 Temporary planning and costs of thesis development

In this section we present the cost of development of the master thesis. We consider direct and indirect costs of the work. The direct costs are expanses that could be easily connected to the work/product etc. This includes for example items such as software, equipment, labour, raw materials. On the other hand, indirect costs go beyond the costs associated with creating a particular product. For example, the materials and supplies needed for the company's day-to-day operations (office rental, desktop computers, cell phones). These costs contribute to the company as a whole, but they are not assigned to particular work/project.

As the result, in our case, the costs are divided into:

1. Direct costs (c_{direct}):
    - Labour cost (c_{labour})
    - Software cost ($c_{software}$)
2. Indirect costs ($c_{r_indirect}$)
    - Total indirect costs (office rent, desk, electricity etc.) is assumed to be proportional to direct costs.

In the calculations the following values are assumed:

- Time frame of work (T): 20 weeks
- Work week time (t_{week}): 32.5 h/week
- Pay rate - cost of employment for employer ($p_{employer}$): 25 EUR/h
- Cost of software (c_{PF}, c_{ML}): 1500 EUR (DigSILENT Power Factory), 2000 EUR (MATLAB)
- Indirect costs (office rent, electricity, desk, water) are estimated as 25% of direct costs ($r_{indirect}$)
- VAT 21% (Spain)
- Additional time for further development: 20 weeks

Hence, the cost of the master thesis development till now is:

$$C_{total} = c_{direct} + c_{indirect}$$

where direct cost is:

$$c_{direct} = c_{labour} + c_{software} = p_{employer} \cdot t_{week} \cdot T + c_{PF} + c_{ML}$$

and indirect cost is:

$$c_{indirect} = r_{indirect} \cdot c_{direct}$$

Thus, excluding VAT, the values are:

$$c_{labour} = 16250 \text{ EUR}$$

$$c_{software} = 3500 \text{ EUR}$$

$$c_{direct} = 19750 \text{ EUR}$$

$$c_{indirect} = 4937.5 \text{ EUR}$$

And the total cost, including VAT is:

$$c_{total} = 29871.88 \text{ EUR}$$

which gives the average value per hour:

$$c_{perHour} = 45.96 \text{ EUR/h}$$

For the purpose of further development (for example implementation of resonance mitigation methods), the time frame of next 20 weeks is assumed. The cost of labour is obviously proportional to the working time, however due to the fact that the employer will not pay again for the licences of the software, the value per hour for total project of 40 weeks will decrease to the level of 41.88 EUR/h.

Reference

[1] REN21, *Renewables 2016 - Global Status Report. Renewable Energy Policy Network for the 21st Century.* 2016.

[2] WWEA, *Qarterly Bulletin.* 1 March 2016.

[3] GEWC, *Global Wind Report - Annyal Market Update.* 2015.

[4] EWEA, *The European offshore wind industry - key trends and statistics 2015.* February 2016.

[5] G. F. Reed, H. A. A. Hassan, M. J. Korytowski, P. T. Lewis, and B. M. Grainger, "Comparison of hvac and hvdc solutions for offshore wind farms with a procedure for system economic evaluation," in *Energytech, 2013 IEEE*, pp. 1–7, May 2013.

[6] C. Buchhagen, C. Rauscher, A. Menze, and J. Jung, "Borwin1-first experiences with harmonic interactions in converter dominated grids," in *International ETG Congress 2015; Die Energiewende-Blueprints for the new energy age; Proceedings of*, pp. 1–7, VDE, 2015.

[7] J. Das, *Power System Harmonics and Passive Filter Designs.* IEEE Press Series on Power Engineering, Wiley, 2015.

[8] F. De La Rosa, *Harmonics and Power Systems.* Electric Power Engineering Series, CRC Press, 2006.

[9] J. Arrillaga and N. Watson, *Power System Harmonics.* Wiley InterScience electronic collection, Wiley, 2004.

[10] M. Bradt, B. Badrzadeh, E. Camm, D. Mueller, J. Schoene, T. Siebert, T. Smith, M. Starke, and R. Walling, "Harmonics and resonance issues in wind power plants," in *Transmission and Distribution Conference and Exposition (T D), 2012 IEEE PES*, pp. 1–8, May 2012.

[11] I. A. report prepared by Load Characteristics Task Force., "The effects of power system harmonics on power system equipment and loads," *IEEE Transactions*, 1985.

[12] R. H. Park, "Two-reaction theory of synchronous machines generalized method of analysis-part i," *Transactions of the American Institute of Electrical Engineers*, vol. 48, no. 3, pp. 716–727, 1929.

[13] W. Xu, Z. Huang, Y. Cui, and H. Wang, "Harmonic resonance mode analysis," *IEEE Transactions on Power Delivery*, vol. 20, pp. 1182–1190, April 2005.

[14] G. C. Verghese, I. J. Perez-arriaga, and F. C. Schweppe, "Selective modal analysis with applications to electric power systems, part ii: The dynamic stability problem," *IEEE Transactions on Power Apparatus and Systems*, vol. PAS-101, pp. 3126–3134, Sept 1982.

[15] R. Bellman, R. E. Bellman, R. E. Bellman, R. E. Bellman, and E.-U. Mathématicien, *Introduction to matrix analysis*, vol. 960. SIAM, 1970.

[16] I. J. Pérez-Arriaga, G. C. Verghese, and F. C. Schweppe, "Selective modal analysis with applications to electric power systems, part i: Heuristic introduction," *ieee transactions on power apparatus and systems*, no. 9, pp. 3117–3125, 1982.

[17] L. Pham, "A review of full scale converter for wind turbines," *URL https://www. academia. edu/5759035/A_Review_of_Full_Scale_Converter_ for_Wind_Turbines*, p. 8.

[18] H. Liu and J. Sun, "Voltage stability and control of offshore wind farms with ac collection and hvdc transmission," *IEEE Journal of emerging and selected topics in power electronics*, vol. 2, no. 4, pp. 1181–1189, 2014.

[19] J. Sun, "Impedance-based stability criterion for grid-connected inverters," *IEEE Transactions on Power Electronics*, vol. 26, no. 11, pp. 3075–3078, 2011.

[20] R. D. Middlebrook, "Input filter considerations in design and application of switching regulators," *IAS'76*, 1976.

[21] H. Liu and J. Sun, "A study of offshore wind hvdc system stability and control," in *Proceedings of 10th International Workshop on Large-Scale Integration of Wind Power into Power Systems as well as on Transmission Networks for Offshore Wind Power Plans*, 2011.

[22] J. Sun, "Small-signal methods for ac distributed power systems–a review," *IEEE Transactions on Power Electronics*, vol. 24, no. 11, pp. 2545–2554, 2009.

[23] Z. Bing, K. J. Karimi, and J. Sun, "Input impedance modeling and analysis of line-commutated rectifiers," *IEEE Transactions on Power Electronics*, vol. 24, no. 10, pp. 2338–2346, 2009.

[24] M. Cespedes and J. Sun, "Impedance modeling and analysis of grid-connected voltage-source converters," *IEEE Transactions on Power Electronics*, vol. 29, no. 3, pp. 1254–1261, 2014.

[25] E. Larsen, G. Drobnjak, and H. Elahi, "Standardization of vsc-hvdc interface with offshore wind generation," *Proc. 11th Int. Workshop Large-Scale Integr. Wind Power Power Syst.*, 2012.

[26] IEC, "Series 61000 standards," from 1990.

[27] CENELEC, "En 50160 - voltage characteristics of electricity supplied by public distribution systems," Brussels, 1994.

[28] IEEE, "Recommended practice and requirements for harmonic control in electrical systems," 1992.

[29] K. N. B. M. Hasan, K. Rauma, A. Luna, J. I. Candela, and P. Rodríguez, "Harmonic compensation analysis in offshore wind power plants using hybrid filters," *IEEE Transactions on Industry Applications*, vol. 50, no. 3, pp. 2050–2060, 2014.

[30] X. Chen, C. Y. Gong, H. Z. Wang, and L. Cheng, "Stability analysis of lcl-type grid-connected inverter in weak grid systems," in *Renewable Energy Research and Applications (ICRERA), 2012 International Conference on*, pp. 1–6, IEEE, 2012.

[31] M. Amin, M. Molinas, and J. Lyu, "Oscillatory phenomena between wind farms and hvdc systems: The impact of control," in *2015 IEEE 16th Workshop on Control and Modeling for Power Electronics (COMPEL)*, pp. 1–8, IEEE, 2015.

[32] EWEA, "The european offshore wind industry - key trends and statistics 2013," tech. rep., European Wind Energy Association, Brussels, Belgium, 2014.

[33] H. Bailey, K. L. Brookes, and P. M. Thompson, "Assessing environmental impacts of offshore wind farms: lessons learned and recommendations for the future," *Aquatic biosystems*, vol. 10, no. 1, p. 1, 2014.

[34] S. Dolman and M. Simmonds, "Towards best environmental practice for cetacean conservation in developing scotland's marine renewable energy," *Marine Policy*, vol. 34, no. 5, pp. 1021–1027, 2010.

[35] P. T. Madsen, M. Wahlberg, J. Tougaard, K. Lucke, and P. L. Tyack, "Wind turbine underwater noise and marine mammals: implications of current knowledge and data needs," *Marine Ecology Progress Series*, 2006.

[36] J. Tougaard, O. D. Henriksen, and L. A. Miller, "Underwater noise from three types of offshore wind turbines: Estimation of impact zones for harbor porpoises and harbor seals," *The Journal of the Acoustical Society of America*, vol. 125, no. 6, pp. 3766–3773, 2009.

[37] M. Wahlberg and H. Westerberg, "Hearing in fish and their reactions to sounds from offshore wind farms," *Marine Ecology Progress Series*, vol. 288, pp. 295–309, 2005.

[38] M. Desholm and J. Kahlert, "Avian collision risk at an offshore wind farm," *Biology letters*, vol. 1, no. 3, pp. 296–298, 2005.

[39] T. Tricas and A. B. Gill, "Effects of emfs from undersea power cables on elasmobranchs and other marine species.," 2011.